DESIGN OF SINGLE-LAYER FREE-FORM STEEL STRUCTURES: A CASE STUDY ON THE BRITISH MUSEUM GREAT COURT ROOF

FARUK SERHAT

JULY 2023

DİYARBAKIR

GRADUATE SCHOOL
OF NATURAL AND APPLIED SCIENCES
OF DİCLE UNIVERSITY

DESIGN OF SINGLE-LAYER FREE-FORM STEEL STRUCTURES: A CASE STUDY ON THE BRITISH MUSEUM GREAT COURT ROOF

BY
FARUK SERHAT

IN PARTIAL FULFILLMENT OF THE REQUIREMENTS
FOR
THE DEGREE OF MASTER OF SCIENCE
IN
CIVIL ENGINEERING

JULY 2023

DİYARBAKIR

DESIGN OF SINGLE-LAYER FREE-FORM STEEL STRUCTURES: A CASE STUDY ON THE BRITISH MUSEUM GREAT COURT ROOF

This study, prepared by **Faruk SERHAT** as part of the Dicle University Graduate Education and Examination Regulation, was evaluated by the jury members with the following information and accepted as a **Master's Thesis in the Department of Civil Engineering**.

Prof. Dr. Neslihan DALKILIÇ
Dean, Graduate School of **Natural and Applied Science**

Assoc. Prof. Dr. Mehmet Emin ÖNCÜ
Supervisor, **Civil Engineering Dept., Dicle University**

Examining Committee Members:

Prof. Dr. S. Özgür DEĞERTEKİN (*)
Civil Engineering Dept., Dicle University

Assoc. Prof. Dr. Mehmet Emin ÖNCÜ (**)
Civil Engineering Dept., Dicle University

Asst. Prof. Dr. İbrahim Behram UĞUR
Civil Engineering Dept., Şırnak University

APPROVAL

Date: *03.07.2023*

(*) Write the title, name and affiliation of the head of the examining committee in the first row.
(**) Write the title, name and affiliation of the superviso in the second row.

To My Son…

I hereby declare that all information in this document has been obtained and presented following the Thesis Manual (prepared by the Dicle University Graduate School of Natural and Applied Sciences), academic rules and ethical conduct. I also declare that, as required by these rules and conduct, I have fully cited and referenced all material and results that are not original to this work. I shall be solely responsible if any evidence is found against my declaration.

Name, Surname: Faruk SERHAT

Signature: ……………………………

ACKNOWLEDGMENTS

I would like to express my sincere gratitude to all those who have provided invaluable assistance in completing my MSc thesis. A special thanks go to my advisor, Associate Prof. Dr. Mehmet Emin ÖNCÜ and Prof. Dr. S. Özgür DEĞERTEKİN, who has offered unwavering guidance throughout the process.

I would also like to thank my wife, mother, and brothers, sisters for their steadfast support throughout the thesis.

.

CONTENT

LIST OF FIGURES

ANNEX LISTS

LIST OF TABLE

ANNOTATION AND SYMBOL

Symbol	**Explanation**
C_{dir}	Directional Factor
C_e	Exposure coefficient
c_o	Orography Factor
c_{pe}	External Pressure Coefficient
c_{pi}	Internal Pressure Coefficient
c_{pnet}	Net pressure coefficient
c_r	Roughness Factor
C_{season}	Seasonal Factor
C_t	Thermal coefficient
F_u	Tensile Strength
F_y	Characteristic Yield Stress
G	Dead Load
I	Building importance coefficient
k_l	Turbulence Factor
k_r	Terrain Factor
l_v	Turbulence intensity
m	Reduction value depending on roof slope (α)
n	Live load participation coefficient
R	Rain Load
s	Snow load on the roof [kN/m^2]
s_k	Characteristic value of snow on the ground at the relevant site [kN/m^2]
ρ	Air Density

Annotation	**Explanation**
TSC 2018	Turkish Seismic Code Published In 2018
TSC 2007	Regulation on Buildings to be Constructed in an Earthquake Zone 2007
AISC 360-10	Specification for Structural Steel Buildings
TSSC 2016	Turkish Steel Structure Code (The Regulation on Design, Calculation and Construction Principles of Steel Structures 2016)
TS EN 1991-1-3	General actions -Snow loads
TS EN 1991-1-4	General actions -Wind actions
LRFD	Load and Resistance Factor Design

ABSTRACT

ANALYSIS AND DESIGN OF SINGLE-LAYER FREE-FORM STRUCTURES: A CASE STUDY ON THE BRITISH MUSEUM GREAT COURT

Serhat, Faruk

Master of Science in Department of Civil engineering

Supervisor: Associate: Doç. Dr. Mehmet Emin Öncü

July 2023, 186 pages

Single-layer free-form systems have become increasingly popular in architectural design projects as they offer the opportunity to create unique and visually stunning structures. These designs have gained global attention due to their impressive appearance and ability to push boundaries creatively. Using single-layer systems is environmentally friendly and reduces construction waste by using less material than traditional construction methods. Nowadays, many architectural projects incorporate single-layer free-form systems to construct exceptional and one-of-a-kind buildings. This thesis comprehensively examines the technical details of single-layer free-form systems from architectural and engineering perspectives, including connection types such as rigid, semi-rigid, and hinged connections. The study thoroughly examines the welded and bolted connection details at the nodal points of single-layer free-form systems and their advantages and disadvantages. This thesis examines the architecture of the Queen Elizabeth II Great Court British Museum, considered one of Europe's most significant courtyard roof projects. The structure of a single-layer free-form building in Istanbul's Yeşilköy neighborhood, Bakırköy district, is analyzed using the SAP2000 program. The critical joint is also analyzed as a welded and bolted connection using Ansys for comparison. A uniform profile section is selected for the building's structural design to make the design more accessible. Various loads, including static loads, snow loads, earthquake loads, and wind loads, are numerically evaluated based on relevant codes such as Turkish Seismic Code (TSC 2018), Turkish Steel Structure Code (TSSC 2016), TS EN 1991-1-3:2009, and TS EN 1991-1-4:2005. Two different analysis cases are conducted for the single-layer free-form system under symmetric and asymmetric load combinations. The results are presented in tables and visual representations for comparative evaluations. The structural analysis indicates that the deflection values are similar, but the welded connection provides more stability compared to the bolted connection regarding torsion. The maximum stress calculated in the analysis of the welded connection is approximately 60% higher than that of the bolted connection. In comparison, the maximum deflection calculated in the bolted connection analysis is approximately 65% higher than that of the welded connection.

Keywords: Single-layer free-form structure, Structural steel nodes, SAP2000, ANSYS

ÖZET

TEK KATMANLI SERBEST FORMLU ÇELİK YAPILARIN TASARIMI: İNGİLİZ MÜZESİ ÇATISI ÖRNEĞİ İNCELEMESİ

Serhat, Faruk
Yüksek Lisans, İnşaat Mühendisliği
Danışman Doç. Dr. Mehmet Emin Öncü
Temmuz 2023, 186 sayfa

Tek Katmanlı Serbest Şekilli sistemler, son yıllarda mimari tasarım projelerinde kullanılarak benzersiz ve özgün yapılar inşa edilebilmektedir. Bu tasarımlar, etkileyici görünümleriyle hem yerel hem de uluslararası düzeyde büyük ilgi görmektedir. Tek katmanlı serbest şekilli sistemlerin kullanılması, yaratıcı, sınırları zorlayan ve etkileyici tasarımların hayata geçirilmesini sağlamaktadır. Ayrıca bu sistemler yapıların dış görünüşüne ve işlevselliğine farklı bir boyut kazandırmak için tercih edilmektedir. Geleneksel yöntemlerden farklı olarak tek katmanlı sistemler daha az malzeme kullanılarak inşa edilebilmektedir. Bu da yapıların daha çevreci olmasını ve inşaat sırasında oluşan atıkların azaltılmasını sağlamaktadır. Bu tez kapsamında Tek Katmanlı Serbest Şekilli sistemlerin tasarım mühendisliği açısından teknik detayları ayrıntılı şekilde ele alınmış bu sistemlerin birleşim tipleri ile rijit, yarı rijit ve mafsallı birleşimler incelenmiştir. Tek Katmanlı Serbest Şekilli sistemlerin düğüm noktalarındaki birleşimleri kaynaklı ya da bulonlu olarak yapılabilmektedir. Çalışmada düğüm noktasının kaynaklı ve bulonlu birleşim detayı, avantaj ve dezavantaj açısından ayrıntılı bir şekilde incelenmiştir. Bu tezde, Avrupa'nın en büyük avlu üzeri örtme projelerinden biri olan Queen Elizabeth II Great Court British Müzesi mimarisi örnek alınarak; İstanbul İli, Bakırköy İlçesi, Yeşilköy mahallesinde inşa edileceği varsayılan Tek Katmanlı Serbest Şekilli bir yapının analizi SAP2000 programı ile yapılmıştır. Ayrıca, yapısal analiz sonucunda belirlenen en kritik düğüm noktasının kaynaklı ve bulonlu olarak analizi de ANSYS programı ile yapılmıştır. Yapı tasarımında profil kesiti uygulama kolaylığı açısından tek tip bir profil seçilmiştir. Modele etki eden sabit yükler, kar, deprem ve rüzgar yüklerinin sayısal değerleri Türkiye Bina Deprem Yönetmeliği (TBDY 2018), Türkiye Çelik Yapı Yönetmeliği (TÇYY 2016), TS EN 1991-1- 3: 2009, TS EN 1991-1-4: 2005 Yönetmelikleri ışığında incelenmiş, yapısal analiz için tüm hesaplamaları yapılmıştır. Tek tabakalı serbest formlu sistem için iki farklı durum analizi yapılmıştır. İlk durumda, moment 2-2 zayıf yönü serbest bırakılarak bir analiz gerçekleştirilmiştir. İkinci durumda ise düğüm noktası rijit birleşimli olarak analiz edilmiştir. Bu analizler, simetrik ve asimetrik yüklerin oluşturduğu yük kombinasyonları altında gerçekleştirilmiş ve sonuçlar karşılaştırılmıştır. Yapılan analiz sonucunda elde edilen sonuçlar karşılaştırmalı olarak tablo ve görsel olarak sunulmuştur. Sehim değerleri açısından yapı analizinde aynı sehim değerleri elde edilmiştir. Ancak burkulma açısından kaynaklı düğüm noktasının bulonlu düğüm noktasına göre daha stabil olduğu görülmüştür. Elde edilen veriler ve yapılan karşılaştırmalar neticesinde; kaynaklı düğüm noktası analizi sonucunda hesaplanan maksimum gerilme değerinin bulonlu düğüm noktasına göre yaklaşık %60 oranında arttığı tespit edilmiştir. Sehim değerinde ise bulonlu düğüm noktası analizi sonucunda hesaplanan maksimum sehim değerinin kaynaklı düğüm noktasına göre yaklaşık %65 oranında arttığı tespit edilmiştir.

Keywords: Tek katmanlı serbest şekilli yapı, Çelik düğüm noktası, SAP2000, ANSYS

1. INTRODUCTION

In recent years, the use of single-layer free-form constructions in architectural design has become increasingly widespread, enabling the realization of creative, boundary-pushing, and impressive designs. Single-layer constructions are preferred by architects and civil engineers to add a different dimension to the exterior appearance and functionality of structures. Such designs emphasize the aesthetic appearance while allowing them to be lighter and more flexible, thereby reducing construction costs.

Single-layer constructions, unlike traditional methods, can be built using fewer materials. This feature of single-layer construction contributes to the buildings being more environmentally friendly and reduces waste during construction. In many architectural design projects today, unique and distinctive buildings are being constructed using single-layer constructions. The impressive appearance of these designs attracts attention both locally and internationally.

Single-layer free-form structures serve as the main load-bearing system and provide secondary support for the exterior cladding system. Additionally, they can be utilized as an elegant element in interior decoration. These structures fulfill the role of the primary load-bearing system while also providing secondary support for the external cladding system. Moreover, they can be employed as a stylish element in interior design.

As the span of structures increases, the importance of load-bearing systems also increases. Wide spans are commonly used in stadiums, exhibition halls, cultural centers, event venues, sports facilities, production facilities, and shopping malls. Due to the necessity of using wide spans in these buildings, the design of wide-span systems has become an integral part of engineering requirements today. Single-layer free-form structures offer contemporary architectural design options combining aesthetics and simple geometry. They provide more flexibility and design uniqueness compared to other load-bearing systems. However, it is essential to note that they may come with higher material and production costs. Therefore, the design and construction of such structures should be carefully planned, considering factors such as budget and timing.

The connections that constitute single-layer free-form structures are fundamental complementary components and load transfer points that give the structure its unique shape. Each structure's connections have specific characteristics tailored to the structure, such as its geometry, static requirements, architectural preferences, and steel detailing factors. Therefore, the design of nodes requires special consideration. If desired, nodes in single-layer free-form structures can be designed as entirely bolted connections or concealed bolted connections.

Single-layer free-form structures stand out as visually striking and functionally high-performance buildings. Essential factors to consider in designing such structures include the design of nodes, material selection, production processes, aesthetic preferences, and specific.

1.1 Design Process

The design process in the context of this work involves several steps, each contributing to the final result.

The first step is "General Information and Classification of Free-form Systems." It involves comprehensive study and understanding of free-form systems, including their definition, characteristics, applications, and classification. This step is fundamental for subsequent design and analysis as it provides necessary background information and a common language for discussing the particularities of free-form structures.

The second step involves a detailed "Case Study" of existing free-form structure. The specific structure studied in this thesis are "The British Museum Great Court Roof". The British Museum Great Court Roof was studied in terms of its overall structure, while the Tornado Roof Structure was examined focusing on its nodes. These studies provide practical insights into the behavior of free-form structures and nodes under real-world conditions.

Next, a "CAD Model" is created to represent the studied structures in a virtual environment. This step is crucial for subsequent analysis as it allows for precise manipulation and examination of the structure, including its geometry, materials, and connections.

"Defining Parameters" is the next step where key parameters such as material properties, loading conditions, and boundary conditions are defined. These parameters are critical for accurately simulating the behavior of the structure.

Following this, the "The British Museum Great Court Roof Structure Analysis" is conducted. This step involves the application of the defined parameters to the CAD model and the simulation of its behavior under various conditions using SAP2000.

The subsequent step involves performing "Case 1 and Case 2 Analysis".

In Case 1 analysis, it was assumed that the frame elements M2, the bending moment in the 1-3 plane (about the 2-axis), did not take any moment. This scenario was modeled as bolted in the node analysis using ANSYS. On the other hand, in Case 2 analysis, the nodes were considered to transfer all forces. This scenario was modeled as welded in the node analysis.

Finally, "Evaluation and Comparison of Results" involves the review of the analysis results, comparison against known performance of the actual structures, and drawing conclusions regarding the performance and design of the free-form structures.

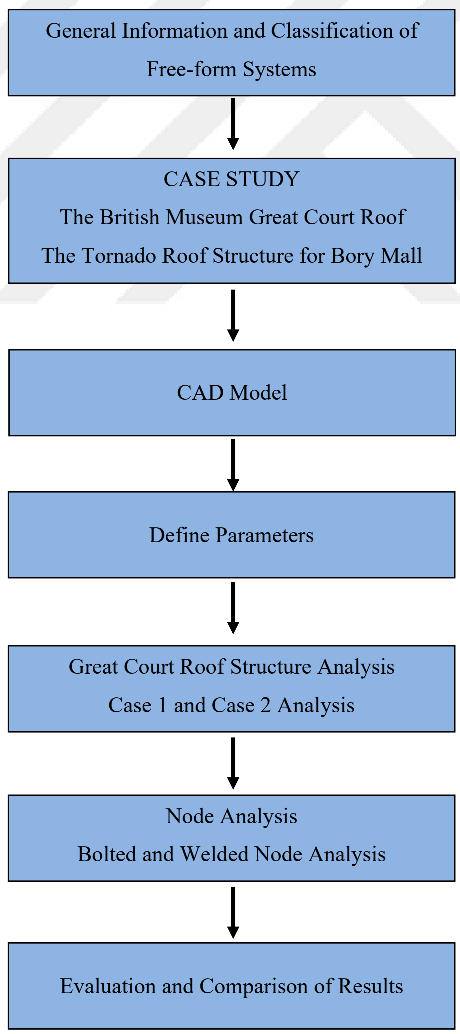

Figure 1.1 Design process of case study

2. LITERATOR REVIEW

A succinct overview of the findings regarding single-layer free-form systems in literature is presented below.

(Harris et al., 2008), explores the design and construction of free-form structures, focusing specifically on the grid shell located at the Savill Garden in the United Kingdom. It highlights the significance of inhibiting rotation in the node, as it directly influences the in-plane shear stiffness of the structure. The paper delves into the project's context and objectives, emphasizing integrating the grid shell within the natural landscape. The design process is meticulously described, showcasing the utilization of computational tools and sustainable design principles. The construction phase is also outlined, underscoring the collaborative efforts and innovative techniques. Overall, this paper offers valuable insights into the design and construction of grid shell structures, making it a valuable reference for future endeavors.

(Ahmed & Stutzki, 2015), the paper states that bolted connections can only achieve semi-rigid connections in the case of single-layer free-form systems, and it is possible to achieve a clean appearance by hiding the bolts without the need for on-site welding. The paper emphasizes that connections are a significant factor in the cost of the load-bearing system. Curved forms can be designed to meet the desired moment-carrying capacity and allowable rotational freedom with patented semi-rigid bolted connections. It is noted that the installation process in single-layer free-form systems is more precise than in traditional steel structures, and bolt holes that have larger diameters can pose stability problems. The paper also stated wholesale displacement is highly likely due to asymmetric snow loading.

(Ding et al., 2017) the theoretical strut model used in the seismic analysis of single-layer reticulated domes. It explores the background and significance of reticulated dome structures, emphasizing their vulnerability to seismic forces and the crucial need for accurate seismic analysis. The review covers a range of existing models and methodologies employed in this field, focusing specifically on the theoretical strut model. It encompasses relevant research studies, case studies, and design considerations related to the applying of the strut model in the seismic analysis of reticulated domes, highlighting its advantages, limitations, and practicality. This paper offers valuable insights and serves is a valuable resource for researchers, engineers, and practitioners interested in the seismic analysis of single-layer reticulated domes using the theoretical strut model.

(Zhi et al., 2012), the damage caused by earthquakes in single-layer lattice systems, the effects of parameters such as span length, height/span ratio, and roof weight on the extent of damage were investigated. Analyses were conducted for different earthquake magnitudes using various parameters, and based on this information, a risk assessment methodology was proposed in the paper.

Another study examined the influence of material and geometric properties of nodes, eccentricity, and their impact on moment-rotation behavior. It was noted that numerical analyses yielded results very close to experimental findings. The three characteristics significantly affecting the moment-rotation curve were rotational stiffness, moment resistance, and rotational capacity.

These studies provide valuable insights into the effects of parameters and characteristics on the damage and behavior of single-layer lattice systems subjected to earthquakes. The findings contribute to developing a risk assessment methodology and enhance the understanding of the moment-rotation behavior of node points, particularly considering the influence of material and geometric properties and eccentricity.

(Li et al., 2015), An examination of the nonlinear behavior of a column-supported dome under seismic effects was conducted in this study. It is the only known study focusing on the supporting system's influence on the dome's dynamic behavior. The dome was assumed to consist of rigid node points, and it was observed that the domes collapsed at significantly lower acceleration values compared to columnless models, highlighting the importance of column stiffness in withstanding earthquakes.

(Xiong et al., 2017) The bending stiffness of the node point is of great importance in the buckling behavior of single-layer space systems. The influence of nodes made of aluminum alloy on the structural behavior was investigated. It was noted that aluminum alloy nodes have lower stiffness, making them more susceptible to buckling than steel nodes.

(Mittendorf & Dodson, 2015) Structural nodes play a crucial role in gridshell structures as they are essential for transferring loads. These nodes are pivotal in the design and construction of the structures, given their complex geometry, topology, and the significant forces they need to accommodate within a relatively small volume.

(Tonelli et al., 2016) Grid shell structures, lattice structures, are extensively employed in civil infrastructure, such as expansive commercial buildings and stadiums. However, in the design and fabrication of gridshell structures, the structural connections, commonly called to as nodes, have been identified as a bottleneck or a challenging aspect of the process.

(Saraç, 2005) designed the optimum design of single-layer free-from domes under snow and wind loads. It has been demonstrated that the geometry must be divided into triangles to avoid stability problems if rigid connections are not used, and asymmetric loads must be included in the loadings.

(Hwang et al., 2009) The effect of hole characteristics in bolted connections on stability in grid-type structures has been investigated by modeling the connections using the finite element method.

(Dragone, 1979), Wind loads affecting the domes and their distributions have been studied, and it has been revealed that a pressure force is generated on the dome on the side where the wind comes from, and a suction force is generated on the dome on the side where the wind goes.

(Williams, 2000) The first examples of free-form surfaces date back to the 1920s when thin concrete shells started to be used as roof structures. Generating free-form surface structures with adequate structural strength, stability, and elegance of form was a challenge since limited tools and knowledge existed then. Since then, numerous methods of form generation have been developed. The most frequently used ones are geometry-based methods, physical models, and digital methods.

2.1 Purpose of the Thesis

This thesis examines the preferred Single-Layer Free-Form systems from architectural and engineering perspectives. One of Europe's most giant courtyard covering projects, the Queen Elızabeth II, Great Court British Museum, was selected and modeled as a Single-Layer Free-Form System. The numerical values of the dead loads, snow, earthquake, and wind loads affecting the model were calculated, and they were analyzed in accordance with the TSC 2018, TSSC 2016, TS EN 1991-1- 3:2009, TS EN 1991-1-4:2005 codes. The analyses determined internal forces and displacements, and the results were evaluated.

3. MATERIALS AND METHODS

3.1 General Information and Classification of Free-form Systems

Grid structures have played a key role in construction for many years, offering an efficient and flexible approach to spatial design. Recently, this concept has evolved into Single Layer Free-Form Structures, a significant architectural advancement gaining popularity due to their unique form and increased functionality. These structures, made of an interconnected network of linear elements, challenge conventional architectural boundaries and have revolutionized architectural designs and structural engineering.

Free-form structures, resulting from persistent innovation and advancements in construction technologies, are now a popular solution for architects and engineers. Their benefits include lightweight construction, cost-effectiveness, and speed in construction. Implementation involves using materials like steel, wood, or aluminum and creating an inherent structural rigidity that supports heavy and asymmetrical loads. They are suitable for various structures, from exhibition halls and sports complexes to major transportation infrastructures.

Free-form systems facilitate the creation of planar and curved surfaces through single and double-layer systems. Their benefits extend to environmental sustainability, making them an architectural innovation with societal and environmental benefits. With further advancements in technology and material sciences, these structures have a promising future and potential for further evolution.

These structures are assembled from beam-like elements in a grid pattern to create a shell-like surface. The interconnected components distribute loads and resist deformation, resulting in an efficient system. Single-layer free-form systems are flexible, adaptable, and suitable for various applications. Despite the technological complexity involved in their design and fabrication, these structures offer significant environmental benefits, including reduced material use and the potential for minimizing waste.

Table 3.1 Geometry-based Classification of Free-Form Systems (Kara, 2019)

Plane Surface Free-form Systems	Single Layer			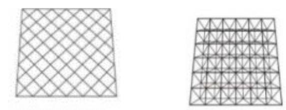
	Double Layer			
Free-form Systems	Single-curved.	Tower/Pyramid (Cylinder/Cone)	Single Layer	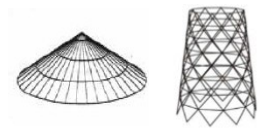
			Double Layer	
		Vault (Cylindrical shell)	Single Layer	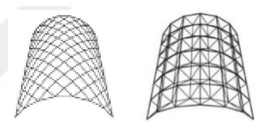
			Double Layer	
	Double-curved	Dome (Spherical, Ellipsoid, Paraboloid)	Single Layer	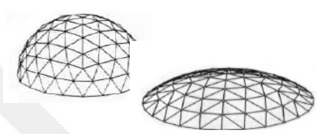
			Double Layer	
		Free-Form	Single Layer	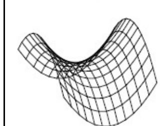

Single-layer free-form and double-layer spatial grid systems differ significantly regarding the section effects in their forms and structural elements. Single-layer systems allow for a wide range of unique and transitional forms, making them well-suited for original designs. On the other hand, double-layer systems are relatively limited in this aspect. Single-layer systems benefit from their ability to accommodate free-form shapes and advancements in material, software, and hardware technologies, enabling them to span much larger openings easily.

3.1.1 Historical development of dree-form structures

Throughout history, structural design has heavily relied on straight lines, orthogonal connections, and repeated elements, primarily due to limitations in technology, knowledge, resources, and production capabilities. This conventional approach contrasts the complexity found in nature, which seldom exhibits straight lines or right angles.

However, rapid advancements in technology and material science have initiated a new era of architectural design, moving away from rectilinear designs towards more intricate and complex structural systems. This transformation underscores the ever-evolving technological landscape, redefining the boundaries of architectural and structural engineering.

At the vanguard of this evolution are single-layer free-form systems, also known as grid shells. Characterized by a network of interconnected linear elements, these structures provide a lightweight, flexible, and cost-effective solution for spatial design. These elements, typically rods or beams, form a continuous shell-like structure, merging function with aesthetics.

Grid shells represent a notable shift from traditional architectural forms, allowing architects and engineers to explore unconventional designs. They also illustrate the transition of grid structures from basic frameworks to intricate, visually pleasing structures.

Given their versatility and ease of construction, grid shells appeal to for various applications, demonstrating their potential and transformative role in the architectural landscape. The ongoing development of these structures embodies the progression of technology and material science, hinting at the limitless possibilities for the future of architecture and structural engineering.

The advent of shell-type structures can be traced back to beehive tombs utilized for interment practices in Spain and Portugal as early as 3000 BC, as depicted in Figure 3.1. This architectural style was subsequently replicated in the beehive houses found in Ireland and Scotland around 2000 BC, demonstrated in Figure 3.2. Both these structural categories were established through the meticulous stacking of stone blocks.

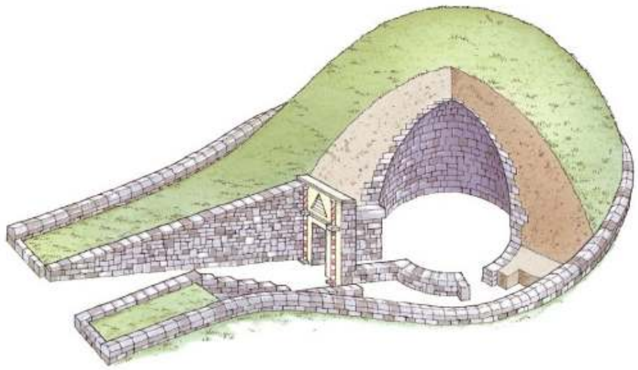

Figure 3.1 Beehive tombs, 3000 BC (Melissa, 2009)

Figure 3.2 Beehive houses in Ireland, 2000 BC (Huth, 2006)

The Persian edifice, Taq-i Kisra, erected in 540 BC as depicted in Figure 3.3, exemplifies an arch structure uniquely constructed using bricks, without including a centering mechanism, a commonly utilized supportive structure. This architectural marvel features a central arch-dome reaching an impressive height of 37 meters and a span measuring 26 meters.

Figure 3.3 Taq-iKisra, Persian monument, 540 BC (Janberg, 2007)

During the Roman era, the construction of arches for utilitarian structures such as aqueducts and amphitheaters gave the Romans the understanding of transmuting out-of-plane forces into orthogonal forces, which were then transferred to foundational elements. This conceptual understanding underpinned the creation of the oldest known concrete shell structure - the Roman Pantheon (Figure 3.4-3.5), constructed in 125 BC. With its impressive 43-meter span, the Pantheon epitomized an extraordinary feat of engineering in its historical context.

Figure 3.4 The Pantheon, Rome/Italy (Wade Fund, 1974)

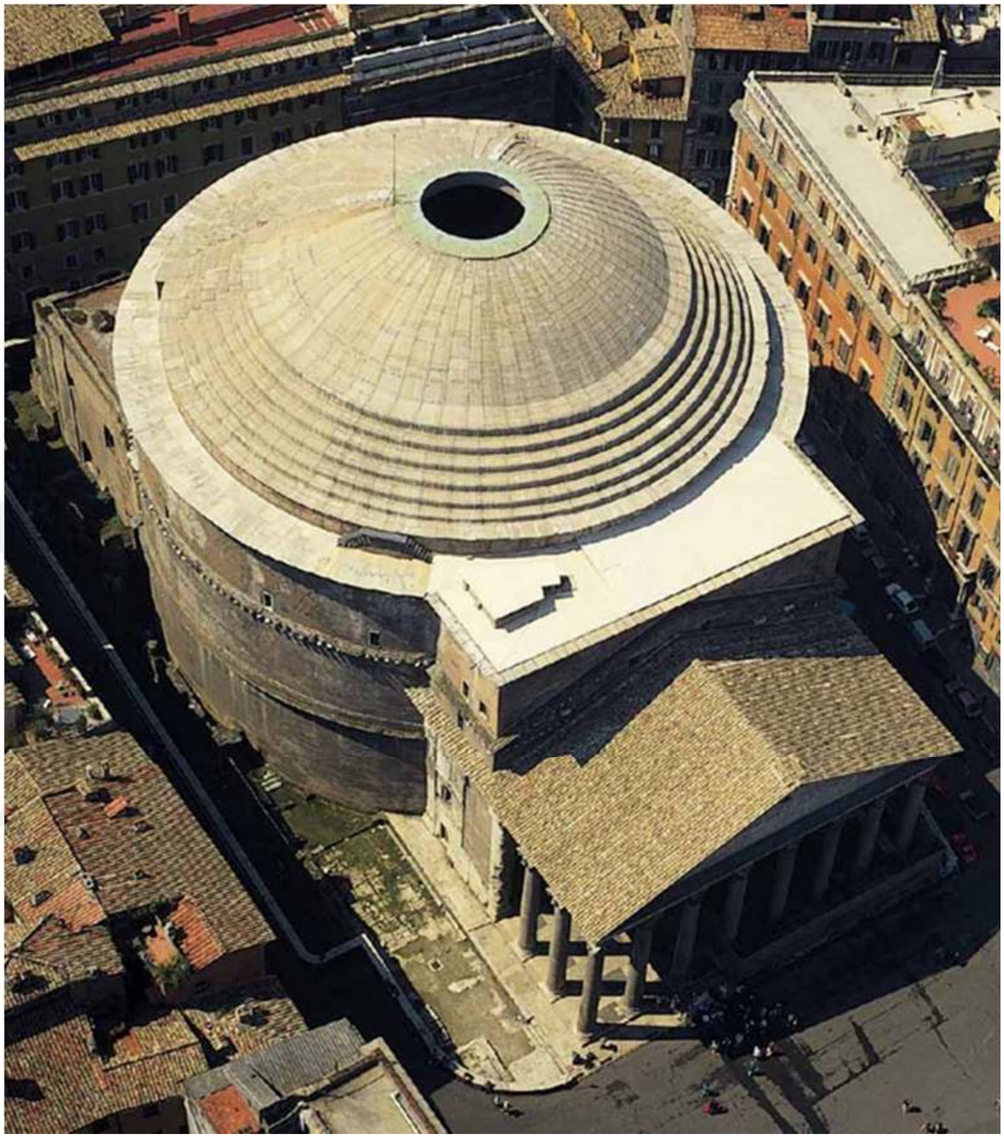

Figure 3.5 The Roman Pantheon, Rome/Italy (Crystal, 2009)

A further example is the dome of Hagia Sophia in Istanbul (Figure 3.6). Despite its construction many centuries ago, with a 32-meter span, the dome of Hagia Sophia maintains its prominence in contemporary architectural appreciation. Divergent from the solid base of the Roman Pantheon, the Hagia Sophia dome is borne by four monumental columns.

Structural features such as hemi domes, abutments, and pendentives were frequently utilized as supporting elements, marking a departure from the architectural methodologies employed in the construction of the Roman Pantheon beginning in the 6th century.

Figure 3.6 Interior of the Hagia Sophia, 6th century (Strelau, 2011)

Incorporating reinforcements, such as steel reinforcing bars, into concrete during the 19th century considerably advanced the capabilities of concrete structures. This innovation allowed these structures to bear special compressive forces and withstand high tensile forces. This enhanced material property facilitated the evolution and proliferation of curved structural forms, specifically shell structures.

The casting method in construction has been instrumental in transforming planar slabs into shell structures characterized by equitable force distribution. However, the cost of formwork and scaffolding continues to present a significant financial burden in constructing these structures, accounting for approximately 50% of the total expenditure, even with the multiple reuses of shuttering.

A noteworthy replication of a natural structure has been accomplished through the innovative combination of grid systems and double-curved shells, resulting in a unique structural system termed a 'grid shell' structure. Deploying a grid system permits dividing the entire structure into simpler elements, circumventing construction challenges associated with erecting comprehensive arch structures. Furthermore, a grid shell structure can effectively harness natural daylight, unlike a fully enclosed concrete shell. The grid shell structure's inception can be attributed to Schwedler, who constructed a steel cupola, depicted in Figure 3.7 as a rooftop for a gas holder from the Imperial Continental Gas Association in Berlin in 1863. This pioneering structural system could span distances between 25 and 40 meters. In 1897, Shukhov, a Russian engineer, erected a steel mill located 150 kilometers southwest of Nizhny Novgorod. This structure encompassed five doubly curved grid shells, spanning 70 meters by 24 meters, as illustrated in Figure 3.8.

While Shukhov introduced the concept of the doubly curved grid shell, he did not fully leverage the structural benefits conferred by the double curvature. It was due to an oversight of the positive influence exerted by the curvature in the cross-direction.

Figure 3.7 Schwedler cupola, J. W. Schwedler, Germany/Berlin (lunamtra, 2008)

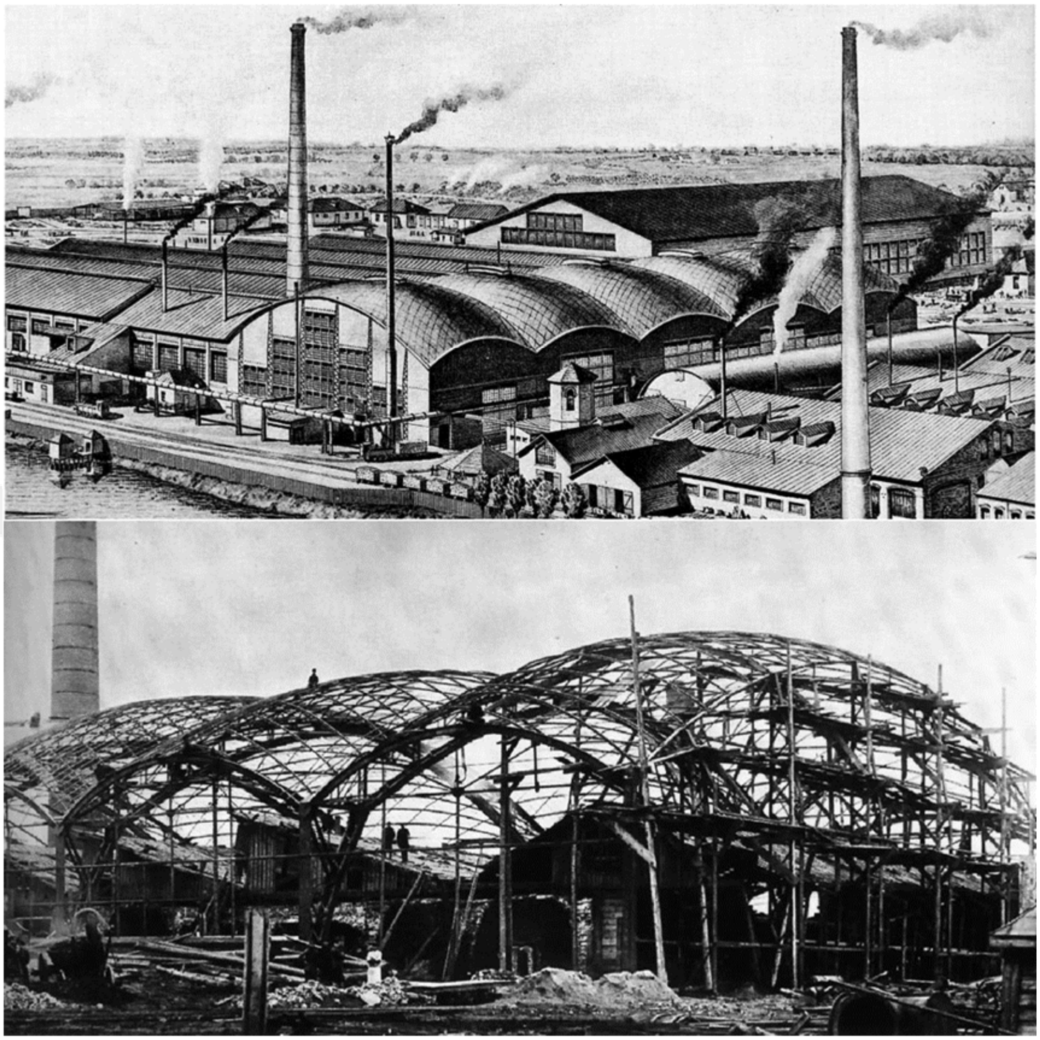

Figure 3.8 Production hall in Vyksa, around 1900 (Janberg, 1897)

A prominent illustration of the synergy between a grid structure and a continuum shell is embodied in Torroja's Fronton Recoletos, constructed in Madrid in 1935, as depicted in Figure 3.9. This architectural masterpiece features a roof composed of a composite of a concrete shell and a triangular grid shell, highlighting the successful marriage of these structural elements.

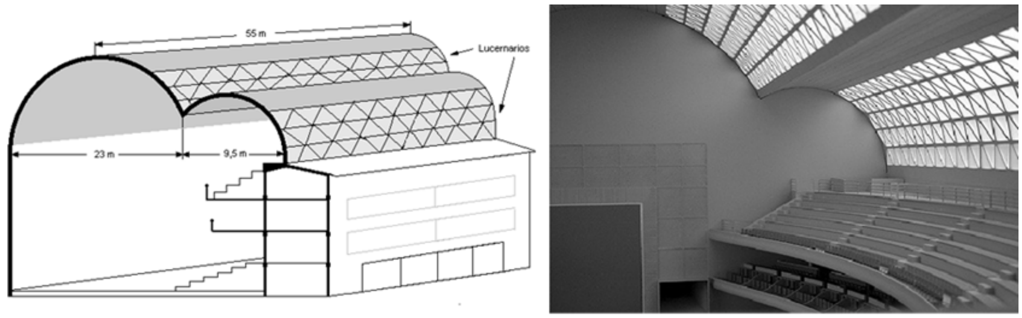

Figure 3.9 Recoletos, Eduardo Torroja, Madrid, Spain,1935. (Paco, 2007)

A prime instance of the integration of grid shell design within reinforced concrete structures is exemplified by the Palazzetto dello Sport. This indoor arena, designed by Pier Luigi Nervi and situated in Piazza Apollodoro in Rome (as represented in Figure 3.10), showcases the adept application of grid shell design principles in reinforced concrete architectural creations.

Figure 3.10 Palazzetto dello Sport, Rome, Italy (DiStefano, 2017)

The advancement of reinforced concrete design principles facilitated the realization of reinforced concrete dome designs in the mid-20th century (Figures 3.11-3.12). Among the pioneers of such design, P.L. Nervi stands out as one of these domes' most proficient and successful architects.

Figure 3.11 Palazetto Dello Sport, Rome/ Italy (Janberg, 2003)

Figure 3.12 Shine Dome, Australia (Wheelahan, 2020)

Given the inherent design and construction complexities associated with reinforced concrete shells, they were largely superseded by discrete steel and timber systems during the 19th and 20th centuries. This transition was precipitated by significant advancements in dome systems composed of bar elements in the early 19th century, leading to the advent of ribbed and transparent wide-span dome systems utilizing cast iron and wrought iron.

An example of such a system is the Bourse de Commerce dome structure, initially designed by F.J. Belanger and F. Brunet in 1813 (Figures 3.14-3.14). This architectural feature is widely acknowledged as marking the inception of single-layer systems in structural design.

Figure 3.13 Bourse de Commerce, Paris / France (Janberg, 2009)

Figure 3.14 Bourse de Commerce Paris / France (Rotunda)

Following the incorporation of steel into these structural systems after using cast iron, novel exemplars surfaced where wide spans were encapsulated by dome structures crafted from steel elements. In the latter half of the 19th century, German engineer Johann Wilhelm Schwedler introduced dome forms that have since borne his name. These dome designs were initially conceived for use in gas storage facilities.

A significant, enduring example from this era is the Fichtebunker, a former gas storage facility in Berlin, which now functions as a luxury accommodation venue (as depicted in Figures 3.15-3.16).

Figure 3.15 Fichtebunker, Berlin / Germany (Schlegelmilch, 2009)

Figure 3.16 Fichtebunker, Berlin / Germany (Schlegelmilch, 2009)

A paramount example of modern lamella domes is the Astrodome (Figure 3.17), conceptualized by architects H. Lloyd and W.B. Morgan in collaboration with the Morris Architects firm and unveiled in 1965. The dome of this architectural marvel, extending 220 meters, is built upon a robust steel framework.

Figure 3.17 Houston Astrodome, Teksas/USA (Chow, 2021).

In 1975, a double-curved wooden shell structure, the Multihalle, was erected in Mannheim, as depicted in Figure 3.18. Unlike Shukhov's grid shell in Vyksa, the Multihalle utilized its inherent double curvature effectively. As outlined in the reference, Otto's application of scale models during the form-finding process realized this feat.

Otto contrived models of varying forms and shapes to investigate the behavior of the grid within a structure, applying minor loads to emulate the structure's weight (Figure 3.19). Unlike their steel counterparts, wooden grid shells can initially be assembled into a planar structure on the ground, attaining their three-dimensional forms by adjusting the boundaries to align precisely with the support locations, as specified in the reference. This type of grid shell is classified as an active bending grid shell. The grid shell explored in this study constitutes a single-layer lattice frame wherein the members are initially fashioned to conform to the final form of the structure, thereby eliminating the presence of active bending moments within the members.

Figure 3.18 Multihalle, Mannheim, Germany, (Bobbarton, 2012)

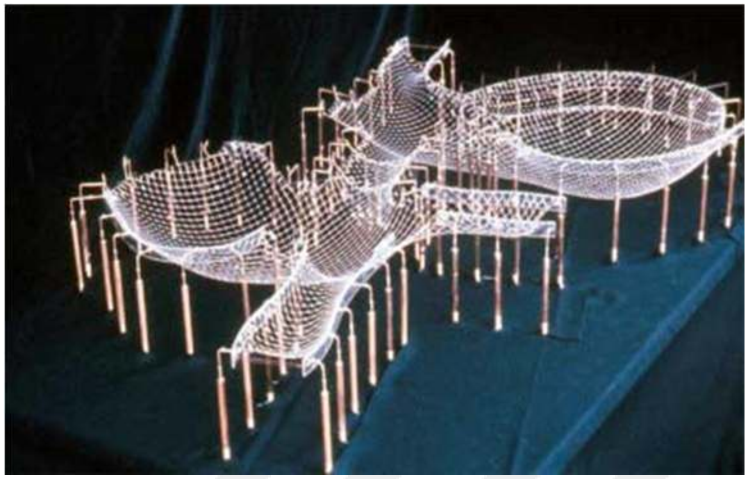

Figure 3.19 Hanging scale model of the Mannheim Multihalle (Liddell, 2015).

The Zeiss Planetarium, conceptualized by the German engineer W. Bauersfeld in the 20th century, has the dual distinction of being both the world's inaugural lightweight thin-shell reinforced concrete dome and the earliest instance of modern geodesic domes, as showcased in Figure 3.20. This dome, featuring a span of 40 meters, was erected in Berlin in 1924, employing approximately 8,000 iron rod elements. Three decades after Bauersfeld's innovation, Buckminster Fuller further advanced these dome structures and introduced the term "geodesic dome" in 1954.

Figure 3.20 Zeiss Planetarium Jena, Berlin / Germany (Janberg, 2020)

As the 20th century neared its conclusion, the quest for lighter yet enduring materials gained prominence. Simultaneously, incorporating cables to bestow rigidity in the design of transparent lamella-style domes with square or rectangular openings emerged as an innovative application. The Osaka Maritime Museum, constructed in 2001, exemplifies this concept, as depicted in Figure 3.21.

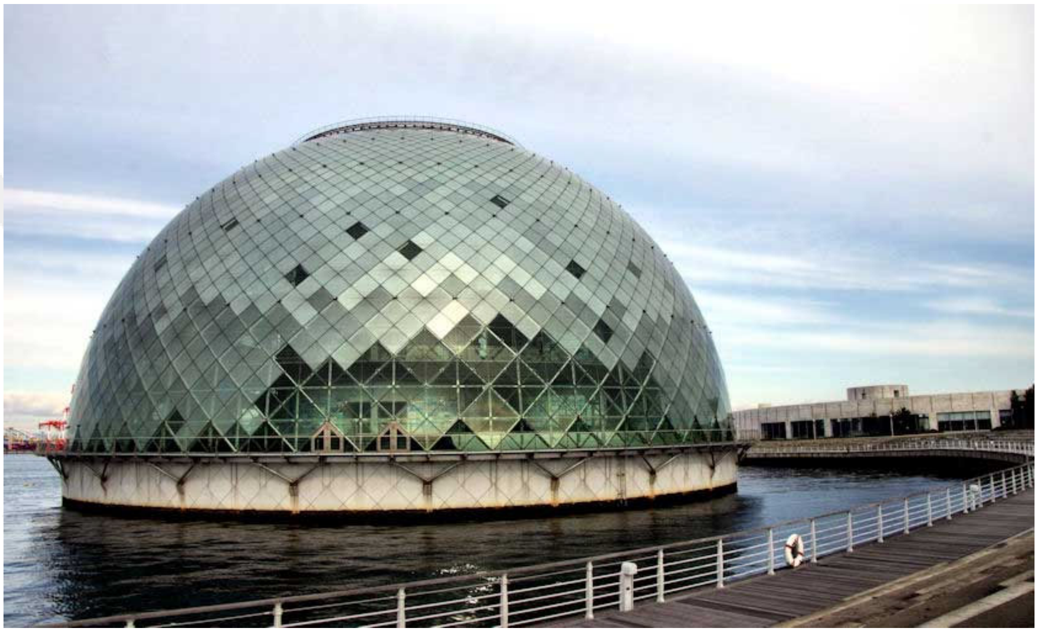

Figure 3.21 Osaka Maritime Museum, Japon (Andreu, 2013)

Another notable progression was the inception of aluminum dome systems. The South Pole Dome, engineered in 1975 utilizing aluminum material, is an exemplar of a single-layer geodesic dome, as shown in Figure 3.22-23.
Presently, domes can be fabricated using three primary types of materials: elements of glass and stainless steel, wood, or aluminum.

Figure 3.22 South Pole Dome interior view, Antarctica (Andrieu, 2000)

Figure 3.23 South Pole Dome exterior view, Antarctica (Cowing, 2013)

The evolution of parametric modeling algorithms, such as Grasshopper, and advancements in flexible, patented joints are capable of moment transfer have facilitated the design of amorphous structures.

One such prominent instance is the Spruce Goose Hangar Dome, erected in 1982, boasting a height of 40 meters and a diameter of 126 meters, predominantly composed of aluminum (see Figure 3.24). While it was initially purposed as an aircraft hangar, it has now become one of the iconic structures of Long Beach, sharing this distinction with the historical ship Queen Mary, moored nearby.

Figure 3.24 Spruce Goose Dome Los Angeles / United States (Murphy, 2008

The world's largest geodesic dome is housed in Japan's Fukuoka Yahuoku Stadium, constructed in 1993, and features a dome diameter of 216 meters in the configuration of a spherical cap (Figure 3.25). This impressive structure serves as a premier example of the massive scales that free-form architecture can reach. Its expansive dome not only provides comprehensive shelter against the elements but also contributes to the distinctive aesthetics of the stadium.

Figure 3.25 Fukuoka Yahuoku , Japan (Sta, 2015)

Another contemporary example is the Desert Dome (2002), acknowledged as the world's largest enclosed desert habitat, cloaking the desert under a glass-clad dome and standing as a symbolic representation of the city of Omaha (Figure 3.26). The structure comprises a geodesic steel dome perched on a reinforced concrete base, with thick acrylic triangular panels employed for the enclosure.

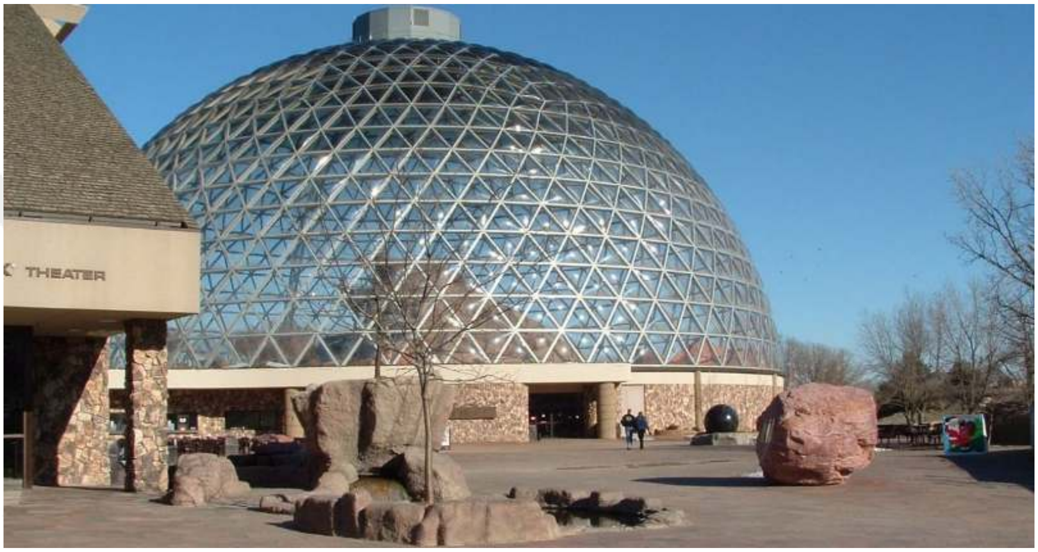

Figure 3.26 Desert Dome, United States (GDR, 2023

The development of single-layer free-form systems was somewhat stalled in the middle of the 20th century, primarily due to fabrication and construction technology limitations. At that time, the design of these structures often involved manual labor and skilled craftsmanship, which made them expensive and time-consuming to build. However, in the late 20th century, digital design tools and new fabrication technologies, such as Computer Numeric Control (CNC) machinery, revived interest in single-layer free-form systems. These advancements allowed designers to generate and analyze complex forms more efficiently and to produce the unique components necessary for their construction. As a result, single-layer free-form systems began to be used more frequently in a range of architectural applications.

Over time, new structural forms of single-layer free-form systems have emerged, including bending-active and tensegrity structures. These innovative structures exploit the inherent flexibility of the individual components to create complex, curved geometries. By embracing the dynamic behavior of the materials, designers created lightweight, efficient, and aesthetically striking structures.

The 20th-century architectural, artistic, and engineering progression is significantly marked by the advent of 'free-form' structures, referring to a departure from conventional geometrical constraints, leading to an exploration of fluid and organic aesthetics. Free-form structures deviated from the then increasingly adopted regular geometrical shapes, evident in architectural marvels like the Greek Parthenon and Egyptian Pyramids rooted in prehistoric design tendencies to mirror irregular natural forms.

The evolution of free-form systems traces back through various architectural and engineering eras, each contributing unique influences. Free-form structures are generally categorized into surface- and network-based systems, defined by their design and construction principles.

Inspired by natural forms, surface-based systems design around a continuous surface and find applications in modern buildings and bridges. They can be further categorized into rigid systems, maintaining their shape under load, and flexible systems, capable of deformation under load and returning to their original shape after load removal.

Network-based systems, characterized by intricate geometry, are dictated by the spatial arrangement and interconnection of individual linear components rather than a continuous surface. They include tensegrity structures, space frames, and lattice structures.

The decision between surface-based and network-based systems is usually project-specific, considering functional needs, aesthetic objectives, site conditions, and construction constraints. As free-form systems evolve, many blur the boundaries between these categories, presenting a hybrid approach to design and construction.

Fast-forward to the mid-20th century, we see a resurgence of free-form structures in architecture, partly due to the development of new materials and technologies.

Material selection is a critical factor influencing the fabrication and installation of Single Layer Free-Form Structures. These structures require materials with strength, durability, and malleability to form complex and unique designs. This section critically analyses the materials commonly utilized in fabrication and how they impact the structure's performance and aesthetics.

In the 20th century, people witnessed a transformation in architectural design principles, driven by the introduction of reinforced concrete, steel, and glass. These materials catalyzed innovation, enabling architects and engineers to explore complex, irregular shapes, thus paving the way for free-form design. As the century drew to a close, the architectural community adopted computational design tools, propelling a digital revolution in the industry. It led to the conception and construction of complex geometries previously thought impossible, bringing free-form design to the forefront of contemporary architecture.

The digital revolution in the late 20th and early 21st centuries further propelled the evolution of free-form systems. The introduction of computational design tools and advanced fabrication technologies allowed designers to conceive, analyze, and construct increasingly complex free-form structures.

Upon determining the desired shape for the Multihalle, Otto utilized the finite element method (FEM) to study the gridshell's behavior. FEM facilitates the visualization of stresses and displacements within structures for an extensive array of static and dynamic analyses, thereby enabling the design and analysis of complex structures.

Structural members can be prefabricated using computer numerically controlled (CNC) machines to circumvent limitations in construction. Consequently, each member can be uniquely designed, culminating in a free-form grid shell structure.

In contemporary times, free-form grid shells have surged in popularity due to their capacity to create beautiful public spaces. Exemplary instances of grid shell structures include the Queen Elizabeth II Great Court (refer to Figure 3.27), which envelops the court of the British Museum in London, and the Kogod Courtyard (refer to Figure 3.28) located within the Smithsonian American Art Museum in Washington.

Figure 3.27 British Museum Great Court Roof, London / England (Diliff, 2013)

Figure 3.28 Smithsonian American Art Museum, Washington (Evanson, 2013)

Gridshell structures, or lattice or reticulated shells, have evolved significantly over a century in aspects such as construction material, grid pattern, structural analysis methods, form-finding methods, manufacturing techniques, and connection details. These lightweight spatial structures provide architects and structural engineers with unlimited design freedom, thanks to their organic shapes, column-free spaces, free-form surfaces, and maximized transparency.

However, the design and manufacturing of structural connections, or nodes, have historically posed significant challenges in grid shell construction, given their complex geometries and the three-dimensional loading conditions applied to these nodes. Nevertheless, recently designed nodes show promise, offering improved aesthetics, high stiffness, high precision, and requiring less labor.

Gridshell structures comprise a single-layer grid of beam members forming shell geometry. Since their structural behavior mimics that of shell structures, understanding shell structures can provide valuable insights into grid shells.

Various classification systems can be applied to structures based on specific criteria, such as shapes, functions, and materials. When approached geometrically, a shell structure's shape can be defined as a curved surface with a minimal thickness (dimension perpendicular to the surface) compared to its in-plane dimensions. Such a surface can be double curved, as in domes and cooling towers, or single curved, like a cylinder.

For their efficiency and unique aesthetics, single-layer free-form structures have become popular in public structures. However, engineering a discrete grid on a free-form surface that aligns with an architect's vision can be complex. These structures offer flexibility and variety in shape, making them highly suitable for meeting diverse architectural modeling needs.

Their emergence signifies a crucial development in creating complex shapes in Architecture, Engineering, and Construction (AEC). With their stunning visual effects and ability to span large, uninterrupted spaces, single-layer free-form structures have become increasingly popular in recent years. They have been used in diverse building types, such as exhibition pavilions, stadiums, assembly halls, and protective shelters. Compared to traditional analytic surface grid structures, single-layer free-form structures offer more flexibility and diversity in shape, better catering to architects' needs for diversified architectural modeling. An excellent example of the geometric term "torsion-free support structure" is the Yas Marina Hotel in Abu Dhabi (Figure 3.29), where smooth skin is divided into straight elements arranged in a specific manner, simplifying node manufacturing.

Figure 3.29 The Yas Marina Hotel in Abu Dhabi (Waagner-Biro Stahlbau)

Indeed, the design and construction of single-layer free-form structures can be intricate, requiring advanced digital tools and technologies. Here, parametric design plays a crucial role, facilitating the creation of intricate shapes and structures that can be swiftly modified or adjusted, thereby marrying aesthetic appeal with functional efficiency.

Digital fabrication, encompassing computer-controlled machines to manufacture complex building components and assemblies, allows for precise component fabrication, reducing errors and wastage. When combined with sustainable materials like bamboo, timber, and recycled materials, the environmental footprint of these structures is further reduced, contributing to their overall sustainability.

Furthermore, sustainable construction methodologies such as prefabrication and modular construction decrease construction waste and minimize resource use, making these structures more eco-friendly. Thus, despite the inherent complexities in their design and construction, the flexibility and diversity of single-layer free-form structures make them attractive for architects, especially considering their capability for architectural modeling diversification.

With the increased utilization of advanced digital tools, sustainable materials, and practices, single-layer free-form structures promise greater efficiency, sustainability, and visual appeal.

The advent of grid structures marks a significant advancement in the evolution of complex shapes in Architecture, Engineering, and Construction (AEC). Their flexibility and diversity perfectly align with architects' needs for diversified architectural modeling. Tools like parametric design and digital fabrication offer innovative solutions to the challenges of designing and constructing these structures.

To conclude, single-layer free-form structures have garnered significant popularity in public structures courtesy of their efficiency and unique aesthetics. Their flexibility and diversity, coupled with applying advanced digital tools and sustainable materials and practices, promise a future where these structures will become even more efficient, sustainable, and visually stunning.

3.1.2 Modern Free-Form Structures and Examples

Modern free-form structures utilize advancements in digital design tools, material science, and fabrication technologies to create previously unattainable designs, marking a new era in architecture and engineering where aesthetics and function uniquely blend. Several structures in the contemporary architectural landscape showcase the free-form systems' flexibility and innovative potential of single-layer free-form systems exemplify this versatility, characterized by their intricate geometries, lightweight features, and expansive span capabilities. These attributes underscore the potential of free-form design to reshape architectural norms and expectations.

Jewel Changi Airport is an exceptional architectural marvel utilizing a free-form system that exudes innovation and functionality (Figure 3.30-31). Located in Singapore, it is a multi-purpose complex featuring the world's tallest indoor waterfall, named the "Rain Vortex" surrounded by a terraced forest setting. The structure's free-form design allows for a naturally intuitive flow of space, enabling visitors to move smoothly through various sections such as retail, dining, hotel, and airport operations. Its glass and steel facade forms a geodesic dome-shaped grid shell that provides transparency, letting in ample daylight and allowing views of the central gardens and falls. The free-form system is especially significant in maintaining the organic, non-linear aesthetic of the waterfall and vegetation, ensuring structural integrity and efficiency. Jewel Changi Airport's design truly revolutionizes the concept of airport infrastructure, blending the realms of retail, leisure, and travel in a stunningly seamless manner.

Figure 3.30 Jewel Changi Airport, Singapore (Hurstley, 2019)

Figure 3.31 Jewel Changi Airport, Singapore (RSP, 2020)

The New Milan Trade Fair in Rho (Figure 3.32-33), Italy, is an iconic example of modern free-form architectural design. Envisioned by Massimiliano Fuksas, this sprawling trade fair complex is known for its remarkable wavy roof, 'The Canopy,' which spans over

1.5 km, binding together various pavilions beneath it. The free-form system allows this enormous undulating glass and steel structure to follow a sinuous, organic pathway, seemingly floating above the more rigid and conventional geometries of the exhibition halls below. This juxtaposition creates a dynamic interplay between the free-form and linear elements. The Canopy's transparency lets in ample daylight, enhancing the visitor experience while promoting energy efficiency. The New Milan Trade Fair exemplifies the adaptability of free-form architecture in creating aesthetically compelling, functional spaces that resonate with the contemporary ethos of design.

Figure 3.32 The New Milan Trade Fair, Italy (Prat, 2005)

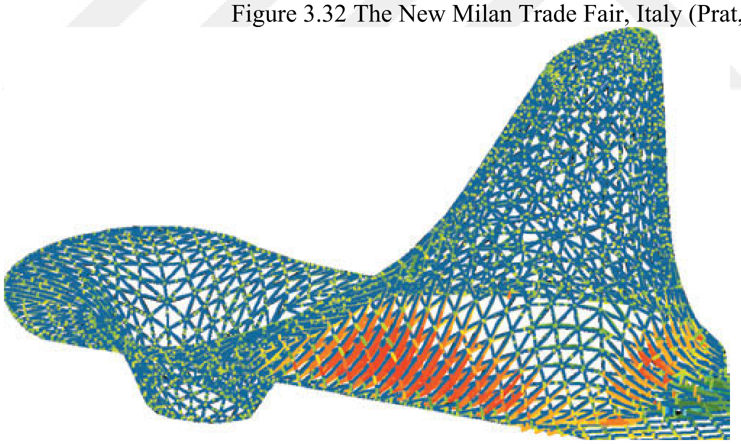

Figure 3.33 The New Milan Trade Fair, Italy (Schlaich, 2005)

Examples of single-layer freeform skylights with organic nodes can be found in some of the world's most iconic architectural structures, such as the cloud-like skylight of the Louvre Abu Dhabi (Figure 3.34-35) and the Glass Hall at the Leipzig Trade Fair. These structures employ unique, single-layer designs with organic nodes to create intricate and visually stunning features. They represent a fascinating and challenging architectural and structural design area, offering unique and visually stunning architectural features.

However, the fabrication and installation of the organic nodes, in particular, often require a high level of precision and expertise. Designers must ensure adequate load transfer and overall structural stability, which can be challenging given the complex geometry of these structures.

Figure 3.34 Abu Dhabi Louvre, UAE (Halbe, 2017)

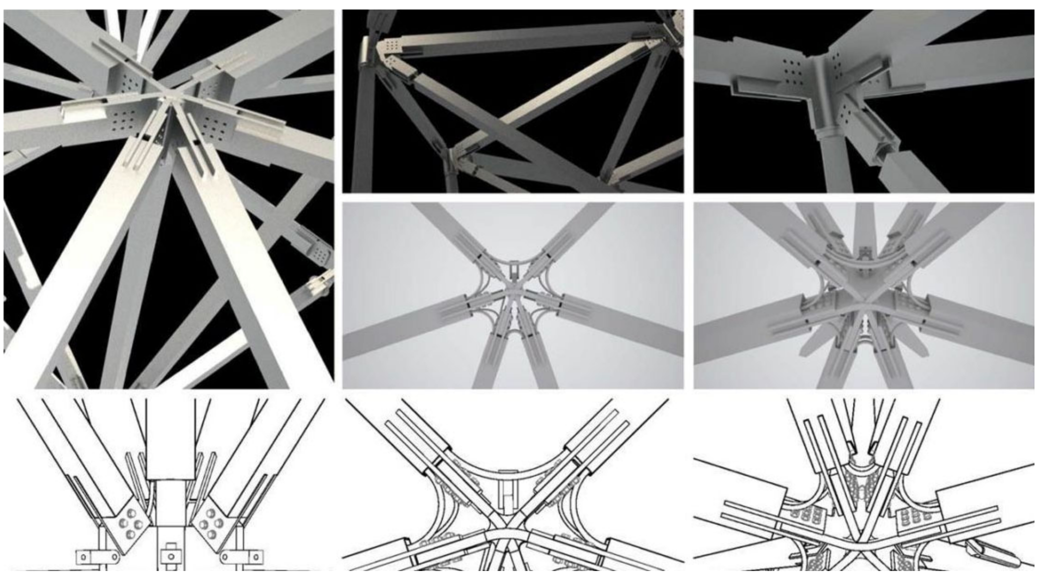

Figure 3.35 Abu Dhabi Louvre Museum, UAE (Joint Details) (Waagner Biro)

The National Aquatics Center, also known as the "Water Cube," in Beijing, China, is a unique free-form structure that has revolutionized the world of architecture (Figure 3.36-37). Designed for the 2008 Olympic Games, its design was inspired by the natural formation of soap bubbles, giving it a unique, organic aesthetic. Its free-form system facilitated the creation of a lightweight and efficient steel space frame that forms the structure's innovative, bubble-like exterior. Covered by Ethylene Tetrafluoroethylene (ETFE), a type of plastic, it boasts exceptional insulation properties and transmits more light than traditional glass, promoting energy efficiency. The Water Cube's free-form design also extends to its interior, housing a range of swimming and diving pools in an environment that evokes the underwater sensation. This iconic structure signifies the potential of free-form architecture to harmonize complex engineering with organic, visually-striking design elements.

Figure 3.36 National Aquatics Center, Beijing / China (Lam)

Figure 3.37 National Aquatics Center, Beijing / China (Interior View)(Arup)

One notable example of a single-layer free-form structure is the Multihalle in Mannheim, Germany. Designed by Frei Otto and Ove Arup, this large timber grid shell is often cited as a seminal example of a single-layer free-form design. Its organic, free-flowing form was achieved by carefully manipulating the timber laths into the desired shape, which involved physical and computational modeling.

Another example of a single-layer free-form structure is the British Museum's Great Court Roof in London (Figure 3.38). Designed by Foster + Partners and Buro Happold, this steel and glass structure is characterized by its complex, undulating geometry. The roof's design was achieved through advanced digital design tools, which allowed the team to optimize the structure's geometry for efficient load distribution and material use.

Figure 3.38 The British Museum in London (Waagner Biro)

A recent example of a single-layer free-form structure is the Centre Pompidou- Metz in France (Figure 3.39). Designed by Shigeru Ban and Jean de Gastines, the structure's roof is a timber grid shell that mimics the form of a Chinese hat. The structure is notable for its complex, curvilinear geometry and the innovative use of laminated timber.

Figure 3.39 Courtesy of Centre Pompidou Metz (Didier, 2010)

Another example is The Sage Gateshead (Figure 3.40), a musical education and performance center in the United Kingdom. The building's distinctive shell-like form was designed by Foster + Partners, and its smooth, curvilinear surface contrasts sharply with the orthogonal forms typically associated with modern architecture. The unique shape of the building was derived through an extensive design and analysis process, including acoustic simulations, to ensure optimal sound performance within the structure.

Figure 3.40 Sage Gateshead, Saint Mary's Square, Gateshead, UK (NGI, 2022)

The Harbin Opera House in Harbin (Figure 3.41), China, designed by MAD Architects, is another excellent example of free-form architecture. The building's design mirrors the undulating landscape of the surrounding area with a smooth, flowing, organic, and dramatic design. The complex was designed using advanced 3D modeling and analysis software, enabling the architects to conceive and realize the ambitious design.

Figure 3.41 The Harbin Opera House in Northeast China's Harbin. (VCG, 2018)

3.1.3 Fabrication and Installation of Single Layer Free-Form Structures

Fabrication and installation are crucial in creating Single Layer Free- Form Structures. Characterized by their complex and irregular geometries, these structures present distinct challenges, necessitating advanced fabrication and installation techniques. This section details these processes, examining traditional methods, technological advancements, and the associated benefits and challenges.

Single Layer Free-Form Structures, also known as single-layer reticulated structures, have become an architectural solution due to their aesthetic appeal, structural efficiency, and adaptability to irregular building shapes. The emergence of such structures has instigated a reassessment of standard fabrication and installation processes in the construction industry. Their unique geometry and inherent structural complexity necessitate using innovative and advanced techniques during construction. The fabrication of single-layer free-form structures traditionally involves intricate processes due to the non-standard nature of their components (Figure 3.42). Conventional fabrication techniques such as welding, bending, and cutting are often employed. However, the complexity of these structures can render these methods time-consuming and costly. Furthermore, the unique geometry of each component in a free-form grid structure often demands a high level of customization, amplifying the complexity of the fabrication process.

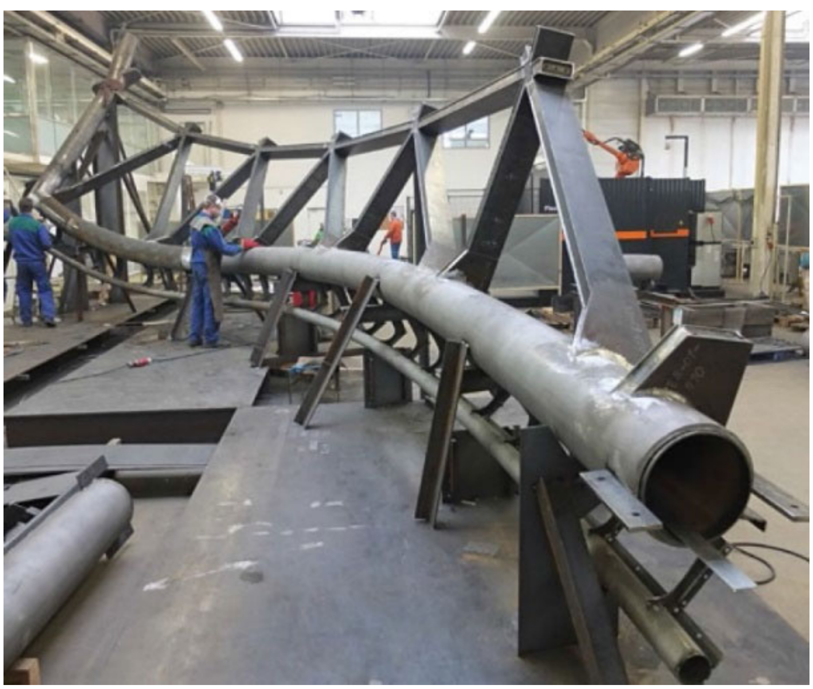

Figure 3.42 Fabrication of edge beam (Seele Pilsen)

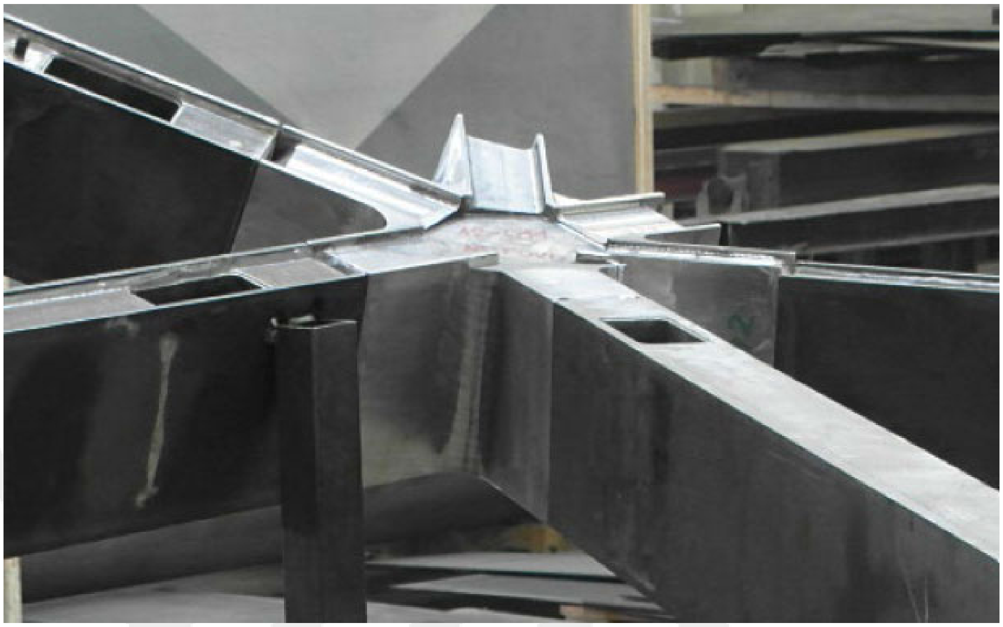

Figure 3.43 Finished node with bolted grid members (Seele Pilsen)

Single-layer free-form structures represent architectural forms characterized by non-uniform, non-regular, and non-linear geometric configurations. These forms are typically generated through algorithms and digital modeling tools, allowing for the creation of complex and unique designs. These distinct designs, in turn, necessitate a shift from conventional fabrication and installation techniques.

3.1.3.1. Preparation: Design and Modelling

Before any fabrication can begin, the free-form grid structure must first be accurately modeled. This process often involves a combination of advanced design software and numerical analysis methods, such as the finite element method. The outcome of this process is a detailed 3D model that precisely defines each component of the grid structure and its relationship to the overall form.

3.1.3.2. Fabrication of Single Layer Free-Form Structures

Fabrication constitutes a critical phase in the realization of Single Layer Free-Form Structures. This stage requires significant precision and coordination to ensure faithful execution of the architectural design. The process commences with digital modeling to delineate the complex geometry of the structure, which is then segmented into manageable parts to facilitate production and assembly.

Figure 3.44 CNC-milled solid grid node (Metal Yapı, 2014)

The fabrication process typically leverages advanced manufacturing techniques such as computer numerical control (CNC) machining (Figure 3.44), 3D printing, and laser cutting. The selection of these processes is contingent on several factors, including the material composition of the structure, design complexity, project budget, and time constraints.

Fabrication techniques for single layer free-form structures have evolved significantly in recent years, spurred by technological advancements and the industry's increasing demand for precision and efficiency. Cutting-edge manufacturing techniques such as 3D printing, CNC machining, and robotic assembly are now increasingly employed in fabricating the individual components of Single Layer Free-Form Structures.

3.1.3.3. Prefabrication

The complexity of single layer free-form structures often necessitates a shift from traditional onsite construction methods to prefabrication. Prefabrication involves manufacturing the components of the structure in a controlled factory environment before transporting them to the construction site for assembly. This approach has several advantages, including increased quality control, reduced in construction waste, and the ability to working independently of adverse weather conditions.

3.1.3.4. Installation

Installing single-layer free-form structures is a critical and intricate process with numerous challenges due to the design's complexity. This stage often calls for advanced construction techniques and equipment, demanding high precision to ensure

the structure aligns accurately with the intended design. The unconventional geometry and complex connections inherent in these structures challenge this process.
The installation process for single-layer free-form structures is intricate, demanding meticulous planning, accurate execution, and extensive coordination among various project stakeholders. This process typically commences with assembling fabricated components on-site, which is then followed by the erection of the structure using cranes or other similar lifting equipment (Figure 3.45).

Figure 3.45 Erection of the canopy on site (Seele-Austria)

Given the complex geometry of Single Layer Free-Form Structures, adopting a systematic installation strategy is crucial to ensure proper alignment and connection of components. This strategy involves using advanced surveying equipment and digital tools to monitor the installation's accuracy closely.

3.1.3.5. Quality Control and Inspections

Quality control and inspections are crucial in the fabrication and installation processes of Single Layer Free-Form Structures. Given the high precision required, regular inspections and rigorous quality control protocols are typically enforced throughout the project to ensure the structure conforms to the design specifications. It may involve using advanced inspection techniques and technologies to ensure accuracy.

The fabrication and installation of single-layer free-form structures are intricate yet compelling processes that amalgamate architectural design, structural engineering, and construction technology. Despite the hurdles posed by their complex geometry, utilizing advanced digital tools and pioneering manufacturing techniques has facilitated the realization of these distinctive structures with exceptional precision and efficiency.

The fabrication and installation of single-layer free-form structures involve a complex fusion of sophisticated design techniques, innovative manufacturing methods, and rigorous planning and coordination. As architectural designs continue to stretch the boundaries of complexity and novelty, it is incumbent upon the construction industry to persistently innovate and adapt in order to actualize these visionary designs successfully.

3.2 Single-Layer Free-form Systems and Analysis Principles

3.2.1 Structural analysis in free-form structures

The architecture and construction industries have seen a significant shift in the last few decades, characterized by embracing free-form structures. This shift from conventional geometric designs to non-repetitive and unconventional forms has opened up new possibilities in architectural aesthetics. However, it has also presented new structural analysis and feasibility checks challenges. A comprehensive investigation into the principles and methods of structural analysis is performed for free-form structures. It is an exploration of the intersection between creative architectural design and the principles of structural engineering.

Numerical analysis of free-form structures is integral to their stability, safety, and performance. The irregular geometries of these structures necessitate advanced analytical techniques to predict their behavior under varying load conditions. Numerical analysis helps decipher these challenges utilizing computational models and simulations.

The application of numerical analysis aids in evaluating the structure's stability, dynamic response, and load-bearing capacity. Simulations provide a precise understanding of structural behavior, enabling the identification of potential design issues. The numerical analysis considers various factors like the materials' properties, structural geometry, loading, and boundary conditions.

Structural analysis techniques fall into two categories: approximate and numerical methods. The former, including hand calculations and simplified models, are utilized in the preliminary design phase. These provide a swift understanding of structural behavior.

Structural analysis is imperative due to their unconventional geometries in the context of free-form structures. The unique and complex designs of free-form structures demand comprehensive analytical approaches.

Structural analysis forms the backbone of any engineering design process. It involves evaluating a structure's ability to withstand various loads without experiencing failure or excessive deformation. This process often involves determining the distribution of internal forces, moments, and reactions for traditional structures. However, due to their complex geometries, irregular forms, and sometimes unusual material usage, free-form structures demand a more nuanced structural analysis approach.

The critical challenge in the structural analysis of free-form structures is their geometric complexity and non-linear behavior. The unconventional design often features curvature, asymmetry, and irregularly shaped members, which make it difficult to use standard analytical methods. This complexity requires a more sophisticated approach, often involving computational analysis and numerical techniques such as the finite element method (FEM).

Non-Linear Analysis

Due to the potential for large deformations and material non-linearities under loads, free-form structures often require a non-linear analysis. Unlike linear analyses, which assume small deformations and a linear stress-strain relationship, non-linear analyses account for large deformations and more accurately reflect the behavior of materials under high-stress conditions. Non-linear analysis can provide a more realistic prediction of a free-form structure's behavior under various load conditions, thereby helping to ensure the structure's safety and reliability.

Boundary Conditions

Boundary conditions significantly influence the structural analysis of free-form structures, defining how structures interact with their surroundings and directing load distribution. Their careful identification and precision are essential for predicting a structure's behavior and ensuring stability. The irregular shapes of free-form structures add to the complexity of defining their boundary conditions.

These conditions include how the structure is supported, such as through fixed, hinge, roller, elastic, or foundation supports, each with its own characteristics and potential for movement. They also define how external forces, including gravity, wind, seismic activity, or the structure's weight, are applied to the structure, affecting its behavior. Incorrect definitions of boundary conditions can lead to many errors, potentially resulting in unsafe designs. Hence, engineers must accurately identify these conditions, relying on a comprehensive understanding of the structure and its environment. Computer-aided engineering (CAE) tools can assist in defining and applying boundary conditions systematically, allowing for visual representation and aiding in identifying and resolving potential issues.

In summary, correctly identifying boundary conditions is vital in the structural analysis of free-form structures, especially with the ongoing advancements in free-form architecture. Therefore, careful understanding and attention to boundary conditions remain critical.

Finite element method (FEM), computational tools and software

The finite element method (FEM) is a powerful tool for analyzing complex structures. It involves discretizing the structure into smaller, manageable parts called 'elements, interconnected at 'nodes.' Each of these elements is analyzed independently under the influence of external loads, and the overall structural response is then assembled from these individual analyses. FEM is especially valuable in the case of free-form structures, as it accommodates complex geometries and various degrees of freedom.

Computational tools and software, particularly those employing the Finite Element Method (FEM) or similar numerical methods, are integral to analyzing free-form structures. By discretizing the structure into smaller elements, these tools enable engineers to tackle the complex geometries of free-form structures systematically and efficiently.

Computer-Aided Design (CAD) and Computer-Aided Engineering (CAE) software are instrumental in this process. These tools allow for precise geometric modeling and facilitate robust structural analysis under various loading and boundary conditions. They accommodate both linear and non-linear analyses, making them versatile tools for tackling the diverse challenges of free-form structures (Figure 3.46).

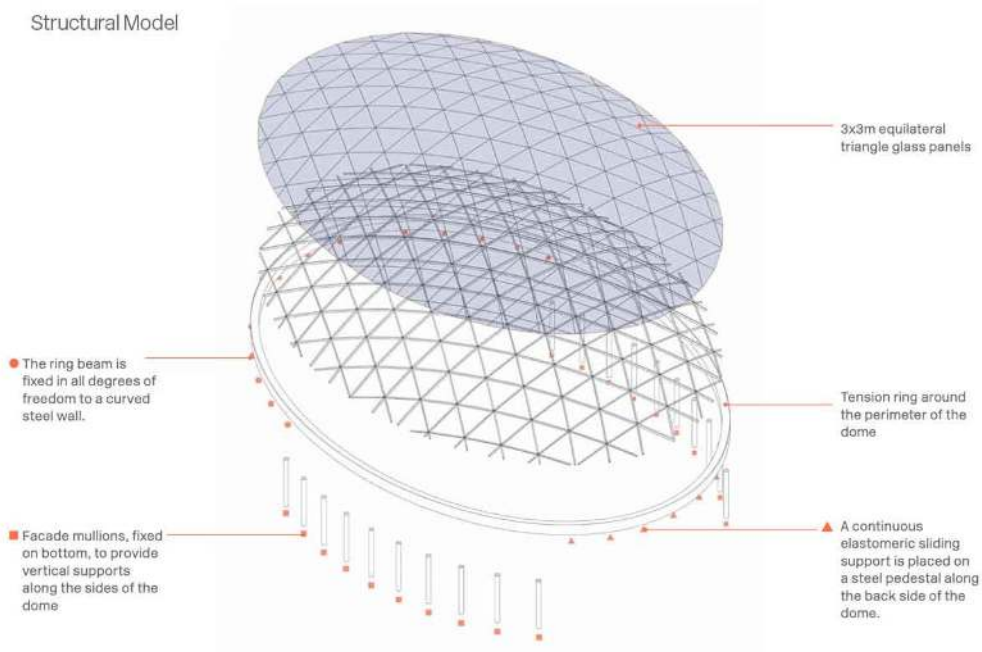

Figure 3.46 Iona Skydome structure model (Eckersley O'Callaghan, 2018)

Finite Element Analysis (FEA) is a standout among numerical methods, known for its ability to handle complex structures and challenging load conditions. By dividing the structure into finite elements, each governed by a set of equations, FEA enables a comprehensive description of the structure's behavior. FEA allows for an in-depth understanding of how the structure responds to different load conditions, critical to ensuring its safety and stability (Figure 3.47).

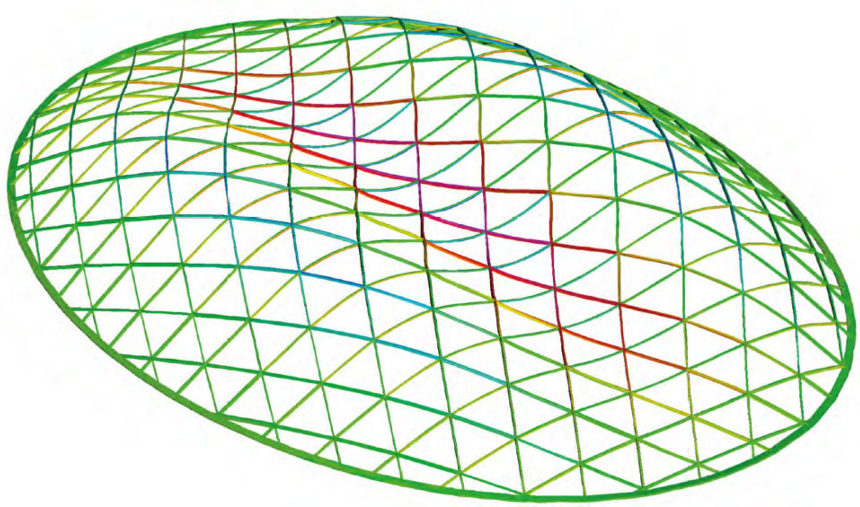

Figure 3.47 Iona Skydome analysis model (Eckersley O'Callaghan, 2018)

However, while these tools offer advanced capabilities, it is essential to remember that they are aids to the engineer's analysis and judgment. They should not replace a solid understanding of structural mechanics principles. Furthermore, because they rely heavily on the input data, the results obtained from these tools are only as good as the data provided. Therefore, a careful definition of the problem, including the structure's geometry, material properties, loads, and boundary conditions, is paramount to achieving accurate results.

Using computational tools and software like CAD, CAE, and FEA is crucial to the structural analysis of free-form structures. They allow for the efficient handling of the complexities associated with these structures and provide engineers with the resources needed to ensure these unique and aesthetically pleasing structures are also structurally sound and safe.

In summary, the structural analysis of free-form structures is a complex but necessary component of their design process. It ensures that architectural and aesthetic ambitions are not compromised by structural inefficiencies, contributing to the creation safe and efficient structures and aesthetically pleasing masterpieces.

The complexity and challenges associated with the structural analysis of free-form structures also create a landscape rife with opportunities for innovation and discovery. As architects continue to push the boundaries of design, engineers need to ensure these intricate structures' safety, efficiency, and reliability.

Numerical methods provide a way to meet these needs. By facilitating detailed analyses that account for complex geometries and load conditions, these methods can help predict the behavior of free-form structures under various scenarios. Through the creation of mathematical models, defining material properties and boundary conditions, performing analyses, and interpreting results, engineers can derive valuable insights into a structure's behavior. These include the distribution of stress and strain, structural deformations, and reactions at supports - all critical factors for determining a structure's safety and effectiveness.

However, while numerical analysis offers a powerful toolset, it should not exist in a vacuum. It must be supplemented with a thorough understanding of structural mechanics principles and the exercise of sound engineering judgment. The validation of results for plausibility and a closer examination of critical regions of the structure are necessary to ensure the model's accuracy and the safety of the final design.

Although challenging, the field of structural analysis for free-form structures is crucial. It requires advanced techniques, software tools, and a deep understanding of structural behavior and design principles. As the architectural world increasingly embraces free-form structures, the demand for sophisticated structural analysis methods that cater to these unique and complex forms will grow. These methods present a fascinating avenue for the evolution of engineering practices, with exciting implications for the future of architecture and construction.

Example of Numerical Analysis

To understand the role of numerical analysis in the context of free-form structures, let us consider the following case study

The Sage Gateshead: The Sage Gateshead is a concert venue in England with a free-form glass and steel structure. Its unique shape necessitated advanced numerical analysis methods to understand how the structure would behave under various loads and to design the appropriate structural elements (Figure 3.48).

Figure 3.48 Sage Gateshead United Kingdom (Clerk, 2018)

3.2.1.1. Global Stability in Single-Layer Free-Form Systems

Single-layer free-form systems require detailed design, analysis, and assembly to ensure safety and stability. A critical factor in the structural integrity of these systems is global stability, which refers to the ability of the entire structure to maintain its shape under various loads. Unlike local stability, which focuses on individual components, global stability considers the stability of the whole structure, preventing instability forms like buckling, torsion, or sway.

Given their lightweight and relatively flexible nature, maintaining global stability in single-layer free-form structures is a major concern. These structures are designed to form a stable three-dimensional figure, with stability achieved through the complex interplay of tensile and compressive forces.

Factors influencing global stability include the geometrical configuration of the structure, properties of the connectors, and loading conditions. For example, larger curvatures or arch-like configurations in the structure can enhance stability. Similarly, connector properties such as rotational stiffness can impact stability. If connectors allow excessive rotation under load, it may cause instability; if they are too stiff, they might lead to more significant bending moments and potential component failure. Load conditions, including their size and direction, also significantly influence stability.

Various methods like analytical models, numerical simulations, and experimental testing are utilized to assess the global stability of single-layer free-form structures. These methods help identify potential instability mechanisms and enable the design of appropriate countermeasures.

Factors Affecting Global Stability

Several factors can influence the global stability of a free-form structure:

Form: The geometric form of these structures can significantly affect load distribution and resistance to deformation. Complex curvatures and non-orthogonal configurations in free-form structures can enhance structural stability by channeling forces along multiple paths, efficiently distributing stresses, and mitigating the risk of failure from localized overloading.

Node Instability: Significant displacements can occur between neighboring nodes due to the unbalanced axial load from the elements connected to a node. This condition is called snap-through instability and falls into the category of nonlinear behavior from a geometric standpoint.

Element Buckling: Even with a partial or overall loss of strength in an element, partial or general collapse can occur. This problem can be avoided by ensuring sufficient bending stiffness.

Material Properties: The characteristics of the materials, including strength, elasticity, density, and durability, play a pivotal role in maintaining system stability. Materials like certain steels or composites with high tensile strength and elasticity are beneficial due to their ability to resist deformation under load. Additionally, materials resistant to environmental factors ensure long-term stability.

Support Conditions: The stability of a single-layer free-form system is greatly influenced by its support conditions. The design of supports must account for the nature of loads, both static and dynamic, and the geometric configuration of the structure. The positioning, type, and number of supports significantly impact the force transfer from the structure to the ground, which subsequently affects the structure's balance and stability.

Load Distributions: Both internal and external load distributions impact the structure's stability. Internally, the configuration and connection of elements dictate how loads are shared, while externally, the structure must endure loads such as gravity, wind, and seismic activity. Uneven or unexpected load distributions can lead to structural instability, causing excessive deformations, material failure, or even structural collapse.

"Global stability" refers to the entire structure's ability to maintain its general form under loading. Global stability analysis aims to ensure the structure remains stable and not experience instability forms like buckling, torsion, or sway under expected loads and influences. Geometric configuration, material properties, loading conditions, and boundary conditions influence the global stability of a free-form structure.

The evaluation of global stability in free-form structures is performed using computational analysis methods, with Finite Element Analysis (FEA) being a common approach. This technique simulates the structure under various loading conditions, enabling engineers to identify potential stability issues and adjust the design accordingly to maintain global stability under all anticipated conditions.

Ensuring global stability is crucial for free-form structures, which often involve complex geometries and unconventional forms. Engineers can ensure these structures remain stable and safe under all expected conditions through careful design, rigorous analysis, and suitable materials and construction techniques.

3.2.2 Node design

In single-layer free-form systems, the nodal points or connectors form a crucial design aspect, influencing the structure's behavior, feasibility, and aesthetics. These junctions, known as organic nodes in freeform skylights, allow for complex and beautiful patterns of light and shadow, enhancing a building's interior and exterior.

These organic nodes are custom-designed to accommodate connections at various angles, facilitating the creation of unique freeform structures. Careful design and analysis of these nodes are essential, with engineers utilizing computational tools for optimization to ensure structural integrity and visual appeal.

Nodes are categorized broadly into rigid, semi-rigid, and flexible types. Rigid nodes, designed to transfer moments, lock the angle between elements and are commonly found in shell structures. Semi-rigid nodes permit some rotation, providing flexibility in grid geometry, and are used in structures like reticulated domes. Flexible nodes allow significant rotation and are typically used where grid geometry needs to be adaptable, as in deployable structures.

The choice of node type depends on the project's specific needs, including structural requirements, geometric constraints, and construction logistics. Thus, single-layer freeform skylights with organic nodes represent a significant architectural innovation, offering unique structural and aesthetic benefits despite their design and construction challenges.

When designing nodes for gridshell structures, several factors must be taken into consideration:

Load Transfer: The nodes must be designed to efficiently transfer loads between members and prevent stress concentrations that could lead to premature failure.

Fabrication and Installation: The nodes' design should consider the fabrication process and the ease of installation. This design considerations such as the type of materials being used, the necessary machinery and tools, and the level of skill required for installation (Figure 3.48).

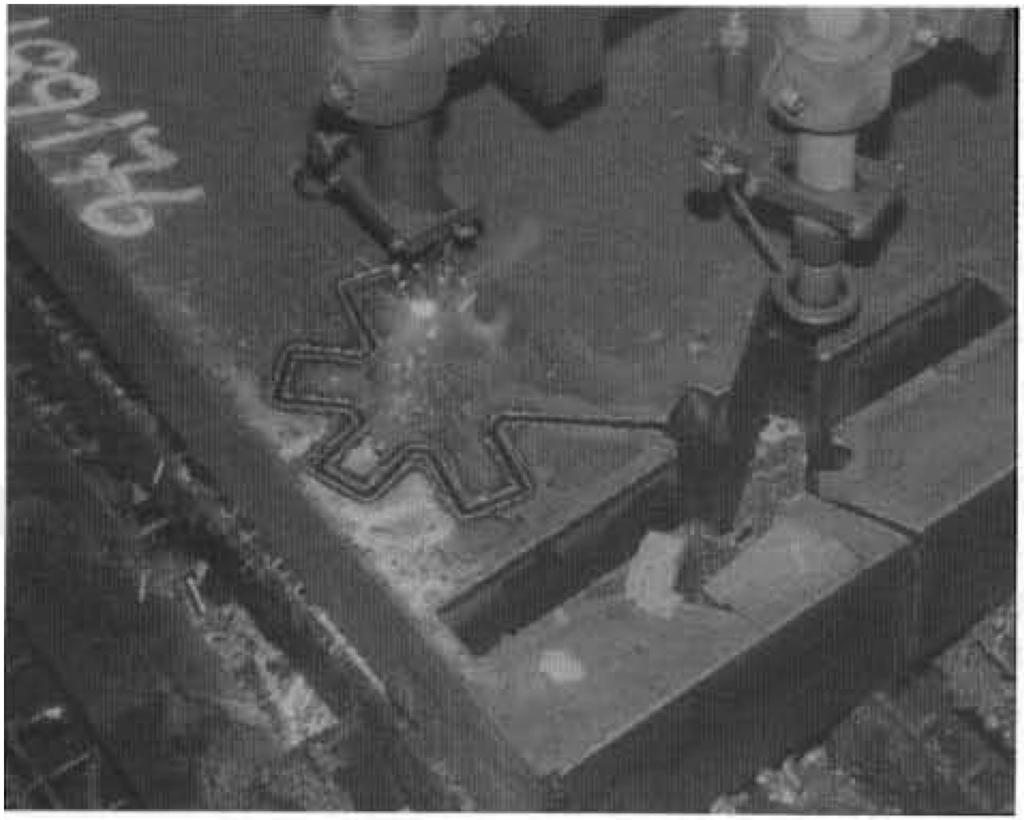

Figure 3.49 Autogenous cutting of nodes from the plate (Waagner Biro)

Aesthetics: The design of the nodes should align with the overall architectural vision of the structure. This process can be critical in grid shell structures, where the nodes can be a prominent visual feature.

Maintenance and Inspection: Nodes should be designed for easy inspection and maintenance over the structure's lifespan. These checks include considerations such as the accessibility of the node and the ease of replacing components if necessary

3.2.3 Node analysis in single-layer free-form systems

With their complex and non-regular geometries, free-form structures depend heavily on grid member connections or node connectors. These are points where two or more structural members meet and connect, enabling the transfer of forces and moments between them. With meticulous design and execution, these connections significantly contribute to the structure's strength, stability, and stiffness.

The connection type selection and specifics in single-layer free-form systems depend on factors like span distance and load transfer requirements. Typically, the connections used in these systems can be divided into two main groups: hinged connections and moment-transferring connections.

Moment-transferring connections can further be subdivided into fully rigid and semi-rigid categories. Fully rigid connections completely restrain relative rotational movement between connected elements, requiring the connection point to possess sufficient rigidity and strength to maintain zero relative rotational movements. Semi-rigid connections, in contrast, do not entirely restrain this rotational movement.

In both cases, the non-linear behavior of materials and geometry must be considered, which can considerably complicate the analysis. Consequently, the material details and connection methods used in single-layer free-form systems significantly influence the resulting architectural and engineering designs.

Types of Grid Member Connections

Grid member connections in free-form structures can be broadly classified into three categories (Figure 3.50):

Rigid Connections: Rigid joints, crucial in structural engineering, are designed to transfer various forces including bending moments, axial, and shear forces - between connected members. They maintain the angular relationship between these members, providing high structural rigidity. This rigidity is beneficial in preserving the structure's form and resisting dynamic loads like wind or seismic activities. However, these joints are more complex and costly to fabricate than flexible connections.

Moment-transferring connections, a type of rigid joint, are specifically designed to transfer bending moments between the connected elements. They lend stiffness and stability to the system, and are utilized when substantial load transfer and resistance to deformation are necessary.

Pinned or Flexible Connections: Pin-connected joints, designed to transfer shear and axial (tension or compression) forces between connected members, allow for rotational movement at the connection. These joints are typically easier to construct and analyze but offer less rigidity than rigid connections.

Hinged connections allow rotational movement between the connected elements, providing flexibility and accommodating shape and form changes. They are generally used in systems where limited or no moment transfer is desired or required, lending more flexibility to the structure's design and movement.

Semi-Rigid Connections: These types of joints balance the simplicity of pin-connected joints and the rigidity of fully rigid joints. They are designed to allow a limited amount of rotation under load, providing flexibility in the structure while maintaining a significant degree of rigidity.

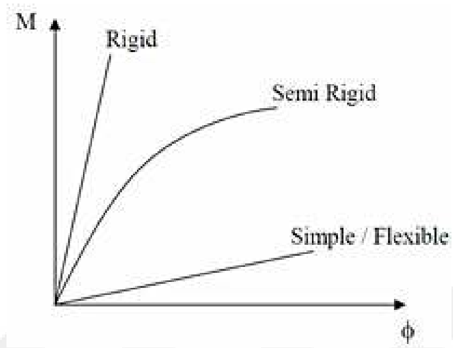

Figure 3.50 Comparing rigid, semi-rigid, and simple connections (Graitec)

The choice between these connections will depend on several factors, including the loads the structure must resist, the materials used, and the desired aesthetic effect. For example, pin-connected joints can give the structure a delicate, lightweight appearance, while rigid joints can convey a sense of solidity and strength.

In addition to the choice of connection type, other essential considerations in the design of grid member connections include the connection's capacity (its ability to carry loads without failing), its stiffness (its resistance to deformation under load), and its durability (its ability to withstand environmental conditions such as moisture and temperature changes).

Designing these connections can be challenging due to the complex forces in a free-form structure, but computational design and analysis tools can be beneficial. These tools can simulate the structural behavior of different connection designs under various loading conditions, allowing engineers to optimize their designs for efficiency and safety.

Design Considerations

The detailed design of grid member connections in free-form structures involves several important considerations:

Load Transfer: The connection must safely transfer the forces and moments between the connected members. It requires a detailed understanding of the loading conditions and the flow of forces through the structure.

Structural Integrity: The connection must not compromise the structural integrity of the members it connects. It often involves careful detailing to avoid stress concentrations, which could lead to premature failure.

Fabrication and Installation: The connection design must also consider practical considerations, such as ease of fabrication and installation. Connections that are overly complex or difficult to install can significantly increase the cost and timeline of the Project (Figure 3.51).

Figure 3.51 British Museum Great Court Roof, glass installation (Waagner Biro)

Aesthetics: In free-form structures, aesthetics are often as important as structural considerations. The connections should therefore be designed to complement the overall aesthetic of the structure.

Examples of Grid Member Connections in Free-Form Structures

To better understand the role and importance of grid member connections in free-form structures, let us examine a few examples:

Case Study 1: The British Museum Great Court Roof: This free-form structure consists of a complex grid of steel members creating a unique, undulating geometry. The connections between these members were meticulously designed to ensure structural integrity while maintaining the overall aesthetic.

Case Study 2: Paveletskaya: This structure comprises a grid of interconnected steel members. The connections between these members were designed with particular attention to steel's unique properties and limitations as a construction material. The detailed design of grid member connections in free-form structures is crucial to their structural design. These connections must be robust, efficient, and carefully detailed, ensuring they can adequately transfer forces and moments, maintain structural integrity, and complement the structure's aesthetic.

3.2.4 Connection types of single-layer free-form systems

Designing the connection points is one of the most critical issues for the production and assembly of single-layer Free-form carrier systems at optimum cost and time. Classifying the connection points used in single-layer Free-form systems is generally tricky. Many types differ in terms of geometric features. According to a research study, 250 connection forms have been encountered or suggested. However, it has not been proven whether a large part of these are successful designs or not due to the complexity of their design. (Heki, 1984)

Representation of nodes and members in the system. (Figure 3.52).

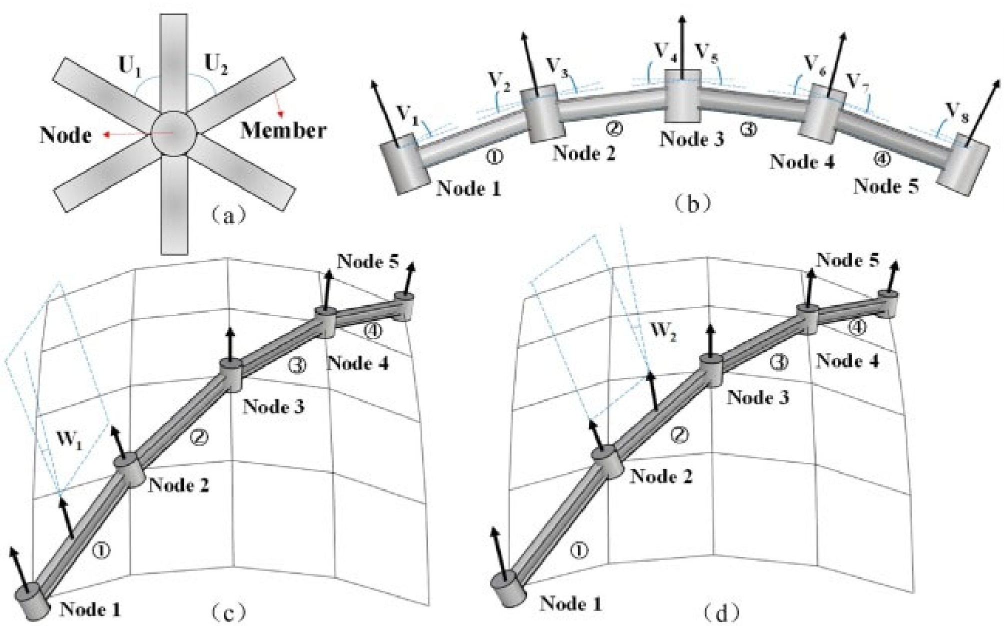

Figure 3.52 Node and member representation in joints. (Quan, 2022)

Connections can be made either by welding or by bolting. Welded connections appear to be an easier option in terms of design due to their high rigidity. However, the manufacturing and assembly stages are pretty challenging regarding labor, cost, and timing.

Bolted connections are advantageous in terms of practicality. The bolts used in bolted connections are high-strength and pre-tensioned. While bolted systems have a certain level of rigidity, they do not have rotational restrictions to the extent of welded connections. The axial force level directly influences the bending moment capacity of a node in the members connected to that node. Members with a closed box section are preferred to resist lateral torsional buckling problems. The moment-rotation effect can be realistically defined through experiments or qualified finite element programs.

Connections in single-layer free-form systems, often formed at the intersections of linear elements known as nodes, play a critical role in defining the structural behavior of the system. They are responsible for transferring loads between individual components, maintaining the stability of the structure, and defining the deformation characteristics of the system. Welded connections may be an easier option due to their high rigidity. However, the fabrication and assembly stages can be pretty challenging regarding labor, cost, and timing.

In single-layer free-form structures, node connectors play a critical role in the stability and integrity of the structure by serving as the junction point for various structural elements. The design and selection of appropriate node connectors are crucial in the structural design process. Herein, we explore several types of node connectors in constructing single-layer free-form structures.

Nodes in a grid shell structure play a crucial role in the overall stability and integrity of the structure. These nodal points, where multiple structure members intersect and are mechanically connected, are responsible for transferring forces between members. A well-designed node should efficiently transfer loads while maintaining the structure's desired form. In addition, the nodes should be designed to accommodate the different load scenarios the structure will experience.

Types of Node Connections in Gridshell Structures

Various node connections are used in grid shell structures, depending on the design requirements, material choices, and construction techniques. These may include:

1. Bolted Nodes: Bolted nodes are a common type of node used in free-form structures due to their ease of assembly and disassembly. These connectors consist of pre-drilled bolted plates or castings to allow the structural elements to be bolted together. This behavior provides flexibility and ease of modification, as components can be easily replaced or adjusted. Bolted nodes can be used in steel and timber structures, and their strength can be adjusted by varying the number and size of the bolts used. The bolts used in bolted connections are high-strength and pre-stressed. While a bolted system possesses a certain level of rigidity, it does not impose rotational restrictions to the extent of welded connections. The axial force level directly influences the bending moment capacity of a node in the connecting members. Members with a closed box shape are preferred to mitigate lateral torsional buckling issues. Experiments or qualified finite element programs are used to define the moment-rotation behavior realistically.

These are semi-rigid connections that allow for some flexibility at the node.

Bolted nodes are used in the Centre Pompidou-Metz in France. This structure, designed by Shigeru Ban, comprises a network of timber beams that form a complex, undulating roof structure. The timber elements are connected using steel bolted nodes, facilitating easy assembly and the ability to accommodate the unique geometry of the structure.

The node is made from a hollow sphere with openings at the top and the bottom. Each structural member is connected to the node sphere by two bolts mounted from inside the hollow sphere. Horizontal, vertical, and twist angles of structural members at this node can be accommodated by the geometry of the two bolt holes for each member. Direct support of cladding elements by the members across the node connector is not feasible.

In 1994, MERO GmbH, Wuerzburg, Germany, published a series of end-face connectors and the bowl node called “MERO Plus”. One of these node connectors is the cylinder node MERO-1, shown in Figures 3.53 and 3.54. The node is made from a hollow cylinder with openings at the top and the bottom. Two bolts inside the hollow cylinder connect each structural member to the node cylinder. The geometry of the machined plane can accommodate horizontal, vertical, and twist angles of structural members' surfaces at the node. The connection enables the transfer of relatively high bending moments (Stephan et al., 2004).

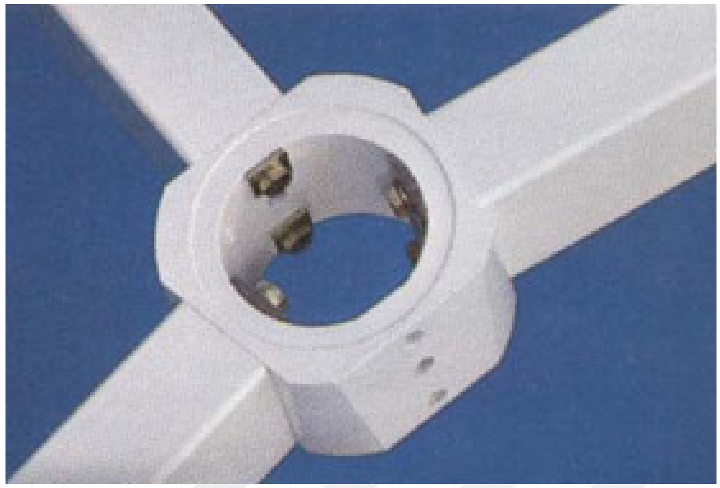

Figure 3.53 End-Face Connector MERO-1 (Stephan et al., 2004)

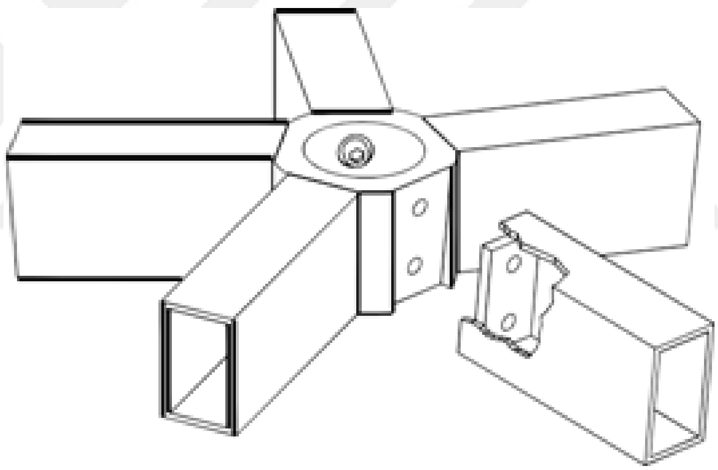

Figure 3.54 End-Face Connector MERO-1 (Stephan et al., 2004)

Another "MERO Plus" connector is the block node MERO-2, which is shown in figure 3.55. The node is cut from a thick plate. Each structural member is connected to the lock node by one or two bolts mounted inside the structural member. Hence, the member must be a hollow section profile like RHS, SHS, or CHS. Alternatively, the members can be welded to the node. The geometry of the machined plane can accommodate horizontal, vertical, and twist angles of structural members' surfaces at the node. The bending capacity is similar to the capacity of the cylinder node MERO-1 (Stephan et al., 2004).

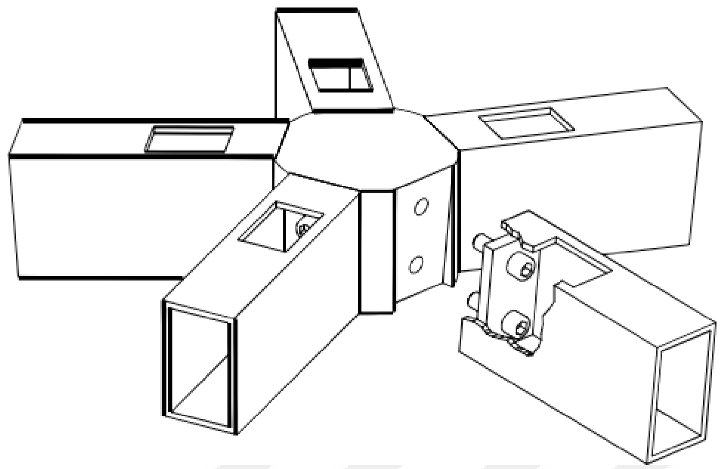

Figure 3.55 End-Face Connector MERO-2 (Stephan et al., 2004)

2. Welded Nodes: In scenarios where additional strength or rigidity is required, welded connectors can be used. These are permanent, rigid connections where members are fused at the node using heat. Welded connectors provide high strength and stiffness, making them ideal for structures subject to high loads or dynamic forces. Welded nodes are commonly used in steel structures. They are formed by fusing the intersecting steel elements using a high-temperature welding process. These nodes provide high strength and rigidity, making them suitable for applications where substantial loads must be transferred between elements. However, installing welded connections can require specialized equipment and skilled labor.

Welded connections are a common type of connection used in single-layer free-form systems, particularly those constructed from steel or other weldable materials. Welding involves fusing the materials at a high temperature, producing a typically rigid and robust connection. This type of connection is well-suited to systems with fixed geometry, and moment-resisting nodes are desirable. One of the critical challenges with welded connections in free-form systems is the difficulty of achieving precise alignments, given the complex and often irregular geometries involved.

The node, shown in the figures 3.56, figures 3.57 and 3.58, is the welded end-face connector WABI-1, which was developed by Waagner-Biro AG, Vienna, Austria, for the courtyard roof of the British Museum in London. The node consists of a star-shaped plate with 5 or 6 arms.

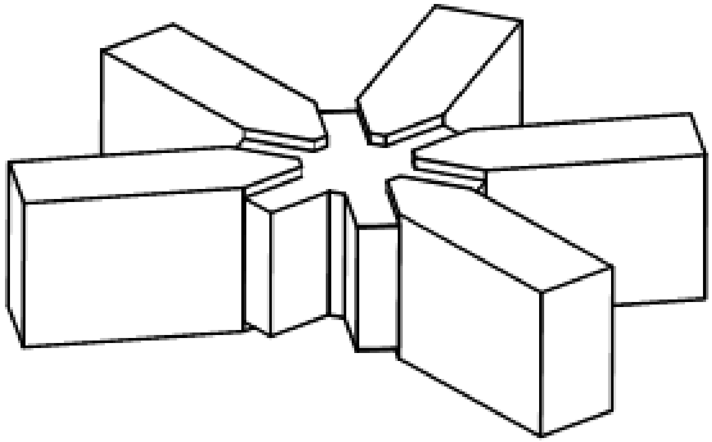

Figure 3.56 End-Face Connector WABI-1 (Stephan et al., 2004)

Figure 3.57 End-Face Connector WABI-1 (Stephan et al., 2004)

Each arm runs between adjacent structural members. These nodes are made from thick plates by cutting perpendicular to the plate surface. The end faces of the structural members have a double miter cut to match the corresponding node gap between adjacent arms. The thickness of the node plate is less than the height of the connected structural members. The top and bottom surfaces of the node plates are connected to the members by fillet welds, and butt welds connect the side surfaces. The geometry of the double miter can accommodate horizontal, vertical, and twist angles of structural members at this node cuts at the end of the members. High bending moments can be transferred up to full member strength. (Stephan et al., 2004)

British Museum, England/ London, employs welded nodes. Designed by Schlaich Bergermann Partner, this lightweight structure consists of a network of cables and struts. The steel struts are connected to the cables through welded nodes, enabling the transmission of tensional forces throughout the structure.

3. Fabricated Nodes: Fabricated nodes assemble individual components to form the complete node. It can be achieved through welding, bolting, or other joining techniques. Fabricated nodes offer a high degree of customization, allowing for the adaptation of the node design to suit specific structural requirements.

These are nodes that are custom designed and fabricated precisely for a project. These are often used in more complex grid shell structures where standard connection methods may not be suitable.

4. Casted Nodes: Cast connectors are often used when complex geometries or non-standard forms are required. Casting allows for complex geometries and offers high load-bearing capacity. Also, Casting allows for the creation of intricate, custom-designed node connectors. These connectors can be made from various materials, including steel, aluminum, and high-strength polymers. The casting process enables the creation of intricate node geometries that would be challenging to achieve with other fabrication methods.

5. 3D Printed Nodes: With technological advancements, 3D printed connectors have become increasingly feasible. These connectors can be custom designed and produced with high precision, making them ideal for single-layer free-form structures with complex geometries. They can be made from various materials, including metal and polymer-based materials.

6. Hybrid Connectors: Hybrid connectors can combine different types of connections. For instance, a cast connector might have pre-drilled holes for bolted connections, combining the geometric flexibility of casting with the ease of assembly provided by bolting.

7. Modular Connectors: These connectors are designed to be part of a modular system, where identical or similar components are repeated throughout the structure. They can simplify the design, fabrication, and assembly process and be particularly useful in large-scale structures.

8. Adjustable Connectors: These connectors allow for adjustments to be made post-assembly, enabling the fine-tuning of the structure's geometry or the accommodation of structural movement. They can be beneficial when precise alignment is critical or the structure is expected to change shape or position over time.

9. Self-locking Connectors:Interlocking nodes use specially designed structural elements that fit together in a specific manner, much like jigsaw puzzle pieces. These connectors are designed to lock into place once assembled, providing a secure connection without additional fasteners. These nodes can often be assembled without additional fasteners, and they provide a visually appealing node design that adds to the aesthetic quality of the structure.

The design of nodes in grid shell structures is critical to the overall structural design process. These nodes play a crucial role in the overall stability and performance of the structure, making their design an area that requires careful consideration and expertise. The selection of the appropriate node connector for a single layer free-form structure requires consideration of numerous factors, including the structural requirements, the complexity of the geometry, the fabrication capabilities, and the desired aesthetics.

4. CASE STUDY

This study examined single-layer free-form systems based on the model of The British Museum Great Court Roof. In order to understand single-layer free-form systems, the roof of The British Museum Great Court was modeled and analyzed, and relevant studies were conducted. Subsequently, the welded to the node and the bolted to the node used in The British Museum Great Court Roof were investigated within the scope of the node detail study. The nodes that were welded and bolted were analyzed.

4.1 The British Museum Great Court Roof

The British Museum, since its opening in 1850, has been an emblem of the grandeur of the British Empire (Figure 4.1). Throughout 150 years, the building has undergone alterations by eight different architects. However, the most remarkable transformation took place in 2000 under the guidance of Lord Norman Foster, with the collaboration of Waagner-Biro. This significant alteration involved the creation of a distinctive free-form roof that now covers the museum's previously inaccessible courtyard, providing a beautiful space for the public to enjoy. With the incorporation of over 3,300 triangular glass panels, this roof has become the most giant covered courtyard in Europe, attracting approximately 5.5 million visitors annually. This renovation effectively doubled the public area within the museum. The glazed roof, spanning 5,900 square meters, comprises 4,878 individual rods, 1,566 individual nodes, and 3,312 insulating glass panels, with a combined weight of approximately 800 tonnes. Additionally, the newly constructed 65-meter-high southern portico, serving as a foyer, is an integral part of this transformed courtyard space (Williams, 2001).

Figure 4.1 The British Museum in London (Waagner Biro)

The British Museum, originally constructed in the 18th century, features a quadrangle layout centered around the iconic Reading Room. Recently, Lord Norman Foster transformed the museum's Great Court, previously occupied by the British Library, into a great public square. This ambitious project involves the construction of an elegant glazed roof spanning an area equivalent to a football pitch. The new space will serve as the central hub of the museum, providing additional gallery space, retail outlets, and an upper-level restaurant for visitors to enjoy.

The project commenced in March 1998 with the demolition of the book stacks surrounding the Reading Room, which had concealed the original classical Georgian stone facades of the Great Court. Construction of the impressive roof structure began in September 1999 and was completed with the de-propping process in April 2000. The entire project is scheduled for completion and public opening in November 2000. The British Museum's Great Court, transformed at the dawn of the 21st century, exemplifies the possibilities of free-form structures in modern architecture. At the heart of the museum, the Queen Elizabeth II Great Court, designed by Foster + Partners and engineered by Buro Happold, opened to the public in December 2000. It encapsulates a pioneering example of a single-layer free-form system, with its iconic tessellated glass and steel roof. This ambitious design turned what was previously an inner courtyard into the largest covered public square in Europe (Williams, 2001).

Figure 4.2 The British Museum in London (Waagner Biro)

Figure 4.3 The British Museum in London (Waagner Biro)

The roof of the Great Court at the British Museum spans the entire area, measuring 95 meters in length and 74 meters in width. It extends from the surrounding buildings to the Reading Room located slightly off towards the north. The roof structure comprises a network of triangular cells, forming a shell-like shape (Figure 4.3). As there is only one line of symmetry due to the position of the Reading Room, the geometry of each node and member within the structure is unique (Williams, 2001).

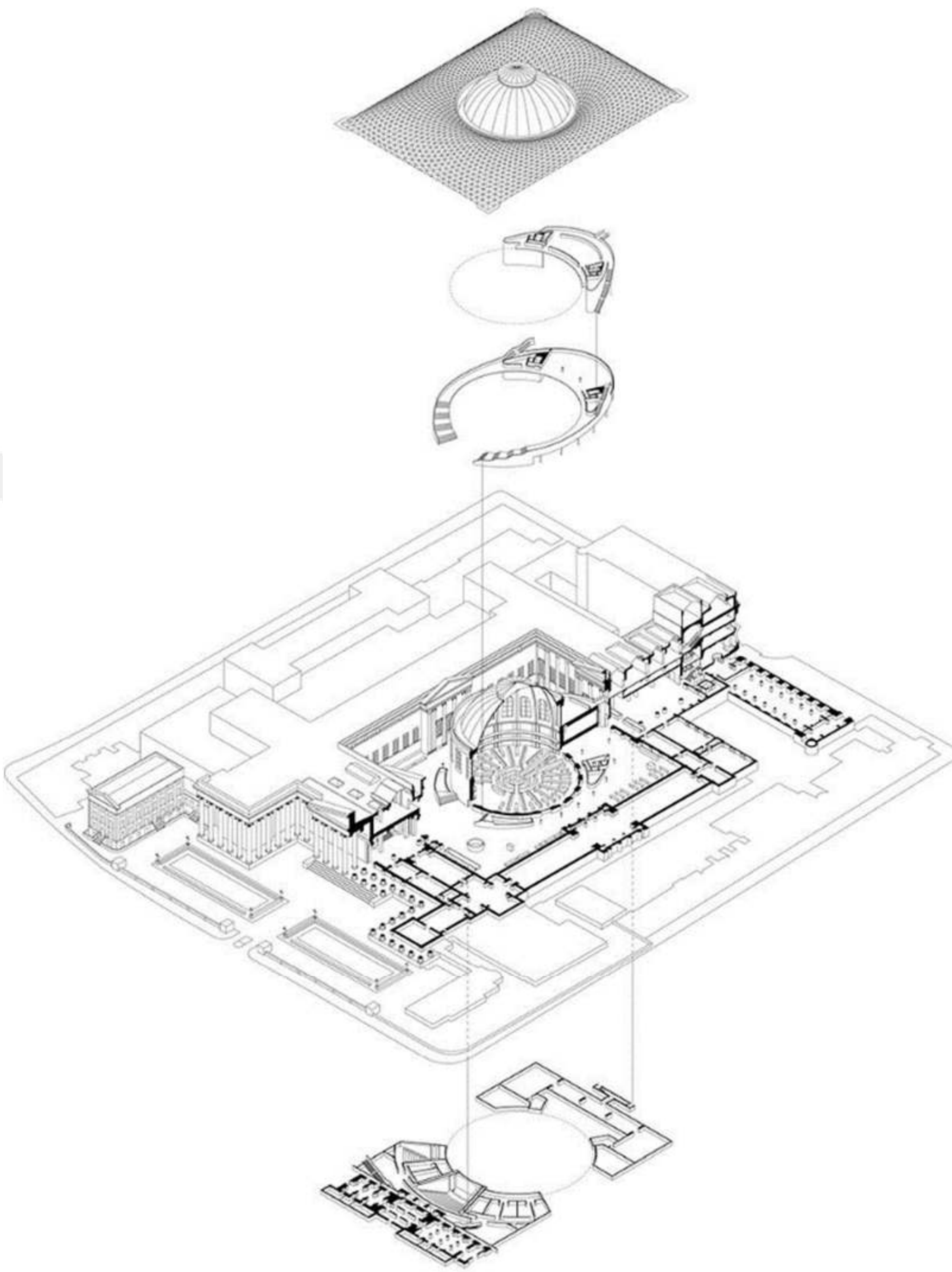

Figure 4.4 Renovation of the British Museum, London (Young, 2000)

Buro Happold developed the final geometry of the roof network and its structural design through a form-finding process. Several factors were considered during this process, including the maximum size of the glass panes from a fabrication perspective and the required glass performance. The resulting network consists of 4,878 members and 1,566 nodes, each distinct. The intricate geometry and individuality of each node and member in the network showcase the complexity and precision involved in the design and construction of the roof structure, allowing for a visually striking and functional space within the Great Court of the British Museum.

Waagner Biro and other contractors were involved in the project from an early stage to provide expertise in buildability, fabrication, and installation. Their knowledge and experience were crucial in ensuring the successful realization of the roof structure.

The roof spans vary in different directions. In the north, the span measures 28.8 meters with an arch height of 5.48 meters. In the east and west, the span is 14.4 meters with an arch height of 5.1 meters. In the south, the span measures 23.8 meters with an arch height of 6.4 meters. These dimensions highlight the variation in the geometry of the roof structure, accommodating the unique requirements and constraints of the Great Court at the British Museum.

The collaboration between Waagner Biro and other contractors allowed for a comprehensive assessment of the project's feasibility and the incorporation of specialized knowledge in the fabrication and installation processes. This collaborative approach ensured that the structural design and construction of the roof met the project's specific demands, resulting in the successful transformation of the Great Court space (Williams, 2001).

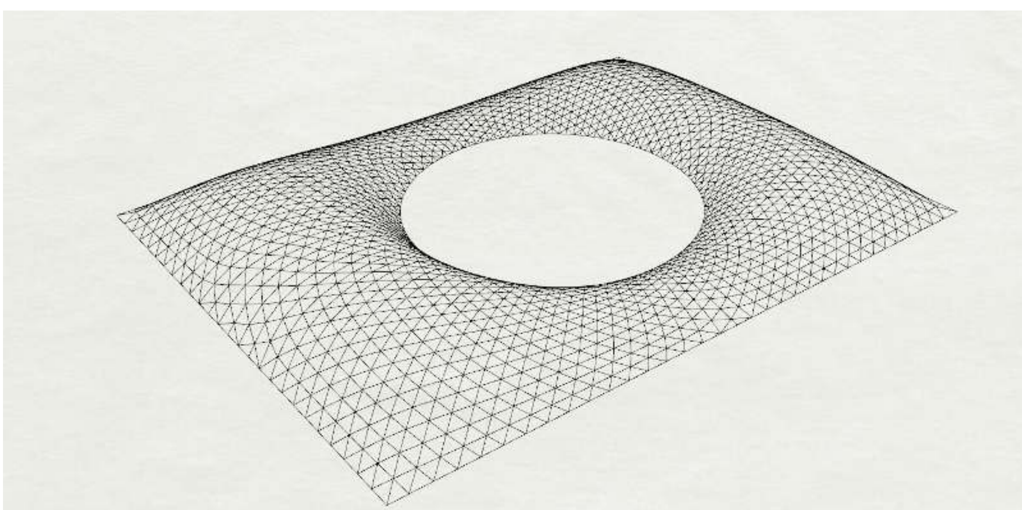

Figure 4.5 Three-dimensional computer model of the roof structure

STRUCTURAL SYSTEM

The roof of the Great Court at the British Museum is supported at two main locations: the Reading Room and the perimeter of the museum buildings surrounding the court. These support points provide the necessary stability and load-bearing capacity for the roof structure.

The Reading Room, located in the middle of the court, serves as one of the primary support points for the roof. Its structural integrity and connection to the roof system ensure stability and transmit loads to the ground.

Additionally, the perimeter of the museum buildings surrounding the Great Court is another support area for the roof. The roof structure is anchored and connected to these buildings to distribute the loads and provide overall stability.

By utilizing these support points, the roof structure achieves its intended function of covering the entire Great Court area, providing a unified and sheltered space for visitors to enjoy. The design and engineering of the roof system ensure that it remains securely in place and effectively supports the weight and forces imposed on it.

A solution was implemented to support the roof structure without imposing vertical loads on the room to address the limitation of the Reading Room in carrying additional loads. It involved the installation of 20 new composite columns positioned evenly around the Reading Room. New foundations at ground level support these columns.

On top of these columns, a circular steel beam is placed to which all incoming roof members are connected. This steel beam serves as a primary support element for the roof structure. Below the steel beam, a large horizontal concrete ring is positioned. This concrete ring is rigidly fixed horizontally to the columns and is crucial in providing lateral stiffness to the roof system.

It is important to note that the vertical loads are not transferred between the concrete ring and the roof structure. Instead, the concrete ring primarily contributes to the lateral stability and stiffness of the roof. Maintaining the overall structural integrity and minimizing potential horizontal movements is crucial. The concrete ring sits on sliding bearings on top of the Reading Room, allowing it to provide stiffness while accommodating any horizontal movements without exerting additional vertical loads on the room.

By utilizing this support system, the roof structure achieves its required stability and load-bearing capacity while ensuring that the Reading Room is not subjected to excessive loads beyond its design capabilities (Williams, 2001).

Figure 4.6 The Great Court roof at night (Waagner Biro)

The roof members at the museum's perimeter are connected to a continuous horizontal steel beam, supported by vertical posts spaced approximately 6 meters apart. These vertical posts are positioned on top of a continuous new concrete ring, added onto the existing wall to distribute the loads. All the posts are supported on sliding bearings to accommodate the absence of horizontal loads perpendicular to the perimeter. The vertical zone between the steel and concrete beam is enclosed with glass panels in the upper part, while operable aluminum panels are used for ventilation underneath.
During the investigation of the existing buildings, it was determined that no horizontal loads perpendicular to the perimeter could be transferred to the building. It necessitated using sliding bearings for the posts and implementing additional measures to provide lateral stability. Cross bracings were incorporated between adjacent vertical posts behind the four porticos, and horizontal lattice beams were added at the four corners to enhance stiffness (Williams, 2001).

These exceptional support conditions have a significant impact on the structural behavior of the roof. The typical "arch effect" cannot be achieved due to the sliding bearings at the perimeter, resulting in the roof structure experiencing significant bending moments, shear forces, and normal forces. It affects the stiffness and deflection characteristics of the roof.

Furthermore, due to the unique support conditions and the need for the entire structure to work as intended, temporary support is required throughout the construction process until the roof is fully completed. This ensures that the structural integrity and stability are maintained during the construction phase until the final configuration of the roof is achieved. During the design process of the roof, various options for the roof members were considered, including solid and hollow sections. The solid version offered slightly slimmer sections, but it required twice the amount of steel compared to the hollow option. However, the significant increase in steel weight associated with the solid version had negative implications on forces, moments, deflections, and especially the buckling factor.

Detailed investigations and discussions were conducted by the Professional Team, considering the special support conditions and the height restrictions of the roof. After careful consideration, the decision was made to prefer the hollow version of the roof members. Structural performance, weight considerations, and overall feasibility likely influenced this choice. The hollow option was deemed more suitable to achieve the desired structural behavior, minimize steel weight, and meet the project requirements (Williams, 2001).

Figure 4.7 British Museum (interior view), London (Waagner Biro)

The structural calculations and analysis for the roof were carried out by both Buro Happold and the Contractor in parallel. This approach allowed for independent verification of the results and facilitated a comprehensive understanding of the structural behavior, enabling the development of relevant connection details and installation methodology.

In the optimization process, the dimensions of the roof section sizes were adjusted. The sections had a standard width of 80 mm to accommodate the glass support detail, while the height varied from 80 mm near the Reading Room to 200 mm at the perimeter, based on the structural requirements.

To achieve sharp edges and optimize the dead load of the steel, welded box sections were utilized. This construction method allowed for different plate thicknesses for the flange and web, contributing to the overall design efficiency.

The calculations were conducted using second-order theory, considering imperfections in the structure. The maximum imperfection value, representing deflection due to the first eigenform for buckling, was applied to cover the worst-case scenario, with a maximum value of 140 mm divided by 200.

Various load cases, including dead load, patterned snow, and wind load, were investigated and combined most unfavorably. The computer model used to simulate the structure aimed to resemble reality closely and included the Reading Room columns, the snow gallery concrete ring, and the vertical posts at the perimeter. Member stresses were calculated using forces and moments from the elastic calculations, factoring in loads, employing second-order theory, and utilizing the plastic section values according to the Eurocode.

An important aspect of the analysis was carefully considering deflections caused by the dead load of the steel structure and the glass. These deflections, which occur once the temporary supports of the roof are removed, had to be accounted for to achieve the final geometry of the roof. It required constructing the roof slightly higher to compensate for the anticipated deflections.

Developing a suitable node detail to connect all members and transfer forces, including bending moments, was a significant challenge in the project. The design had to consider the various angles between incoming members, ranging from a minimum of 26 degrees to a maximum of 110 degrees. Additionally, the twisted orientation of the members relative to each other was essential to accommodate the direct glass support on top of the upper flange (Williams, 2001).

Early applications for the node design involved round and prismatic nodes and triangular frames for each glass pane, which required on-site assembly using intermediate elements. However, these initial designs were unsuccessful in visual appearance and economic feasibility. Several versions (1 to 7) were explored, including sub-versions, and numerous sketches ultimately discarded.

Finally, version 8 emerged as the breakthrough idea. The design met the requirements and was deemed suitable for construction. It marked the successful resolution of the node design challenge and paved the way for further progress in the project.

Figure 4.8 Node with welds (Waagner Biro)

The final design for the node in the project involved cutting it out of a thick plate in the shape of a star with six legs, all perpendicular to the plate surface. The incoming members were positioned between two legs of the node and required a complex end treatment to fit securely. The node was recessed both on the top and bottom to prevent the node from protruding beyond the surface of the member flanges and potentially interfering with the glass above. This recessed design allowed fillet or butt welds along the member flange, providing the necessary structural connection between the node and the members.

The fabrication process for the nodes involved flame-cutting the elements out of steel plates. The suitability of this procedure and the tolerances of the nodes were confirmed early in the project through the production of samples. The positioning of the nodes within the steel plate was automated, considering the different node heights and the production sequence. Data files for the cutting machine were generated automatically and sent directly to the machine. Each node was marked with a number, and the position of this number defined the orientation of the node in the net.

Automation was also pursued member fabrication, although it posed more significant challenges due to the complex end geometry. The main procedure involved the end treatment of the members, which was achieved using a welding robot. The member was fixed on a turntable, and the end in front of the robot was cut using data generated in the design office and directly transferred to the machine. The member was turned 180 degrees in a second step, and the second end was prepared. This procedure required significant development and adjustment of details to ensure the members met the required tolerances. Factors such as gas pressure for cutting the flange and web varied depending on the plate thickness, which was incorporated into the automatically generated data and the end geometry (Williams, 2001).

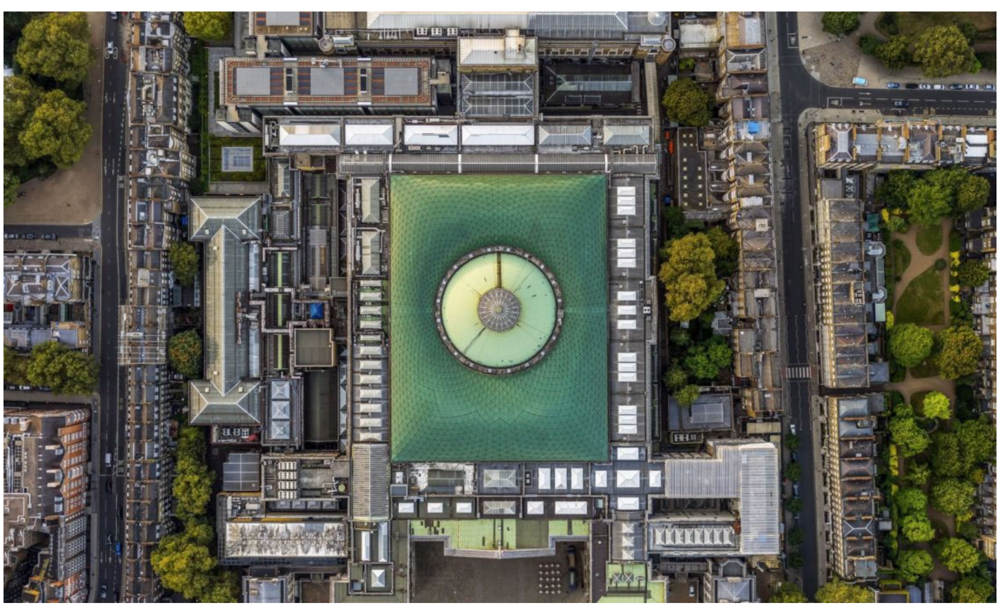

Figure 4.9 British Museum plan view, London (Waagner Biro)

4.2 The Tornado Roof Structure for Bory Mall

The Bory Mall, located in Bratislava, Slovakia, is a contemporary structure that houses one of the country's largest shopping complexes. One of the most distinctive features of this complex is its "Tornado" roof, a stunning example of free-form architecture. The Tornado roof is characterized by a spiraling form reminiscent of a whirlwind, from which it derives its name. Thanks to its organic, free-flowing form, free-form systems offer flexibility and creative solutions to architects and engineers.

The design of the Tornado roof was a highly intricate process, leveraging cutting-edge design tools and software. Given the complexity of the roof's geometry, traditional drafting methods were insufficient. Advanced computer-aided design (CAD) and parametric modeling tools were utilized to articulate the roof's intricate form and to ensure its seamless integration with the rest of the building. (Helbig, 2016)

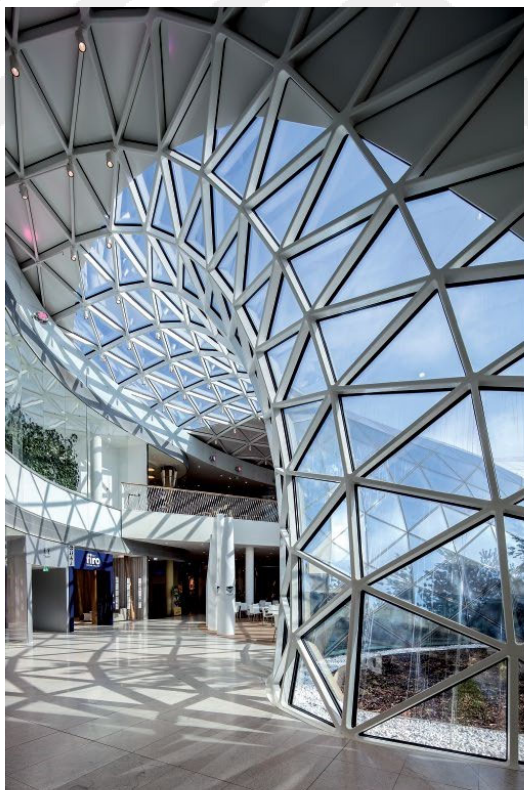

Figure 4.10 “Tornado” facade from inside (Metal Yapi)

The structure of the Tornado roof is a single-layer system comprised of a network of steel members that come together to create the roof's dynamic form. The nodes, or connections between the members, play a critical role in the roof's stability and structural integrity. These nodes were carefully designed to bear the complex load paths arising from the roof's non-standard shape. Notably, the unique spiral form of the roof leads to an uneven distribution of loads, which needs to be carefully accounted for in the design of the nodes and the overall structural system.

Figure 4.11 “Tornado” facade from outside (Metal Yapi)

The construction of the Tornado roof presented significant challenges. Fabrication and assembly of the roof's components must be placed with a high degree of precision due to the complex form of the roof. Moreover, the roof's large span necessitated using lightweight yet strong materials to ensure its structural stability while minimizing its self-weight. Steel was the material of choice due to its inherent strength, ductility, and workability, enabling the creation of the intricate network of members that form the roof's structure (Helbig, 2016).

Numerical analysis

For the ultimate limit state (ULS) analysis, non-linear FE calculations were performed for all load case combinations. The structural model used for this can be seen in Figure 4.12. The structure's design was based on elastic material properties and elastic stress distribution within the sections (elastic–elastic design).

The steel's plastic capacity was only considered in the con- nection design for grid members.

The Tornado roof's structural analysis entailed an array of calculations, encompassing geometric modeling, load analysis, and stress distribution. These calculations were instrumental in assessing the roof's strength, stability, and safety under various loading conditions. Finite Element Analysis (FEA) was employed to simulate the structure's behavior under different loads, providing valuable insights into the roof's stress distribution and potential points of weakness (Helbig, 2016).

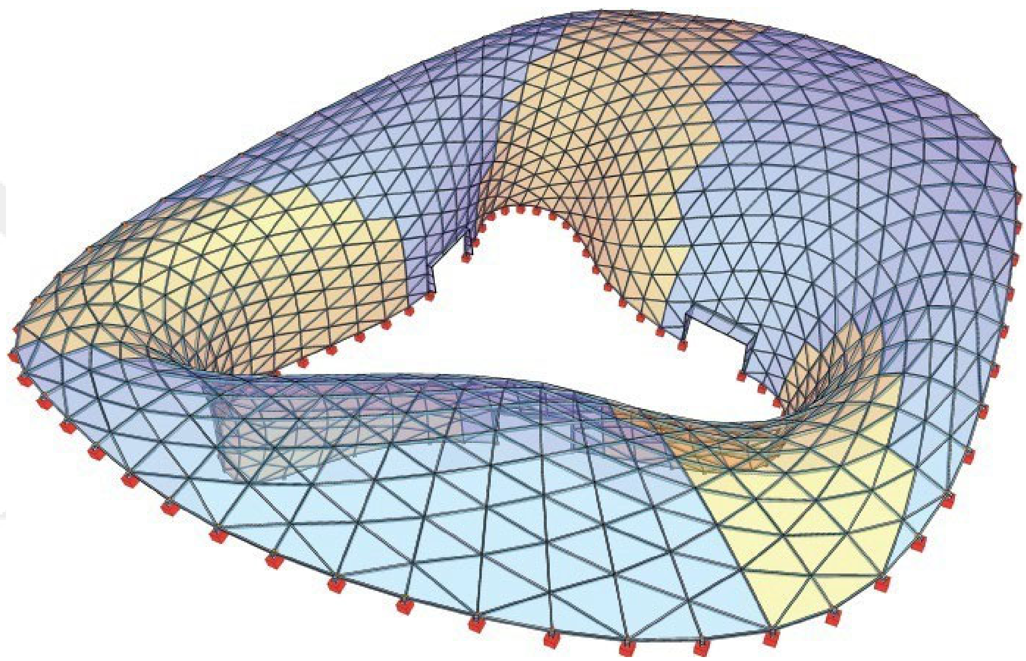

Figure 4.12 Global FE model of tornado facade (Knippers Helbig)

Grid members

All members are made from grade S355 rolled rectangular hollow sections (RHS), varying structural depths according to the grid shell curvature and stiffness. Outer section dimensions are 120x70 mm (in the lower part) and 180x76 mm (in the upper part). At a height of approx. 5 m above the base, there is a transition zone two grid bays wide between the two section depths. The transition is designed so that every node connects grid members of the same depth only. The first step is from 120x70 to 150x76 mm, and the second is from 150x76 to 180x76 mm.

Different wall thicknesses were chosen for each section depth according to internal forces and moments while considering buckling lengths.

Grid member connections

Grid members are either bolted or welded to the nodes; less heavily loaded connections are bolted, whereas those carrying higher loads are welded. All the results of an automatic design process performing all relevant checks for every individual member end were transferred by design tables and graphically. In plausibility checks, for instance, the graphical output helped to identify areas that required more welding. This overview could also be used to adapt the segmentation of the erection to suit the welded connections required (Helbig, 2016).

Grid nodes

The grid nodes were fabricated from grade S355 solid steel blocks milled to an individual shape. Each node was designed by Massimiliano Fuksas Architects according to the adjacent rolled hollow sections (see Figure 4.13). The node shape had a smooth curvature on both the top and bottom, following the grid faces. The node edges were smoothly curved to match the individual incoming rolled member sections. For bolted grid members, threaded holes were prepared in the contact surface of the appropriate members.

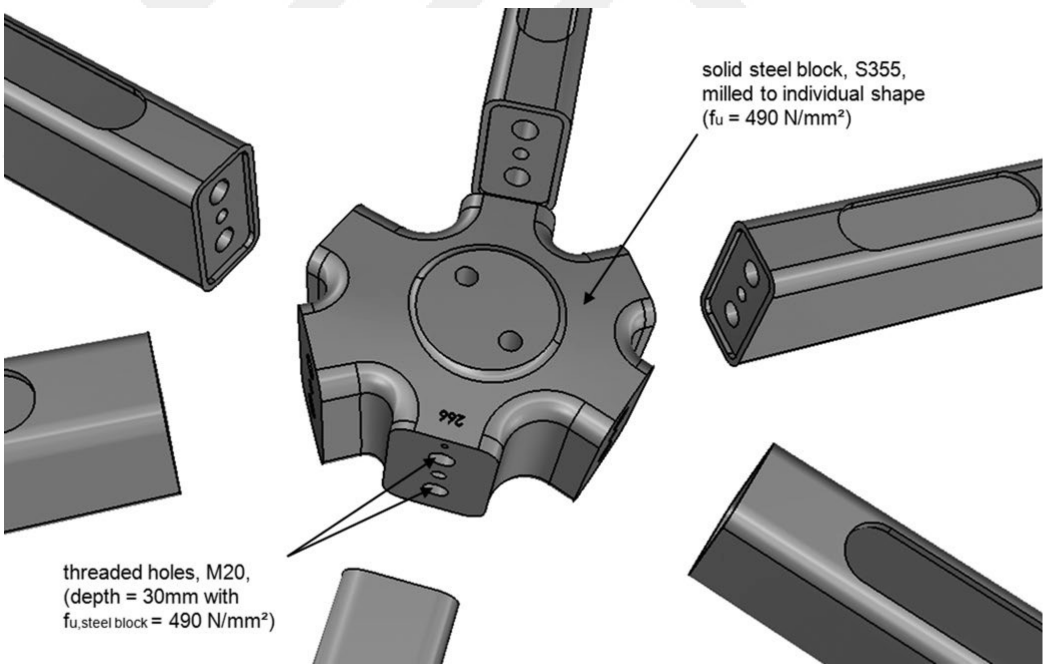

Figure 4.13 3D model of solid grid node (Knippers Helbig)

The node “arms” lengths connecting to the members were designed to allow for sufficient stress redistribution from the hollow section contact surface to the point where neighboring members interact inside the solid steel. This solid section-based stress distribution was used for interaction with adjacent member end stresses (Helbig, 2016).

Fabrication of grid nodes

Based on the individual 3D models the architects provided, the grid nodes were fabricated using CNC milling. All sides of each node connecting to a grid member and all visible nodes had to be milled (see Figure 4.14).

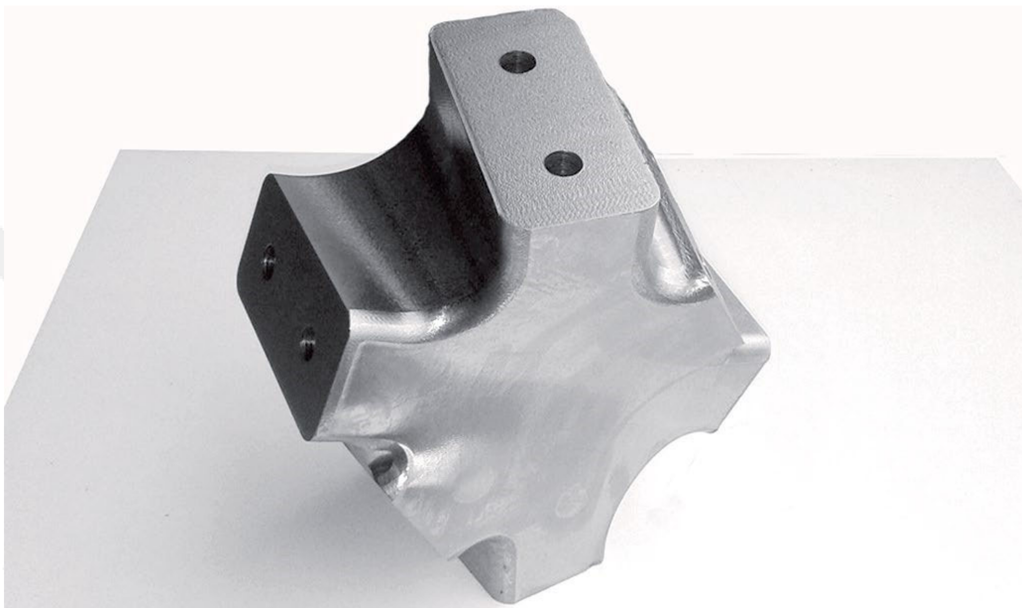

Figure 4.14 CNC-milled solid grid node (Metal Yapı)

On top of the node, one small circular non-milled surface was required to fix the piece to the milling machine (later concealed by the glazing). The piece also serves as a reference surface for the free-form geometry.

Erection

Erection of the facade had to take place after interior work had already begun. The main concrete around the central plaza was temporarily closed until the tornado facade could be waterproof. Erection work was carried out on stepped falsework. However, the number of supported grid nodes was proportionally low since the geometry of the entire facade was primarily assembled via the prefabricated nodes and beams bolted together on site. So the tornado could be erected in vertically sliced segments. Any welding of members was performed on-site after erection. The final coating and local corrosion protection for on-site welding was applied on-site.

For the architect and client, achieving invisible node-member joints and having a high-quality, continuous final coating has always been important criterion. As can be seen in Figure 4.15, this design intent could be realized perfectly.

Figure 4.15 Finished node installed on site (Metal Yapı)

Beyond the structural considerations, the Tornado roof's design also factored in architectural and aesthetic objectives. The dynamic, spiraling form of the roof creates a visually captivating spectacle, setting Bory Mall apart in its architectural distinctiveness. Moreover, the open design of the roof structure permits ample natural light to filter into the mall, enhancing the shopping experience.

The Tornado roof at Bory Mall is a stellar example of a free-form system, showcasing how the confluence of art, science, and engineering can yield breathtaking architectural outcomes. It stands as a testament to the immense possibilities offered by free-form systems, opening the door to new frontiers in architectural design (Helbig, 2016).

4.3 Introduction of Parameters

4.3.1 Purpose and scope

In this thesis, a stability investigation is conducted for a Single-Layer Free-Form structure to be constructed in the Yeşilköy neighborhood of the Bakırköy district in Istanbul.

The British Museum Great Roof's architectural model is the thesis' basis. Within the context of this thesis, the calculated magnitudes of the Dead Load, Cladding Load, Live Load, Snow Load, Earthquake Load, and Wind Load, all of which exert an influence on the Single-Layer Free-Form Structures under investigation, will be determined. Subsequently, a comprehensive analysis will be conducted.

The thesis uses Turkish Standards based on EN (European Norms) to determine the loads applied on the Single-Layer Free-Form Structure. Due to the inadequacy of the codes regarding stability in the Turkish Regulation on Design, Calculation, and Construction Principles of Steel Structures used in our country, the work has been carried out based on EN principles. The codes used in the analysis are listed below.

Table 4.1 The codes used in the analysis

Codes / Standards	Description
TBDY - 2018	Turkish Seismic Code Published In 2018
TSSC 2016	Turkish Steel Structure Code (The Regulation on Design, Calculation and Construction Principles of Steel Structures 2016)
TS EN 1991-1-3: 2009	Eurocode 1: Actions on structures Part 1-3: General Actions – Snow actions
TS EN 1991-1-4: 2005	Eurocode 1: Actions on structures Part 1-4: General Actions – Wind actions
ANSI-AISC 360-16:	Specification for Structural Steel Buildings, 2016

4.3.2 Structural analysis methodology

Several three-dimensional structural finite element models have been created using SAP2000 and ETABS to evaluate the structural response and performance of the structures under gravity, wind, and earthquake loads. The models incorporate all lateral and vertical load-resisting system elements and represent the spatial and vertical distribution of mass and stiffness of all structural elements. Walls are modeled as shell elements, columns as frame elements, and slabs as membrane elements. Generally, the following software will be utilized during the various stages of the design process.

Table 4.2 Software

Software	Description
SAP2000® V.24	3D FEA Analysis & Design
ANSYS	Finite Element Analysis (FEA) Software
Rhinoceros	Computer-Aided Design Software

The structural analysis program uses finite element methods. All load combinations are calculated with second/third order theory, i.e., considering geometrically non-linear effects. Area loads will be automatically converted according to linear or single loads by the FE software.

4.3.3 Load and resistance factors and load combinations

In structural design, load and resistance factors play a crucial role in ensuring the safety and reliability of the structure. Load factors are applied to different loads to account for their uncertainties and variations, while resistance factors incorporate uncertainties in material strengths and structural capacities.

The load and Resistance Factor Design (LRFD) approach is commonly used in modern structural design practices. It involves the combination of loads and assigning appropriate load and resistance factors to ensure that the structure can safely withstand the applied loads.

Load combinations are defined based on different load types and their associated factors. These combinations are determined by considering the simultaneous occurrence of various loads, such as dead, live, wind, snow, and seismic loads. The load combinations are formulated to represent the most critical loading conditions that the structure may experience during its design life.

The design process involves calculating the effects of each load combination on the structural elements and comparing them to the corresponding resistance or capacity of the elements. The design is unsafe if the calculated effects exceed the available resistance or capacity.

The determination of load and resistance factors, as well as the formulation of load combinations, are based on national or international design codes and standards. These codes provide guidelines and requirements for structural design, ensuring the structure's safety, reliability, and serviceability.

In this thesis, load and resistance factors, as well as load combinations, will be determined according to the applicable design codes and standards, such as the Turkish Design Code for Steel Structures (LRFD), to ensure the structural integrity and safety of the Single-Layer Free-Form Structure.

In this thesis, the design and analysis procedures have been carried out using Load and Resistance Factor Design (LRFD) approach based on the Load Combinations provided in the Turkish Earthquake Code 2016 (TÇY 2016) Regulation 5.3. LRFD (Turkish Design Code for Steel Structures) methodology outlined in the regulation has been employed to determine the limit states of the structural system under load combinations.

For wind loads, the principles outlined in TS EN 1991-1-4 will be considered. Similarly, for snow loads, the guidelines provided in TS EN 1991-1-3 will be taken into account.

Regarding structures located in earthquake-prone regions, the conditions specified in the "Turkish Building Earthquake Code" (TBDY 2018) will be the basis for the design of the structural system.

By adhering to these codes and standards, the study aims to ensure that the Single-Layer Free-Form Structure is designed and analyzed by the appropriate safety requirements for various load conditions, including wind, snow, and seismic loads.

$$R_u \leq \phi \, R_n \qquad (4.1)$$

where R_u: Required strength determined by calculation for load combinations, R_n: Characteristic strength, ϕ: Coefficient of strength, ϕR_n: Design strength.

The Load and Resistance Factor Design (LRFD) Load Combinations are as follows:

Table 4.3 Load Combinations for ULS

1	1,4 G
2a	1,2 G + 1,6 (Qr or S or R)
2b	1,2 G + 1,6Q + 0,5 (Qr or S or R)
3	1,2 G + 1,6 (Qr or S or R) + (Q or 0,8W)
4	1,2 G + 1,0Q + 0,5 (Qr or S or R) + 1,6W
5	1,2 G + 1,0Q + 0,2S + 1,0E
6	0,9 G + 1,6W
7	0,9 G + 1,0E

where G: Dead load, Q: Live load, Qr: Roof live load, Q: Snow load, W: Wind load, E: Earthquake effect, R: Rain load, T: Effects of temperature change and/or support collapse, H: Horizontal ground pressure, ground water pressure or bulk material pressure,

Design for Serviceability Limitations

Serviceability Limit States (SLS): These conditions focus on the usability and functionality of the structure under normal service loads. They ensure that the structure remains within acceptable limits of deflection, vibration, cracking, and other serviceability-related criteria.

Usability can be defined as external effects, maintaining the external appearance of the structure under loads, fulfilling the functions expected from it, and providing sufficient comfort. In order to ensure usability, usable limit states are mentioned in TÇY 2016 Regulation Chapter 15.

Under the load combinations determined in the regulation, limit values for behavior variables such as acceleration and displacement of the building system and usability limit states are defined.

In order to control the available boundary conditions, TÇY 2016 Regulation mentions load combinations as follows in Chapter 15:

Table 4.4 Load Combinations for SLS

1	G+ Q
2	G+ 0.5S
3	G+ 0.5Qr
4	G+ 0.5Q+W

where G: Dead load, Q: Live load, Qr: Roof live load, Q: Snow load, W: Wind load,
In the TÇY 2016 Regulation, Section 15 discusses vertical and horizontal displacement checks, vertical vibration checks, comfort checks under wind effects, and displacements caused by temperature changes.

4.3.4 Stability design with general analysis method

Steel structures are predominantly designed based on stability limit states, making stability crucial in structural design. Local instability or buckling in a structural element can lead to localized collapse of the entire structure. Therefore, a stability analysis is necessary to model structural behavior and minimize unstable structural responses.

The General Analysis Method is widely used in stability calculations as it considers material strength degradation and second-order effects in geometry, aided by advancements in computer technology. In this thesis, stability design is conducted using the General Analysis Method.

- The General Analysis Method follows three fundamental application rules:

Second-order effects should be considered to account for nonlinear behavior in terms of geometric conditions.

- Reduction in axial and flexural stiffness is required to incorporate inelastic effects in the material.

4.3.5 General explanations and explanation of the analyzed system

This section examines the characteristics of the single-layer free-form structure under analysis, the design codes utilized in the analysis, and the detailed node analysis of the structure. The front, side, top, and perspective views of the free-form system used in the analysis are depicted in figure 4.16.

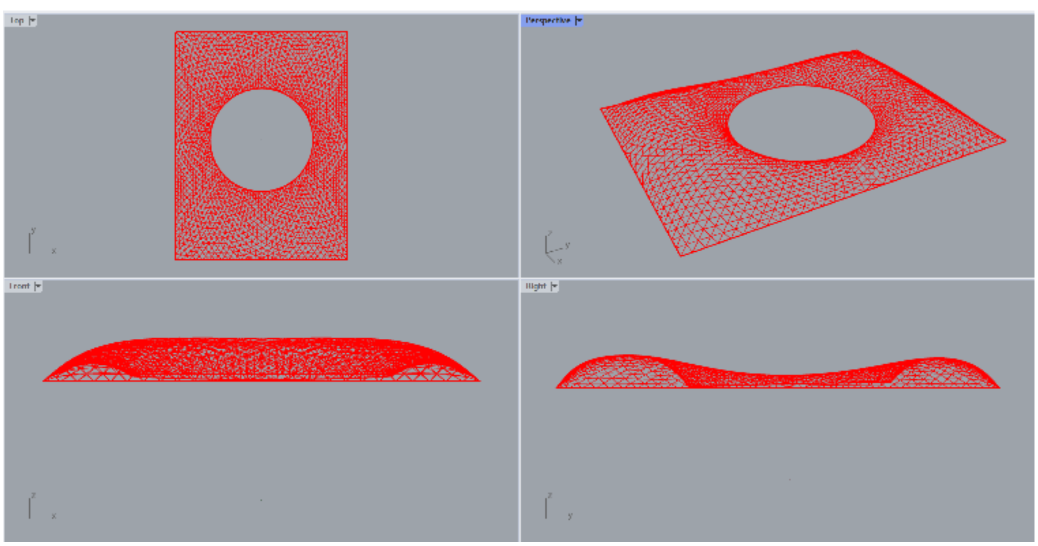

Figure 4.16 The front, side, top, and perspective views of the free-form system

4.3.6 Serviceability criteria

Serviceability Criteria is a critical concept in structural engineering that pertains to the functional usability of a structure under standard operating conditions. It represents the set of conditions that a structure must meet to effectively serve its intended purpose, such as deflection limits, vibration criteria, and durability considerations. These criteria ensure the comfort and safety of the occupants, as well as the longevity of the structure, making them a cornerstone of efficient and effective structural design.

4.3.6.1. Deflection limits

Deflections of structure under serviceability limit state (SLS) load combinations of variable actions. The deflection condition must satisfy the requirement in equation 4.1.

$f < \text{Span}/300 = L/300$ (4.2)

4.3.6.2. Global Buckling

In order to maintain structural stability, buckling analysis will be carried out for each element in the structure. The safety criterion against buckling is that the first buckling mode factor should be at least 1.

4.4 Design Loading

The loads exposed on the structure have been explained in detail in the respective sections.

4.4.1 Dead load

In structures, the loads that continuously affect the structure, such as the self-weight of the structural system, floor and cladding weights, lighting system, installation weights, etc., are referred to as dead loads. In this thesis, the self-weight of the elements is automatically calculated by the SAP2000 program.

The material properties of the structural steel profile used in the building system are as follows. Material Design Properties for Structural Steel S355 according to EN1993-1-1 §3.2.6

- Steel Grade : S355 Grade Steel
- Ultimate Strength, (fu) : 49 kN/cm² (490MPa)
- 0,2 Proof Strenght, (fy) : 35,5 kN/cm² (355MPa)
- Young's Modulus, (E) : 210 000MPa

The dead load due to glass cladding is considered to be 0.60 kN/m^2. The following values are used in the load calculations:

Laminated glass consists of the following layers:

- Fully tempered glass (FT): 10 mm
- Air gap: 16 mm
- Heat-strengthened glass (HT): 6 mm
- PVB interlayer: 1.52 mm
- Heat-strengthened glass: 6 mm
- The total glass thickness is t = 10mm+6mm+6mm=22 mm
- Elastic modulus of glass (E): 70,000 MPa
- Poisson's ratio of glass: 0.23
- Unit weight of glass (γ_{cam}): 25 kN/m^3

4.4.2 Roof live load and maintenance load

Loads that will not remain for a long time during the service life are referred to as movable loads, and unless there are very low probabilities, the structure is not subjected to movable loads. These loads can be applied for cleaning and maintenance on the exterior and interior surfaces of the cladding. The additional service load (Qr) has been defined as 0.25 kN/m^2 to account for a possible additional loading.

4.4.3 Temperature

In this thesis, numerous factors influencing the structural behavior of single-layer free-form systems have been evaluated. However, the potential impact of temperature loads on these systems has been left outside the scope of this study. Temperature loads arise from the thermal expansion and contraction characteristics of materials and can have a decisive effect on structural performance. Particularly in regions where severe temperature fluctuations occur, temperature loads are a significant factor that needs to be considered in structural design and analysis. Nevertheless, in this thesis, the detailed thermal analyses necessary to model and analyze the complex effects of temperature loads have not been conducted. This presents a potential topic for future research, thereby enabling a better understanding of the impacts of temperature loads on single-layer free-form systems and utilizing this information to enhance the system's overall performance.

4.4.4 Seismic load

In analyzing the single-story free-form structure, earthquake loads were considered according to the "TBDY 2018-Turkey Building Earthquake Code" since earthquake loads, although potentially less critical than wind and snow loads, can still affect load combinations.

The chosen location for the structure with high seismic activity is the Bakırköy district in Istanbul, Turkey. By considering the specific seismicity of the region, the appropriate seismic design parameters and loads specified in the TBDY 2018 are applied to the analysis. It ensures that the structure is designed to withstand the expected seismic forces in the given location.

The earthquake force has been calculated based on the seismic design provisions of the "TBDY 2018 - Turkish Building Earthquake Code" using the DD-2 seismic ground motion, which represents rare earthquake ground motions with a 10% probability of being exceeded in 50 years and a return period of 475 years.

For the DD-2 seismic ground motion level, the short period (SS) and 1.0-second period (S1) design spectral acceleration coefficients are provided in the Turkey Earthquake Hazard Maps. These spectral acceleration coefficients are defined as dimensionless factors by dividing the design spectral accelerations for a reference site condition [(VS)30 = 360 m/s] with a damping ratio of 5% by the gravitational acceleration (TBDY 2018).

By using these design spectral acceleration coefficients, the earthquake forces are determined and applied to the analysis of the structure. It ensures that the structure is designed to withstand the seismic forces expected in the specified seismic ground motion level.

Also other accepted coefficients;

- Carrier System Behavior Coefficient was taken as R=3.
- Building Use Categories and Building Importance Factor was taken as I=1.

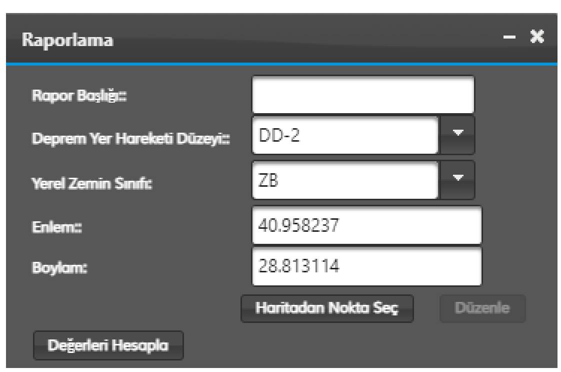

Figure 4.17 Latitude and Longitude

The map spectral acceleration coefficients are converted to design spectral acceleration coefficients by multiplying them with local soil amplification factors. The structures in the model will be analyzed according to the following assumptions:

The analysis will be conducted based on the earthquake ground motion level referred to as DD-2, which has a 10% probability of being exceeded within 50 years. The local soil class is assumed to be "B."

The dimensionless spectral acceleration coefficients obtained from the map provided by AFAD for the study area are S_S = 1.339 and S_1 = 0.362 (Figure 4.2 and Figure 4.3).

The geographical coordinates indicated on the map are 40.95823701749438° latitude and 28.813113634857437° longitude. The local soil amplification factors (F_S and F_1) to be considered based on the local soil classes are presented in table 4.6. and table 4.7. It is stated that linear interpolation can be applied for intermediate values of the map spectral acceleration coefficients in the local soil amplification factor tables. The design spectral acceleration coefficients are calculated according to equations 4.3 and 4.4 as follows:

$$S_{DS} = 1{,}339 \times 0{,}9 = 1{,}205 \tag{4.3}$$

$$S_{D1} = 0{,}362 \times 0{,}8 = 0{,}290 \tag{4.4}$$

The equivalent seismic load method is used for the seismic analysis of the structures. Additionally, one model is also analyzed using the Modal Superposition Method. For any earthquake ground motion level, the Vertical Elastic Design Spectrum graph (Figure 4.20) represents S_{ae}, dependent on T, in terms of acceleration due to gravity. The generated Horizontal Elastic Design Spectrum graph for the model is presented in figure 4.21.

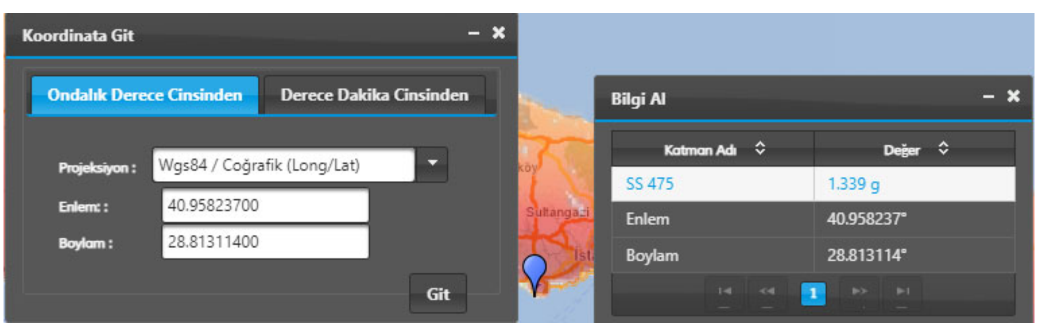

Figure 4.18 S_S Value calculation

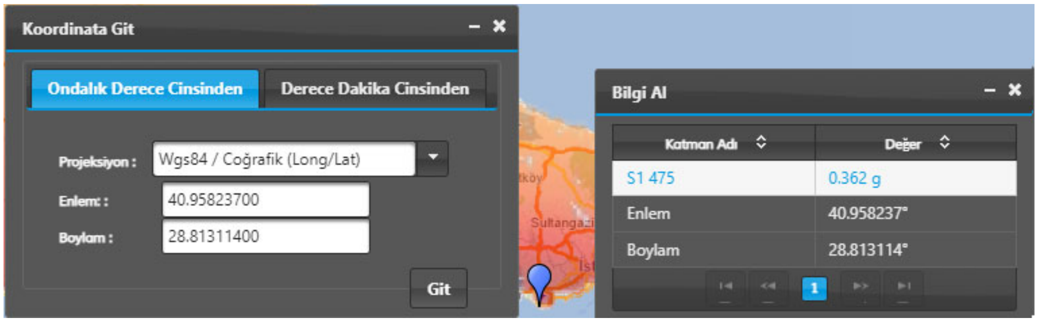

Figure 4.19 S_1 Value calculation

Table 4.5 Soil class table

Local Soil Class	Soil Type	Average at the top 30 meters		
		(Vs)30 [m/s]	(N 60)30 [darbe/30 cm]	(Cu)30 [kPa]
ZA	Soild, hard rocks	>1500	_	_
ZB	Less, moderately strong rocks	760- 1500	_	_
ZC	Very hard stand, gravel and hard clay layers, weak rocks with many cracks	360 – 760	>50	>250
ZD	Meduim dense or dense sand, gravel or very solid clay	180 - 360	15-50	70 - 250
ZE	Loose sand, gravel, or soft to solid clay layers or profiles with a total thickness of more than 3 meters of soft clay layer (Cu< 25 kPa) satsifying PI > 20 and w > %40	< 180	< 15	< 70
ZF	Soils that require site-specific investigation and evaluation: 1) Soils that have the risk of collapse and potential collapse under the influence of earthquakes (liquefiable soils, highly sensitive clays, collapsible weak cement soils, etc.), 2) Peat and/or organic content with a total thickness of more than 3 meters high clays, 3) High plasticity (PI>50) clays with a total thickness of more than 8 meters, 4) Very thick (> 35 m) soft or medium solid clays.			

Table 4.6 Local soil effect coefficients for a short period (TSC2018)

Local Soil Category	Local soil effect coefficients for short period Fs					
	S≤ 0.25	S =0.50	S= 0.75	S = 1.00	S = 1.25	S ≥ 1.50
ZA	0.8	0.8	0.8	0.8	0.8	0.8
ZB	0.9	0.9	0.9	0.9	0.9	0.9
ZC	1.3	1.3	1.2	1.2	1.2	1.2
ZD	1.6	1.4	1.2	1.1	1.0	1.0
ZE	2.4	1.7	1.3	1.1	0.9	0.8
ZF	Special soil behavior analysis will be done					

Table 4.7 Local soil effect coefficients for 1. second period (TSC2018)

Local Soil Category	Local soil effect coefficients for 1.second period F1					
	S≤ 0.10	S =0.20	S= 0.3	S = 0.4	S = 0.5	S ≥ 0.6
ZA	0.8	0.8	0.8	0.8	0.8	0.8
ZB	0.8	0.8	0.8	0.8	0.8	0.8
ZC	1.5	1.5	1.5	1.5	1.5	1.4
ZD	2.4	2.2	2.0	1.9	1.8	1.7
ZE	2.4	3.3	2.8	2.4	2.2	2.0
ZF	Special soil behavior analysis will be done					

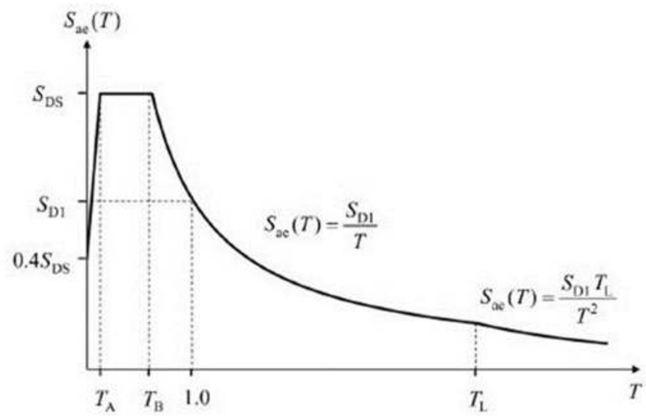

Figure 4.20 Local Ground Effect Coefficient F1 for 1.0 second period

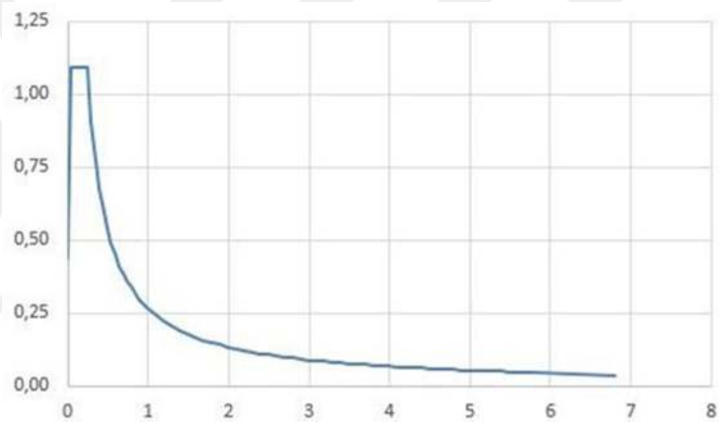

Figure 4.21 TBDY - Horizontal elastic design spectrum graph

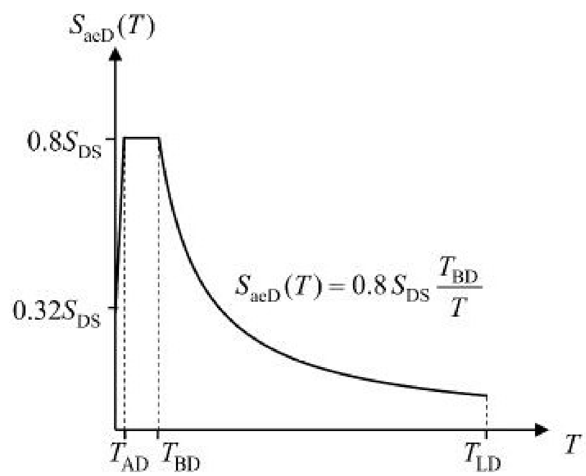

Figure 4.22 Vertical elastic design spectrum graph

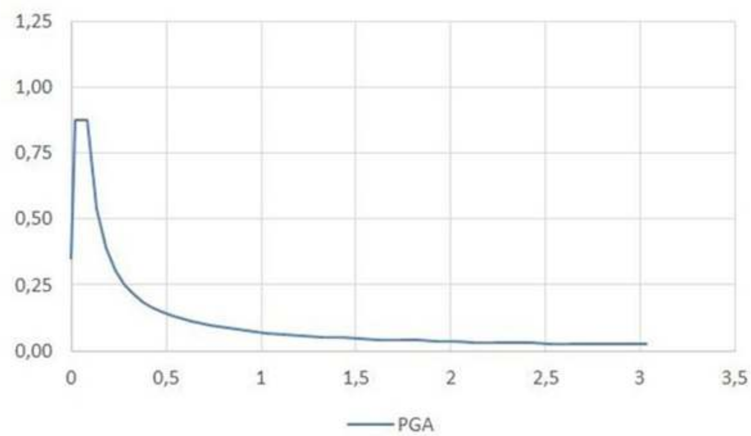

Figure 4.23 Vertical elastic design spectrum

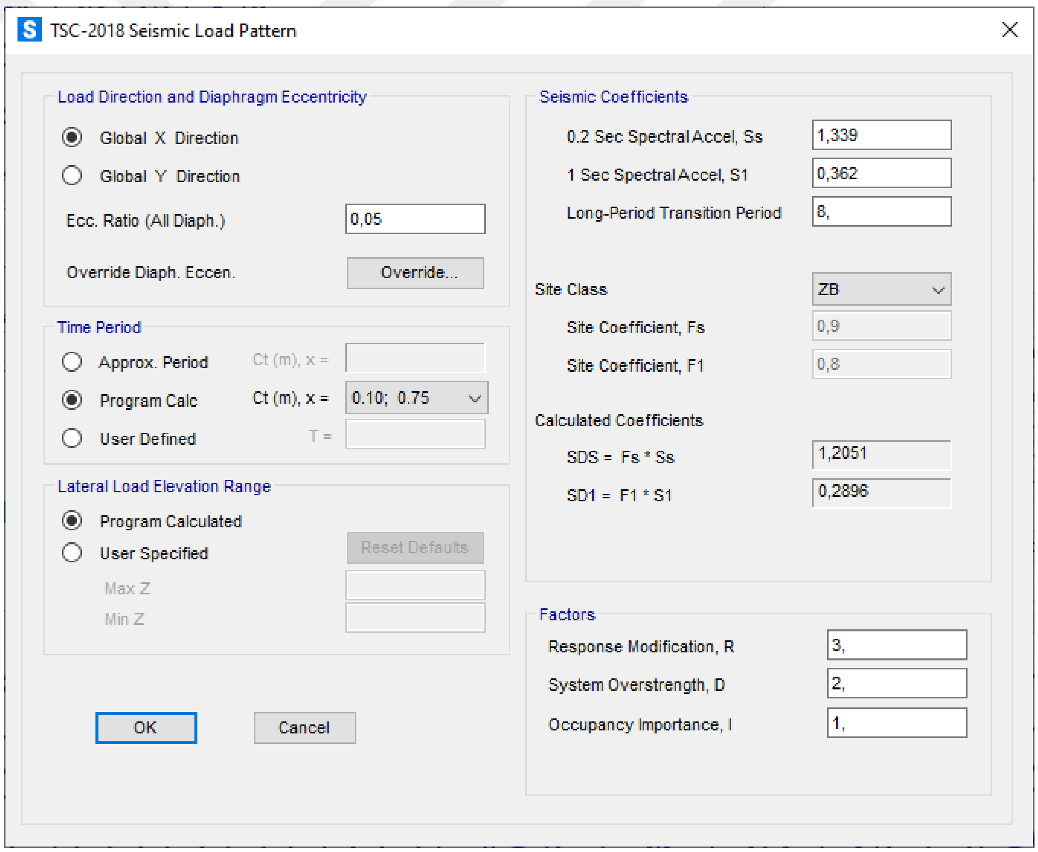

Figure 4.24 Seismic load pattern in the X direction

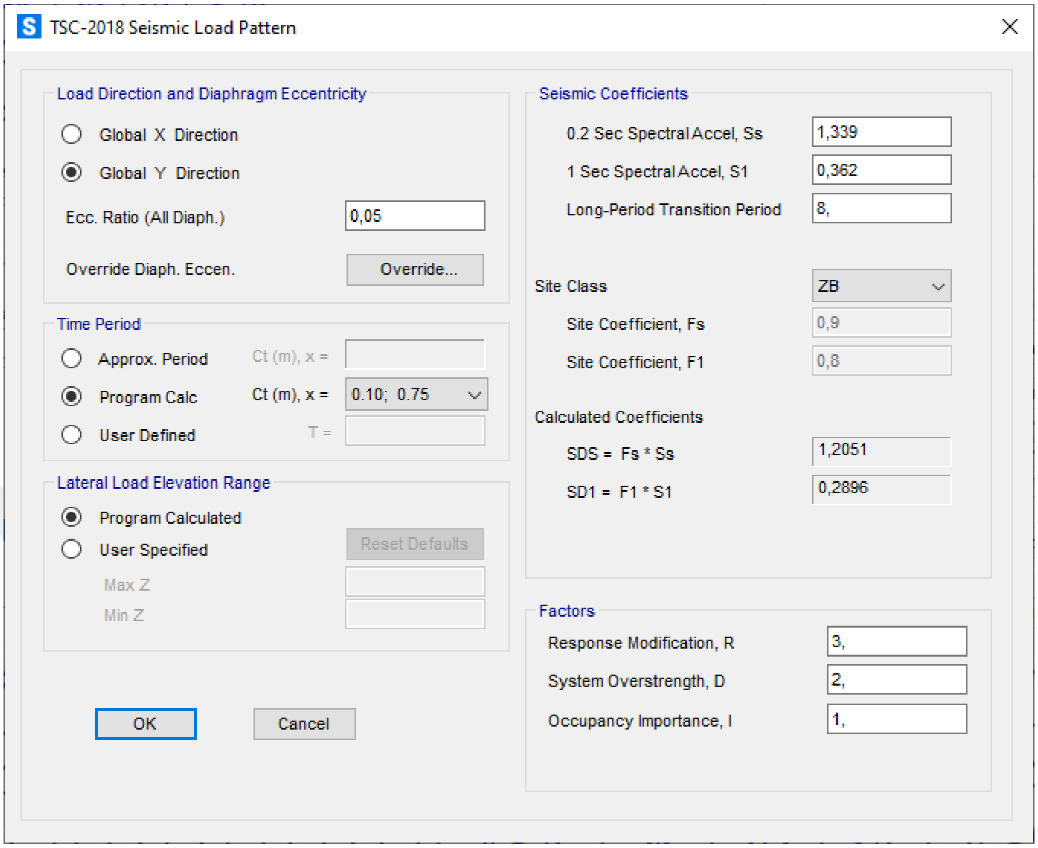

Figure 4.25 Seismic load pattern in the Y direction

4.4.5 Snow load

The stability of single-layer free-form structures is greatly threatened by snow load. Due to its double-curved structure, the fallen snow can accumulate evenly or cause asymmetric loading due to factors such as wind. Therefore, in design and calculations, the different ways in which snow loads can occur should be taken into account (Soare 1963).

Snow loads are calculated according to the TS EN 1991-1-3, considering accumulated and drifting snow loads. The principles applied for cylindrical roofs in the relevant standard are considered.

The structure is located in Bakırköy district of Istanbul, Turkey (elevation: 65 m), and the characteristic ground snow load is defined as 0.75 kN/m^2.

The calculation of the permanent and temporary design roof snow load value is performed according to equation 4.10. The roof snow load is calculated according to TS EN 1991-1-3 as follows:

$$s = \mu_i C_e C_t s_k \qquad (4.4)$$

Where; s: Roof snow load value (kN/m^2), μ_i: Shape factor for snow load, C_e: Surface Exposure Factor, C_t: Thermal factor.

C_e factor is determined from table 4.8 while μi factor is determined from figure 4.28. Considering the location, C_e = 1, C_t = 1 is assumed due to the use of glass cover, and μ_1 = 0.8 is assumed for variable roof slope between 0º-30º. These values are substituted into equation 4.5 to calculate the roof snow load.

The shape factor value for accumulated snow load in case (ii) is determined according to TS EN 1991-1-3 Section 5.3.5.

$$
\begin{aligned}
&\beta > 60^\circ \text{ for} && \mu_3 = 0; \\
&\beta \leq 60^\circ \text{ for} && \mu_3 = 0{,}2 + 10\, h/b
\end{aligned}
\tag{4.5}
$$

The equation for the shape factor value is obtained using the equations provided in TS EN 1991-1-3 Section 5.3.5. According to Note 1 of Section 5.3.5, the recommended upper limit value is 2.00.

Unaccumulated snow load calculation for the given scenario is as follows:

s = 0.8 x 1.0 x 1.0 x 0.75 = 0.60 kN/m^2

The calculation of the accumulated snow load for Case (ii) is as follows:

$s_{\mu 3}$ = 2 x 1.0 x 1.0 x 0.75 = 1.50 kN/m^2

$s_{0.5(\mu 3)}$ = 1.50 / 2=0.75 kN/m^2

The distribution of accumulated and unaccumulated snow load on the structure is shown in Figure 4.26.

Table 4.8 Recommended values of Ce for different topographies

Topography	C_e
Windswept [a]	0,8
Normal [b]	1,0
Sheltered [c]	1,2

[a] *Windswept topography*: flat unobstructed areas exposed on all sides without, or little shelter afforded by terrain, higher construction works or trees.

[b] *Normal topography*: areas where there is no significant removal of snow by wind on construction work, because of terrain, other construction works or trees.

[c] *Sheltered topography*: areas in which the construction work being considered is considerably lower than the surrounding terrain or surrounded by high trees and/or surrounded by higher construction works.

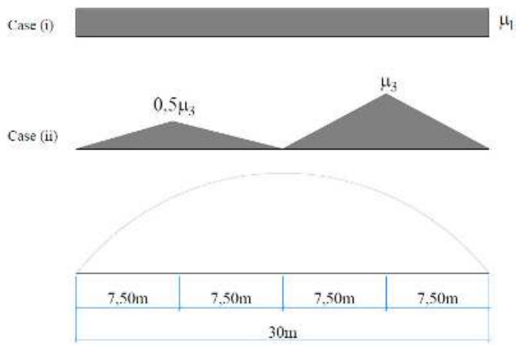

Shape coef.	Coef.	Loading (kN/m²)
μ_1	0.80	0.60
μ_3	2.00	1.50
$0.5\mu_3$	2,00	0.75

Figure 4.26 The distribution of snow load and snow load shape coefficient

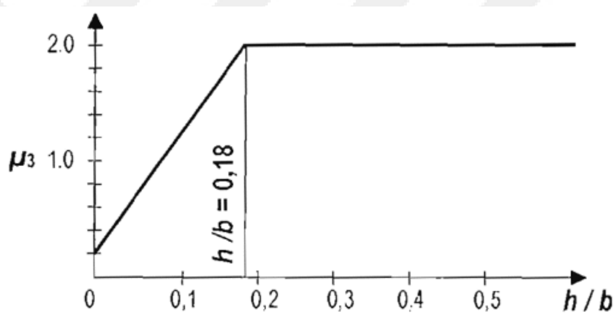

Figure 4.27 Recommended snow load shape coefficient (TS EN 1991-1-3)

Based on this information, a shape coefficient of $\mu_3 = 2$ is chosen.

Angle of pitch of roof α	$0° \leq \alpha \leq 30°$	$30° < \alpha < 60°$	$\alpha \geq 60°$
μ_1	0,8	$0.8(60 - \alpha)/30$	0,0
μ_2	$0,8 + 0,8\ \alpha/30$	1,6	--

Figure 4.28 Snow load shape coefficients (TS EN 1991-1-3)

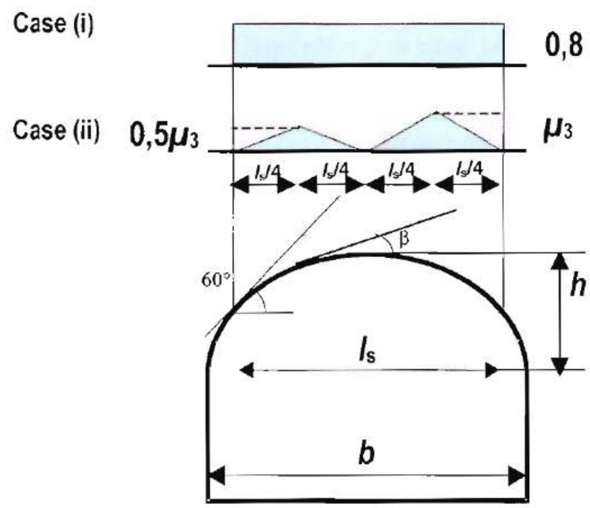

Figure 4.29 Snow load shape coefficients for cylindrical roof

The accumulated snow load, shown in Figure 4.26, was applied using the method given in Figure 4.30 for both fully and half-loaded areas (Figure 4.31-4.32).

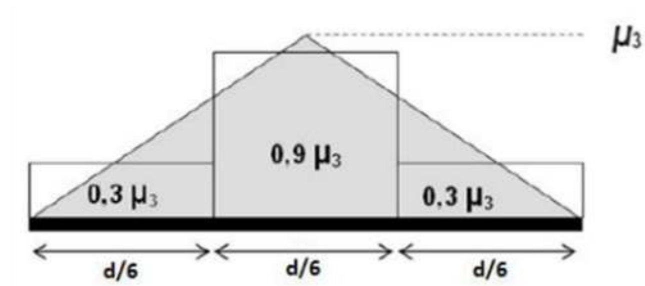

Figure 4.30 Case (ii) drifted snow load shape coefficient (Maten 2011)

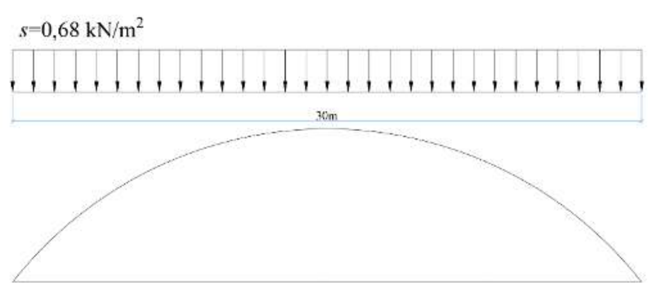

Figure 4.31 Case (i) undrifted snow load distribution

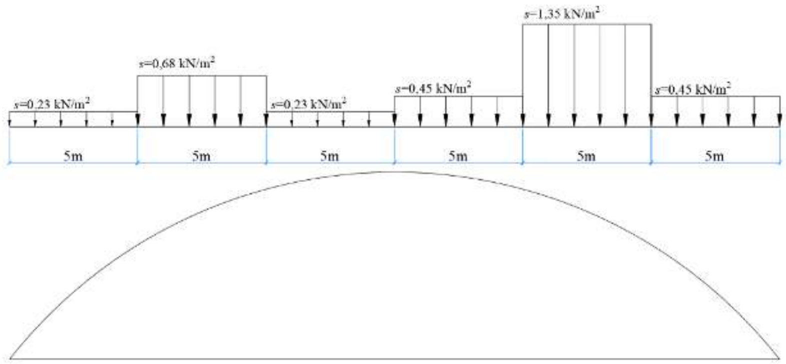

Figure 4.32 Case (ii) drifted snow load distribution

4.4.6 Wind load

Wind load can significantly affect the stability of structures such as high-rise buildings, port structures, low-slope steel structures, high-voltage transmission line towers, double-curved free-form systems, and vaulted structures. Therefore, careful consideration should be given to wind loading in these structures. In modern technology, experimental studies using wind tunnel tests can be conducted to assess wind loads. However, due to the cost involved, this approach is usually chosen for large-scale projects only.

Numerous studies have investigated the effects of wind loads on single-layer free-form structures, leading to a better understanding of their behavior and load distribution. However, wind tunnel tests should always be considered when dealing with large openings because predicting the asymmetric load distribution caused by wind loads can be challenging.

In our country, TS EN 1991-1-4 is used to calculate wind forces. This code includes various parameters for calculating the wind load. In this thesis, the following parameters have been used when calculating the wind loads to be applied to the models.

Wind Load Calculation

Basic wind velocity: v_b = 28 m/s

Terrain category: = II

Reference height from the ground of the examined part of the structure: z_e = 27 m

Terrain category		z_0 m	z_{min} m
0	Sea or coastal area exposed to the open sea	0,003	1
I	Lakes or flat and horizontal area with negligible vegetation and without obstacles	0,01	1
II	Area with low vegetation such as grass and isolated obstacles (trees, buildings) with separations of at least 20 obstacle heights	0,05	2
III	Area with regular cover of vegetation or buildings or with isolated obstacles with separations of maximum 20 obstacle heights (such as villages, suburban terrain, permanent forest)	0,3	5
IV	Area in which at least 15 % of the surface is covered with buildings and their average height exceeds 15 m	1,0	10
NOTE: The terrain categories are illustrated in A.1.			

Figure 4.33 Terrain categories and terrain parameters (TS EN 1991-1-4)

Orography factor at reference height z_e: $c_0(z_e) = 1$

Nationally Defined Parameters

Air density: $\rho = 1.25$ kg/m^3

Calculation of peak velocity pressure

Basic wind velocity

The basic wind velocity, $v_b = 28.00$ m/s.

$vb = cdir \cdot c\ season \cdot vb{,}0$

According to TS EN 1991-1-4, the basic value of the characteristic 10-minute wind speed at 10 meters above ground level in an open area on any day of the year and in any direction is calculated as vb,0. The wind direction factor, cdir, is taken as 1.00 according to Note 2 in TS EN 1991-1-4, Section 4.2. The seasonal factor, cseason, is taken as 1.00 according to Note 3 in TS EN 1991-1-4, Section 4.2. The basic value of the characteristic wind speed, vb,0, is taken as 28 m/s (100 km/h) based on the Design, Calculation, and Construction Principles of Steel Structures.

Peak velocity pressure

The peak velocity pressure $q_p(z_e)$ at reference height z_e includes mean and short-term velocity fluctuations. It is determined according to *EN1991-1-4 equation 4.8*:

$q_p(z_e) = (1 + 7 \cdot I_v(z_e)) \cdot (1/2) \cdot \rho \cdot v_m(z_e)^2$

$q_p(z_e) = (1 + 7 \cdot 0.1589) \cdot (1/2) \cdot 1.25$ kg/m$^3 \cdot (33.47$ m/s$)^2$

$q_p(z_e) = 1479$ N/m^2

$\Rightarrow q_p(z_e) = 1.48$ kN/m^2

How wind loads on vaulted roofs at the Eurocode 1 are calculated:
Specifically, we will show how to use Figure 4.34 from EN1991-1-4, which provides the external pressure coefficients on vaulted roofs with rectangular base:

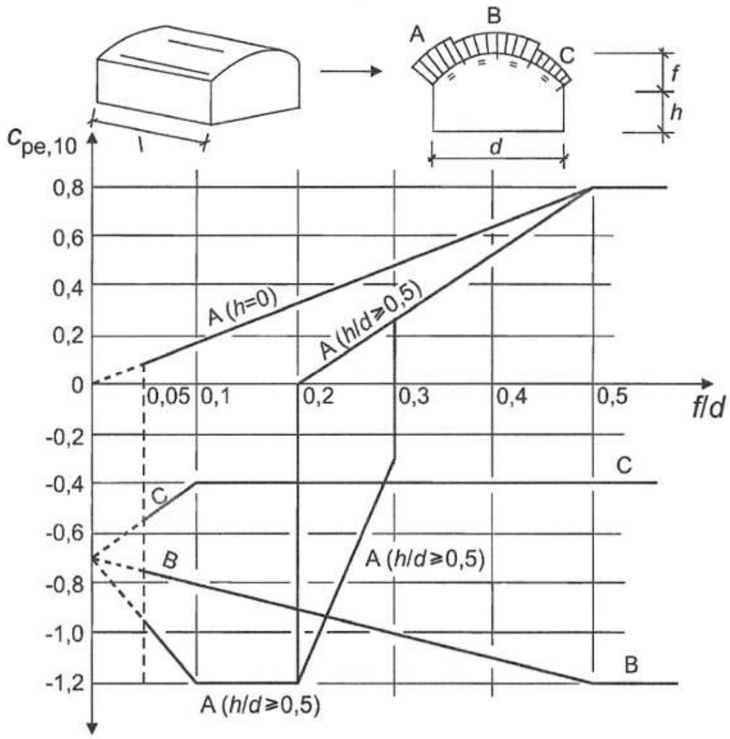

Figure 4.34 Distribution of shape factor (cpe,10) (TS EN 1991-1-4)

We will consider a structure with the following dimensions:

f = 7,30m

h = 19,70m

d = 30,0m

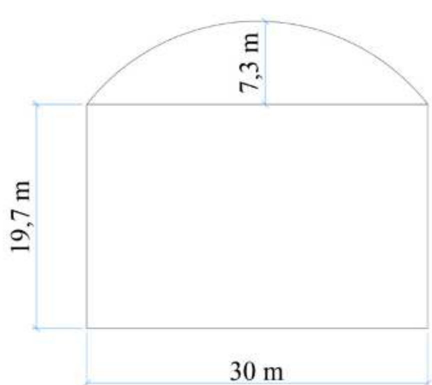

Figure 4.35 Front view of structure

The developed length of the vaulted roof will be split into four equal parts for zone A, zone B (repeated twice), and zone C:

In our case:

f/d= 7,30 / 30,0 =0,24

h/d= 19,70 / 30,0 =0,66

- **<u>For zone A</u>**

We start on the f/d axis until we reach the related to zone A:

We read: **$C_{pe10,A}$= +0,15**

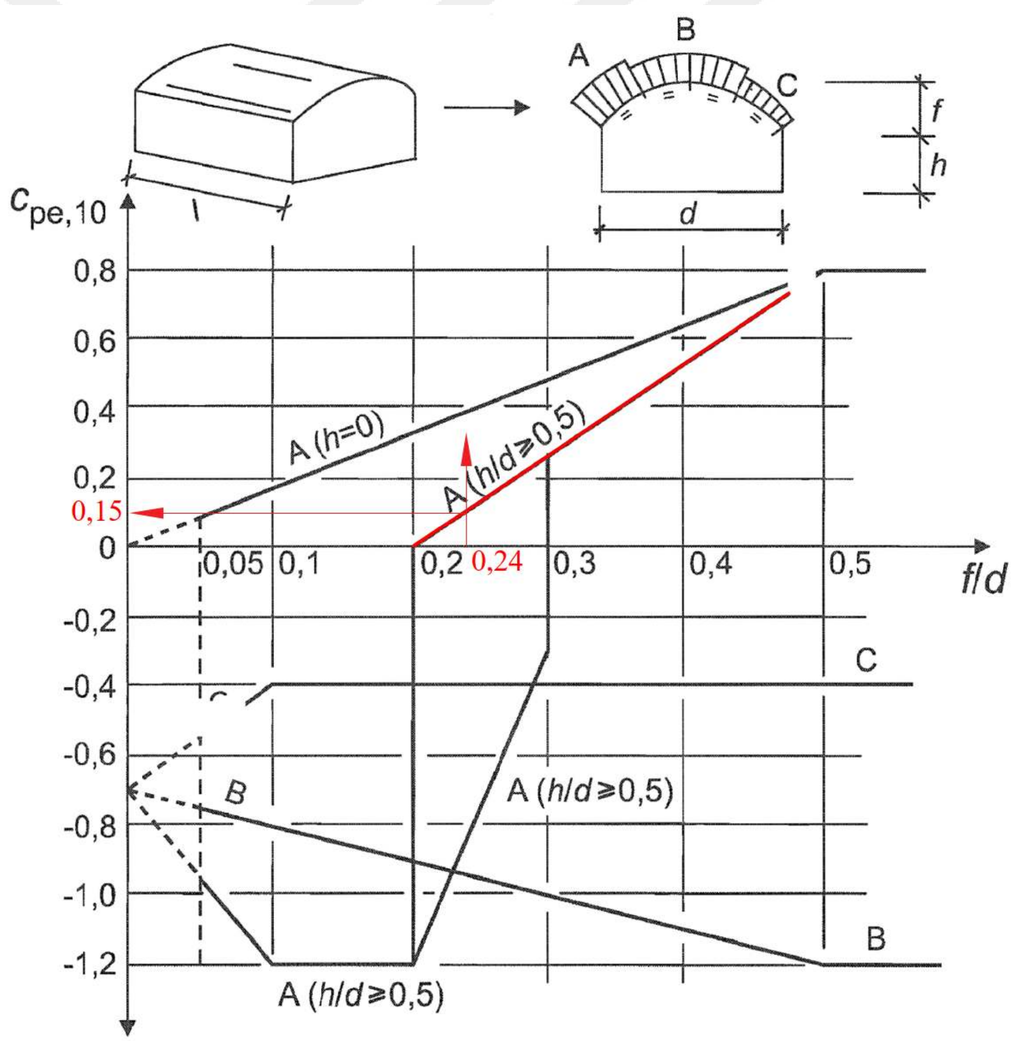

Figure 4.36 Distribution of shape factor (cpe,10) for Region A

- **<u>For zone B</u>**

We start on the f/d axis until we reach the zone B diagram.

We read: $\mathbf{C_{pe10,B} = -0,95}$

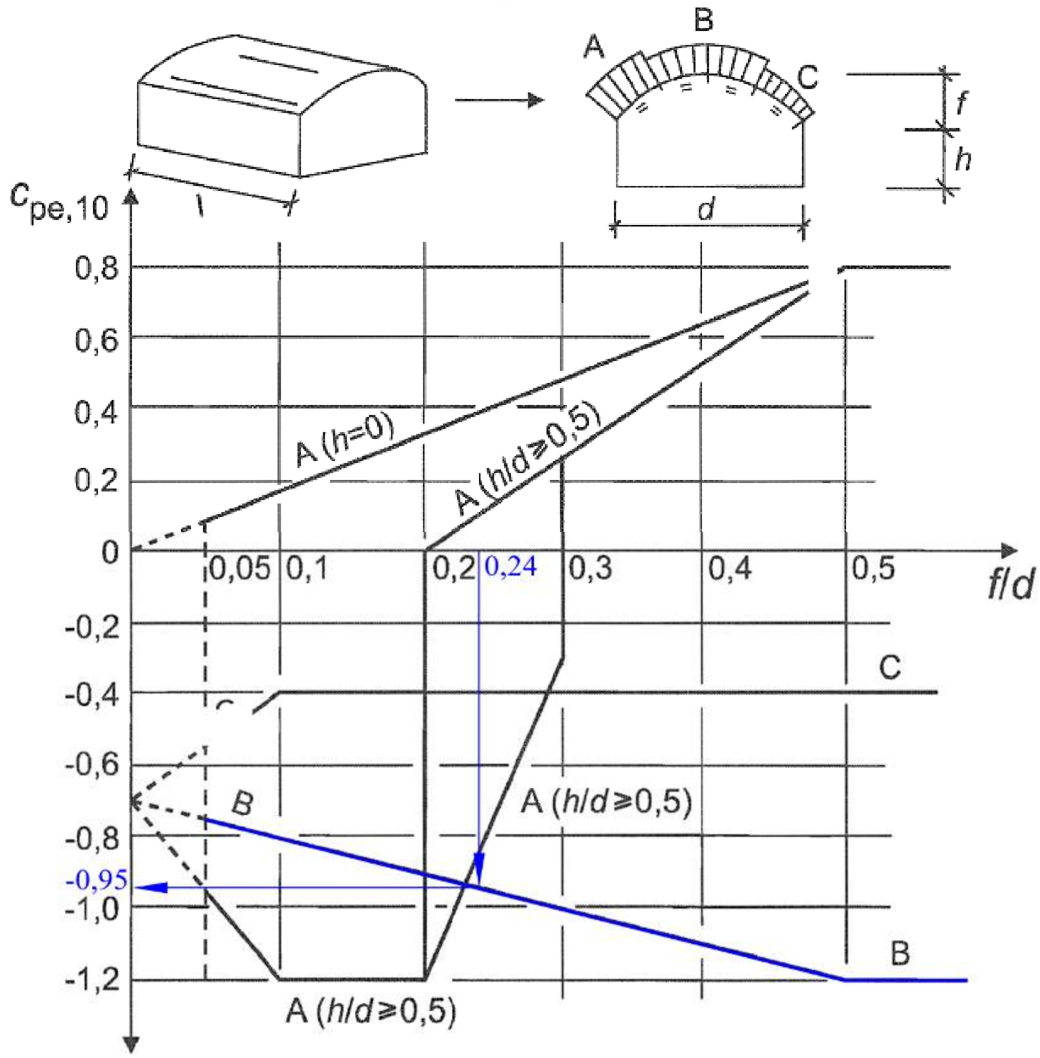

Figure 4.37 Distribution of shape factor ($cpe,_{10}$) for Region B

- **For zone C**

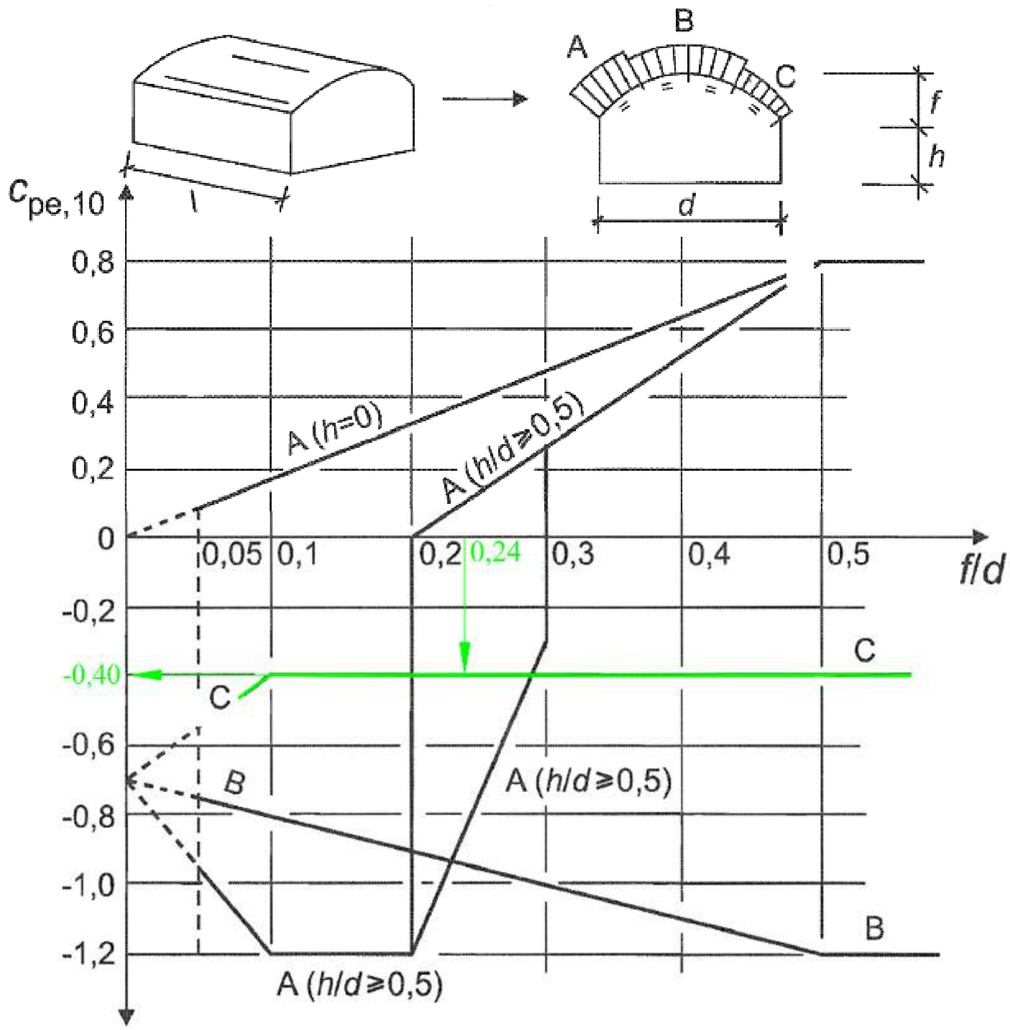

Figure 4.38 Distribution of shape factor (cpe,10) for Region C

We read: $\mathbf{C_{pe10,C} = -0,40}$

In the end:

For zone A => $\mathbf{C_{pe10,A} = +0,15}$

For zone B => $\mathbf{C_{pe10,B} = -0,95}$

For zone C => $\mathbf{C_{pe10,C} = -0,40}$

The ratios h/d = 0.66 and f/d = 0.24 for the modeled free-form system have been calculated. With these values, the external pressure coefficients and wind pressures determined at points A, B, and C are provided in table 4.9.

Table 4.9 External pressure coefficients and wind pressures at points A, B, and C

	A	B	C
C_{pe10}	+0.15	-0.95	-0.40
we(kN/m^2)	+0.22	-1.41	-0.59

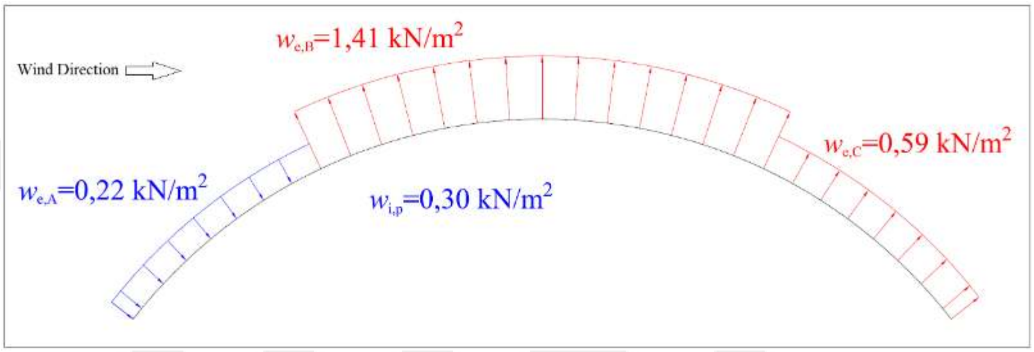

Figure 4.39 The wind pressure distribution

The wind pressure values at the corners of the lightweight cladding elements, intended for load application, have been calculated using interpolation based on the wind pressure values at points A, B, and C. The average of these four wind pressure values has been determined and applied normally to the surface of the cladding element. Due to the double-curved nature of the structures, the surface angles vary at each point. To ensure the closest application of wind loads to the design model, weightless shell elements have been modeled in the trapezoidal areas between the structural systems, and the wind loads have been applied to these surface elements.
The internal pressure coefficient (C_{pi}) is calculated based on the elements on the building facades. However, in this structure, this effect cannot be determined. Therefore, the recommended C_{pi} values of +0.2 and -0.3, according to TS EN 1991-1-4, have been used.

Table 4.10 The internal pressure coefficients (Cpi) and wind pressures

	c_{pi}	w_i (kN/m^2)
Positive	+0.2	w_{ip}= +0.30
Negative	-0.3	w_{in} = -0.45

Table 4.11 External pressure coefficients and pressures at points A, B, and C

	A	B	C
w_e (kN/m^2)	+0.22	-1.41	-0.59
C_{pe10}	+0.30	-0.45	-0.45
w_e (kN/m^2)	+0.52	-1.86	-1.04

The application of positive and negative internal wind pressures on the free-form system is as follows

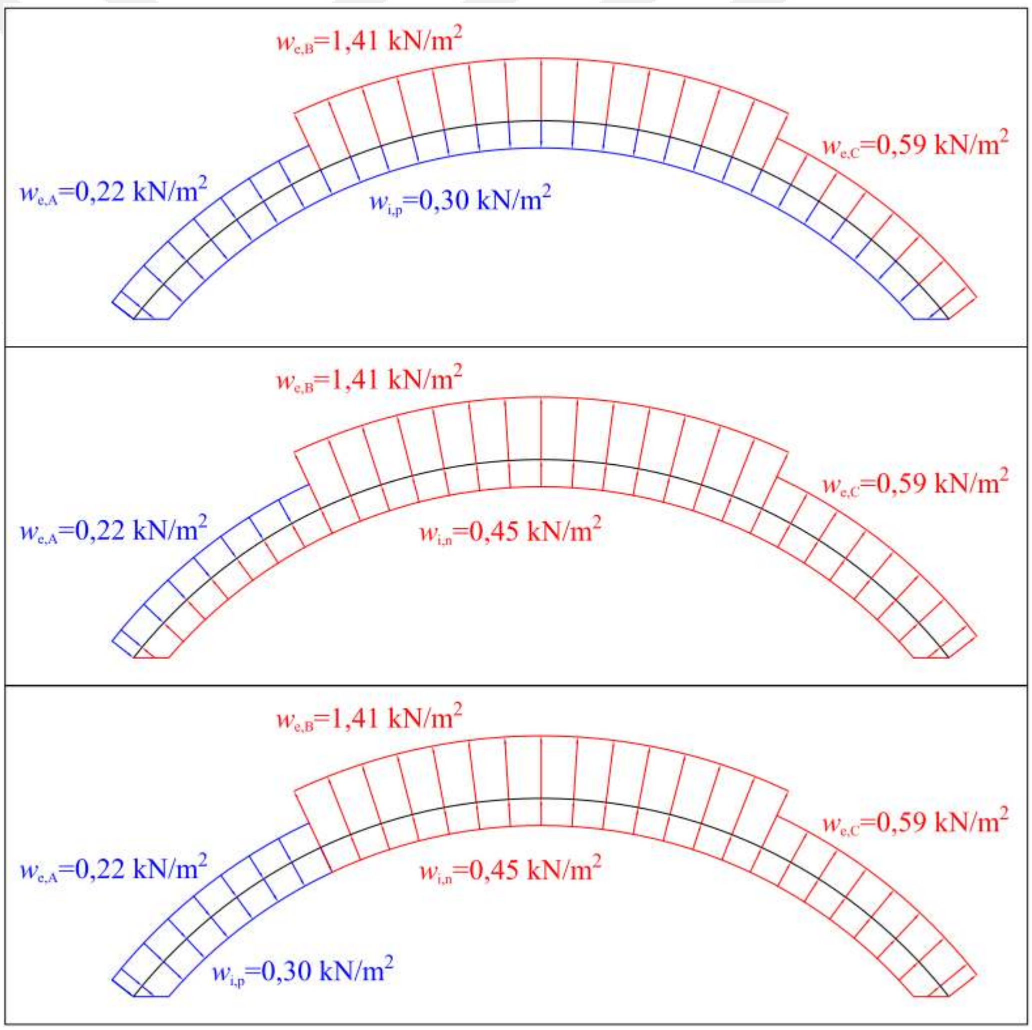

Figure 4.40 The positive, negative, and total internal and external wind pressures

4.5 Analysis and Evaluation of the Model

This section includes the investigated free-form structure's architectural design and static analysis. The architectural design focuses on conceptualizing and modeling the structure, considering its unique and non-conventional shape. Various design parameters such as form, aesthetics, functionality, and spatial organization are taken into account to create the architectural model of the free-form structure. Advanced software tools may generate the digital model, ensuring accuracy and precision.

Following the architectural design, the static analysis of the structure is performed. This analysis aims to assess the structural behavior and response of the free-form structure under different loading conditions. Structural analysis methods, such as finite element analysis (FEA), may be employed to determine the structure's internal forces, stresses, deformations, and stability. The analysis considers the free-form structure's complex geometry and structural elements to ensure its safety, stability, and performance.

The combination of architectural design and static analysis allows for the evaluation of both the aesthetic and functional aspects as well as the structural integrity of the free-form structure. This comprehensive approach ensures the design meets the required performance criteria while maintaining its unique architectural expression.

4.5.1 Description of structural system

The model of The British Museum Great Court Roof was primarily based on the model created by Mirtschin (2012). The CAD model was created by taking into account the geometric formulas in the thesis made by Williams (2001), see Figure 4.41. The CAD model doesn't precisely follow the description from the paper, but the paper allows something similar to be created.

The roof covers the whole area of the Great Court with a length of 97,15m and a width of 73,25m and spans from the edge of the surrounding buildings to the Reading Room in the middle, see Figure 4.42. The whole structure is formed by a net of triangular cells in a shell shape. Because the Reading Room is not exactly in the middle - it is slightly off towards the north - there is only one line of symmetry and therefore the geometry of all nodes and members is different. The roof spans vary in different directions. The span in the north is 29,13 m the arch height 7,30 m, the span in the east and west 14,63 m the arch height 3,55 m and the span in the south 24,03 m, the arch height 6,7 m, Figure 4.42-44.

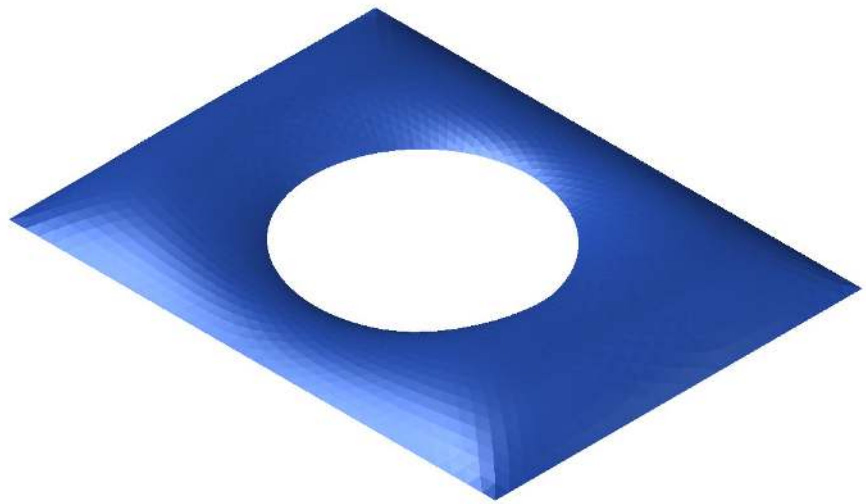

Figure 4.41 Perspective View of Model

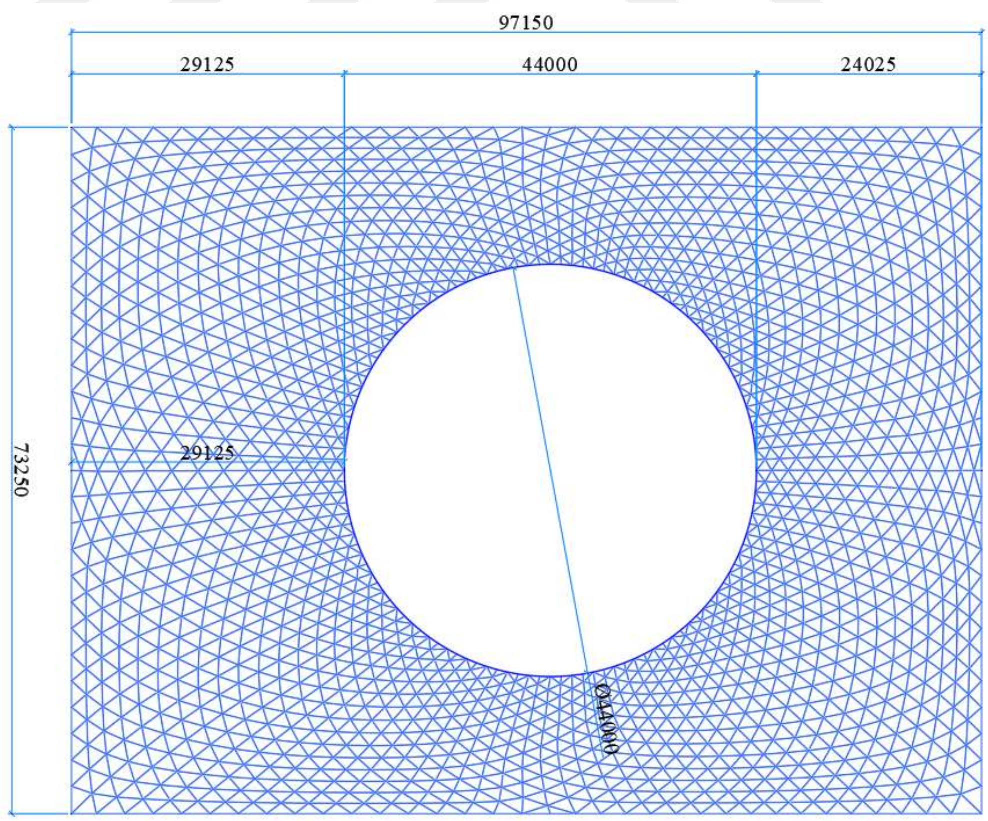

Figure 4.42 Plan view of model

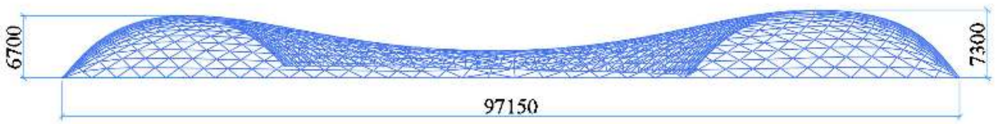

Figure 4.43 Section view of model

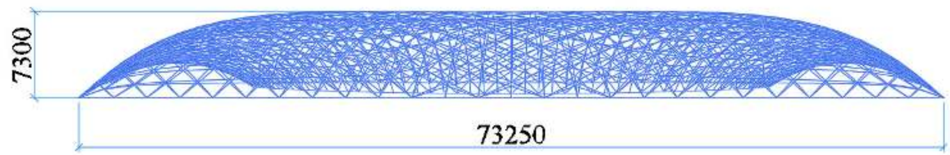

Figure 4.44 Side view of model

For the ultimate limit state analysis, nonlinear FE calculations have been run for all previously defined load combinations.

The structure's design is based on elastic material properties and elastic stress distribution within the sections (elastic–elastic design). Within global member design, no resources are considered based on any plastic deformation of the steel sections.

Accurately generating the structure's geometry in the free-form system is vital to avoid any pre-existing errors during the analysis and assembly stages. The 3D modeling software Rhinoceros 3D has been used in architectural modeling. Grasshopper's parametric modeling tool is integrated into the Rhinoceros program to optimize time and ensure dimension accuracy. The algorithmic tree developed for the free-form system in the software is illustrated in Figure 4.46. Each box in Figure 4.46 contains the parameters that define the structure's geometry. Any changes made to these parameters automatically update the other variables, enabling designers to quickly generate numerous models and conduct multiple analyses within a short period. The free-form visuals created using the program are also presented in Figure 4.47. The created model is transferred to the SAP2000 software for engineering analysis. Below are the plan and elevation views of the single-layer free-form system, which possesses shell behavior and is the subject of investigation in this thesis.

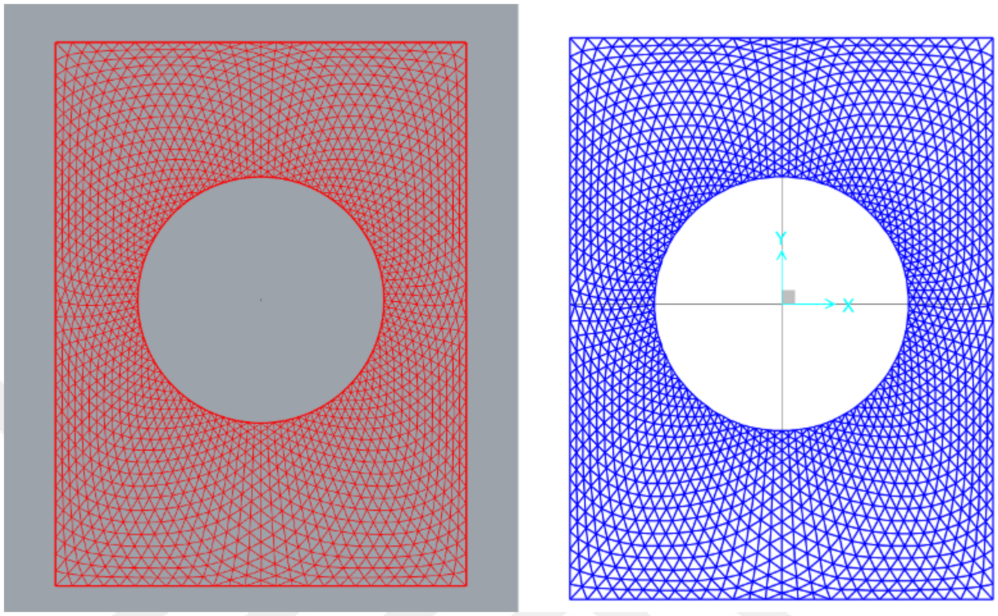

Figure 4.45 Geometry of Free-From, Plan View

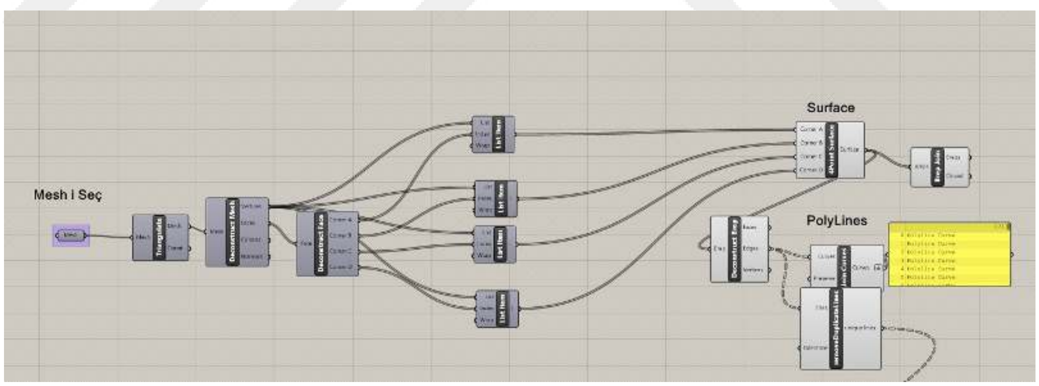

Figure 4.46 Algorithmic tree for the free-form system in Grasshopper software

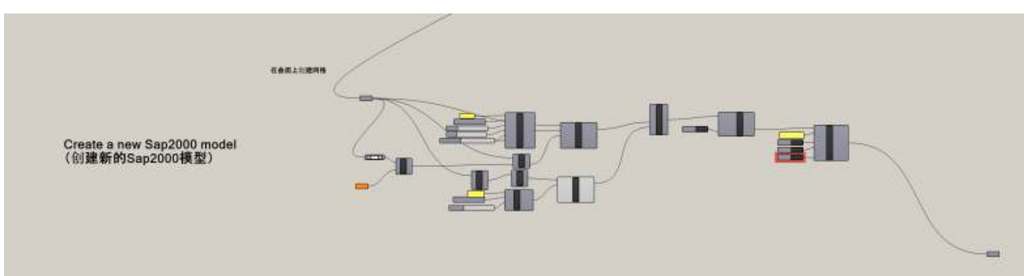

Figure 4.47 The algorithmic tree for data transfer from Grasshopper to SAP2000

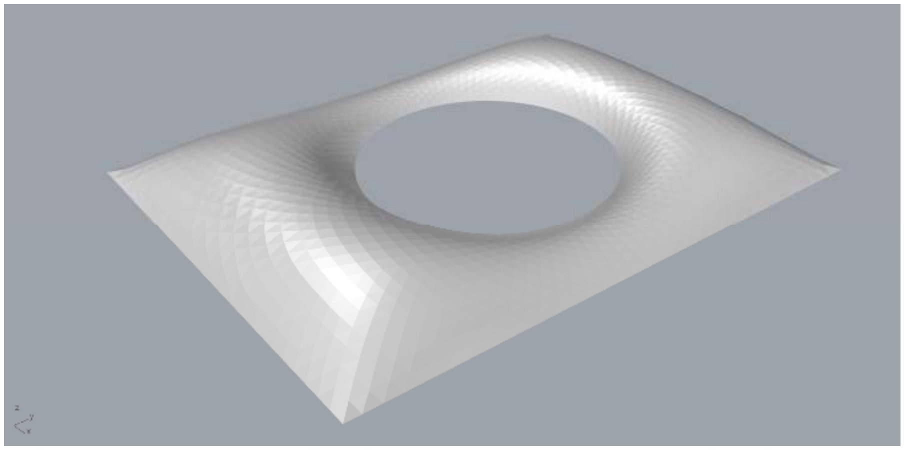

Figure 4.48 Free-form system model in Rhinoceros software

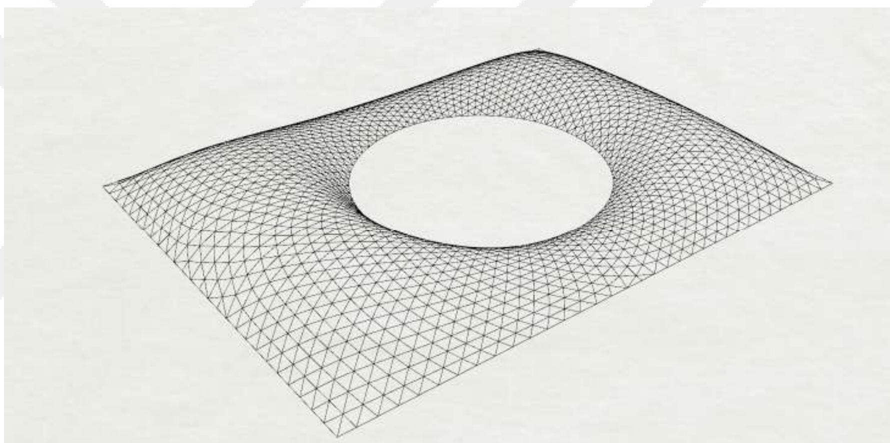

Figure 4.49 Free-form system model in Rhinoceros software

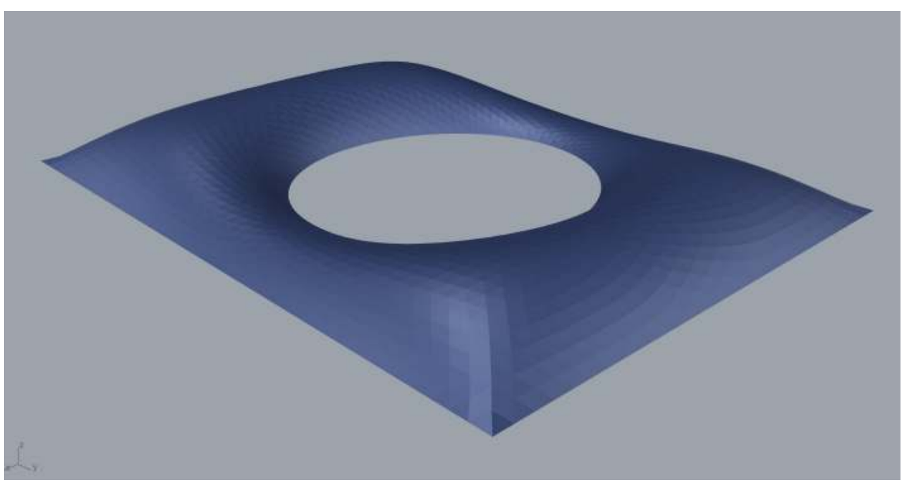

Figure 4.50 Free-form system model in Rhinoceros software

4.5.2 Support conditions

The arrangement of supports used in the structure is as follows.

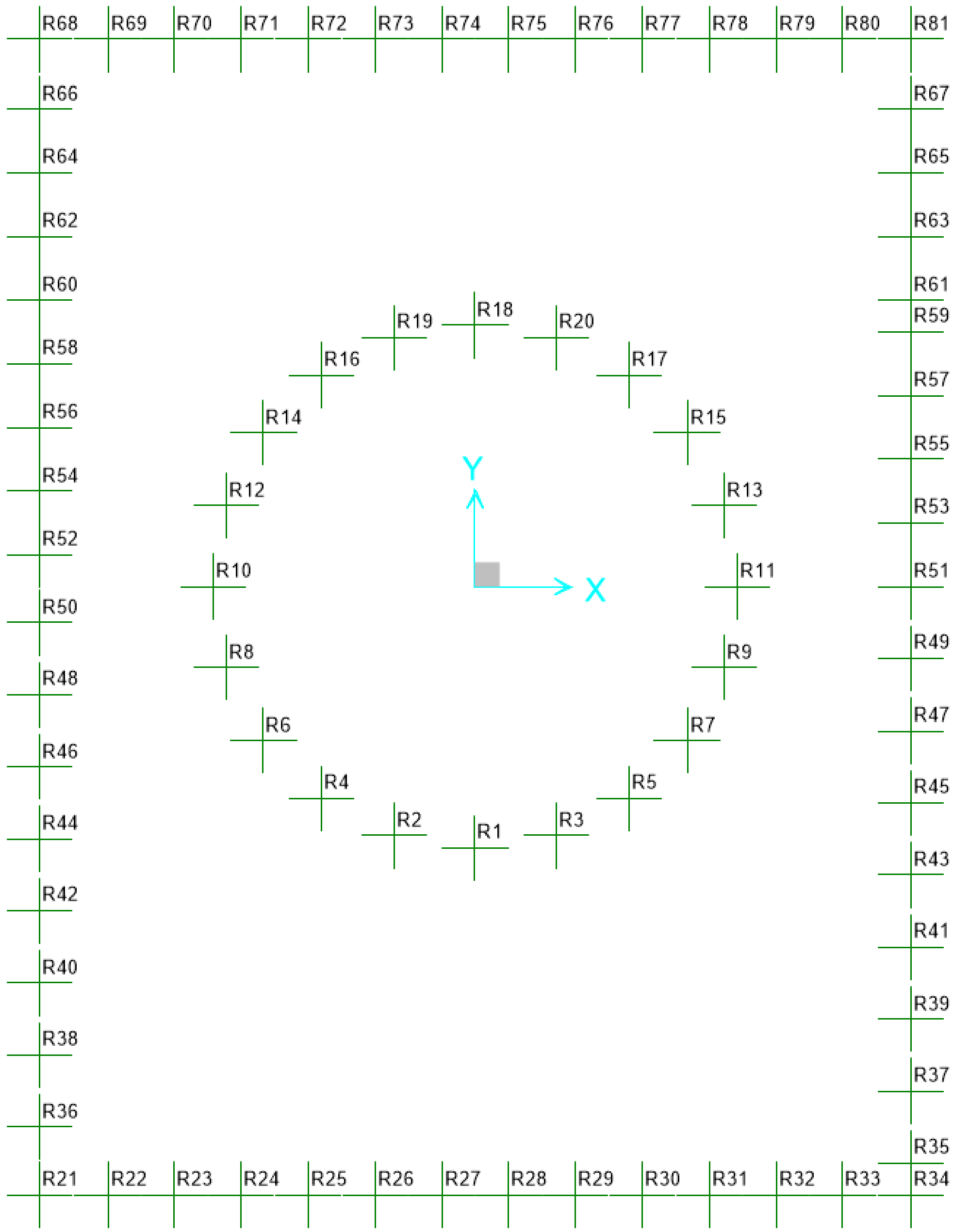

Figure 4.51 Restraint Labels

Table 4.12 Joint restraint assignments

Joint	U1	U2	U3	R1	R2	R3	Joint	U1	U2	U3	R1	R2	R3
Text	Yes/No	Yes/No	Yes/No	Yes/No	Yes/No	Yes/No	Text	Yes/No	Yes/No	Yes/No	Yes/No	Yes/No	Yes/No
R1	Yes	Yes	Yes	Yes	Yes	Yes	R42	Yes	Yes	Yes	Yes	Yes	Yes
R2	Yes	Yes	Yes	Yes	Yes	Yes	R43	Yes	Yes	Yes	Yes	Yes	Yes
R3	Yes	Yes	Yes	Yes	Yes	Yes	R44	Yes	Yes	Yes	Yes	Yes	Yes
R4	Yes	Yes	Yes	Yes	Yes	Yes	R45	Yes	Yes	Yes	Yes	Yes	Yes
R5	Yes	Yes	Yes	Yes	Yes	Yes	R46	Yes	Yes	Yes	Yes	Yes	Yes
R6	Yes	Yes	Yes	Yes	Yes	Yes	R47	Yes	Yes	Yes	Yes	Yes	Yes
R7	Yes	Yes	Yes	Yes	Yes	Yes	R48	Yes	Yes	Yes	Yes	Yes	Yes
R8	Yes	Yes	Yes	Yes	Yes	Yes	R49	Yes	Yes	Yes	Yes	Yes	Yes
R9	Yes	Yes	Yes	Yes	Yes	Yes	R50	Yes	Yes	Yes	Yes	Yes	Yes
R10	Yes	Yes	Yes	Yes	Yes	Yes	R51	Yes	Yes	Yes	Yes	Yes	Yes
R11	Yes	Yes	Yes	Yes	Yes	Yes	R52	Yes	Yes	Yes	Yes	Yes	Yes
R12	Yes	Yes	Yes	Yes	Yes	Yes	R53	Yes	Yes	Yes	Yes	Yes	Yes
R13	Yes	Yes	Yes	Yes	Yes	Yes	R54	Yes	Yes	Yes	Yes	Yes	Yes
R14	Yes	Yes	Yes	Yes	Yes	Yes	R55	Yes	Yes	Yes	Yes	Yes	Yes
R15	Yes	Yes	Yes	Yes	Yes	Yes	R56	Yes	Yes	Yes	Yes	Yes	Yes
R16	Yes	Yes	Yes	Yes	Yes	Yes	R57	Yes	Yes	Yes	Yes	Yes	Yes
R17	Yes	Yes	Yes	Yes	Yes	Yes	R58	Yes	Yes	Yes	Yes	Yes	Yes
R18	Yes	Yes	Yes	Yes	Yes	Yes	R59	Yes	Yes	Yes	Yes	Yes	Yes
R19	Yes	Yes	Yes	Yes	Yes	Yes	R60	Yes	Yes	Yes	Yes	Yes	Yes
R20	Yes	Yes	Yes	Yes	Yes	Yes	R61	Yes	Yes	Yes	Yes	Yes	Yes
R21	Yes	Yes	Yes	Yes	Yes	Yes	R62	Yes	Yes	Yes	Yes	Yes	Yes
R22	Yes	Yes	Yes	Yes	Yes	Yes	R63	Yes	Yes	Yes	Yes	Yes	Yes
R23	Yes	Yes	Yes	Yes	Yes	Yes	R64	Yes	Yes	Yes	Yes	Yes	Yes
R24	Yes	Yes	Yes	Yes	Yes	Yes	R65	Yes	Yes	Yes	Yes	Yes	Yes
R25	Yes	Yes	Yes	Yes	Yes	Yes	R66	Yes	Yes	Yes	Yes	Yes	Yes
R26	Yes	Yes	Yes	Yes	Yes	Yes	R67	Yes	Yes	Yes	Yes	Yes	Yes
R27	Yes	Yes	Yes	Yes	Yes	Yes	R68	Yes	Yes	Yes	Yes	Yes	Yes
R28	Yes	Yes	Yes	Yes	Yes	Yes	R69	Yes	Yes	Yes	Yes	Yes	Yes
R29	Yes	Yes	Yes	Yes	Yes	Yes	R70	Yes	Yes	Yes	Yes	Yes	Yes
R30	Yes	Yes	Yes	Yes	Yes	Yes	R71	Yes	Yes	Yes	Yes	Yes	Yes
R31	Yes	Yes	Yes	Yes	Yes	Yes	R72	Yes	Yes	Yes	Yes	Yes	Yes
R32	Yes	Yes	Yes	Yes	Yes	Yes	R73	Yes	Yes	Yes	Yes	Yes	Yes
R33	Yes	Yes	Yes	Yes	Yes	Yes	R74	Yes	Yes	Yes	Yes	Yes	Yes
R34	Yes	Yes	Yes	Yes	Yes	Yes	R75	Yes	Yes	Yes	Yes	Yes	Yes
R35	Yes	Yes	Yes	Yes	Yes	Yes	R76	Yes	Yes	Yes	Yes	Yes	Yes
R36	Yes	Yes	Yes	Yes	Yes	Yes	R77	Yes	Yes	Yes	Yes	Yes	Yes
R37	Yes	Yes	Yes	Yes	Yes	Yes	R78	Yes	Yes	Yes	Yes	Yes	Yes
R38	Yes	Yes	Yes	Yes	Yes	Yes	R79	Yes	Yes	Yes	Yes	Yes	Yes
R39	Yes	Yes	Yes	Yes	Yes	Yes	R80	Yes	Yes	Yes	Yes	Yes	Yes
R40	Yes	Yes	Yes	Yes	Yes	Yes	R81	Yes	Yes	Yes	Yes	Yes	Yes
R41	Yes	Yes	Yes	Yes	Yes	Yes							

4.5.3 Member sections

The selected profile types for the elements are as follows.

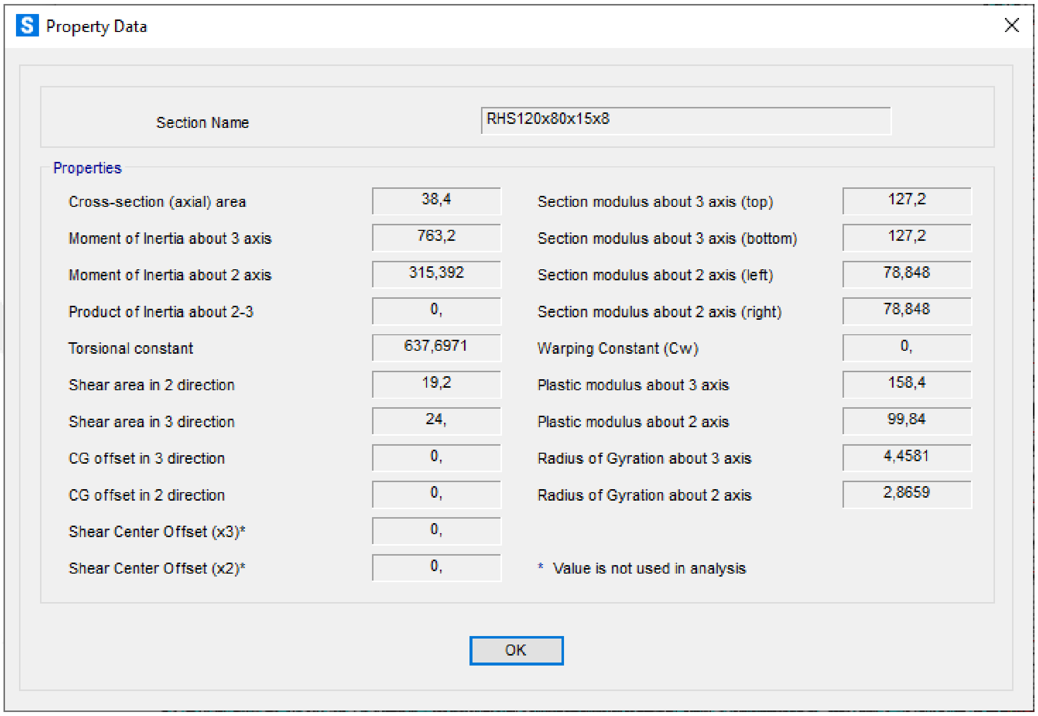

Figure 4.52 Profile Properties

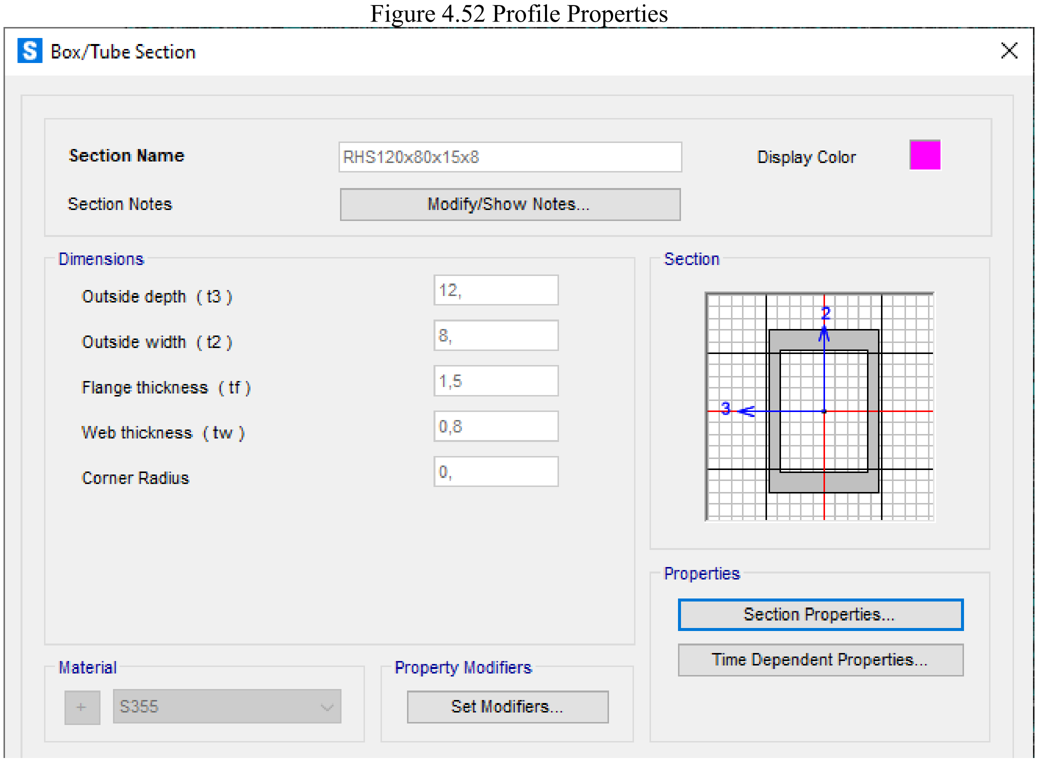

Figure 4.53 Profile Section

4.5.4 Frame's internal forces frame release

The frame's internal assumed for the elements in the software and their local axes are provided in Figure 4.54.

The frame's internal forces are:

- P, the axial force
- V2, the shear force in the 1-2 plane
- V3, the shear force in the 1-3 plane
- T, the axial torque (about the 1-axis)
- M2, the bending moment in the 1-3 plane (about the 2-axis)
- M3, the bending moment in the 1-2 plane (about the 3-axis)

These internal forces and moments are present at every cross-section along the length of the frame.

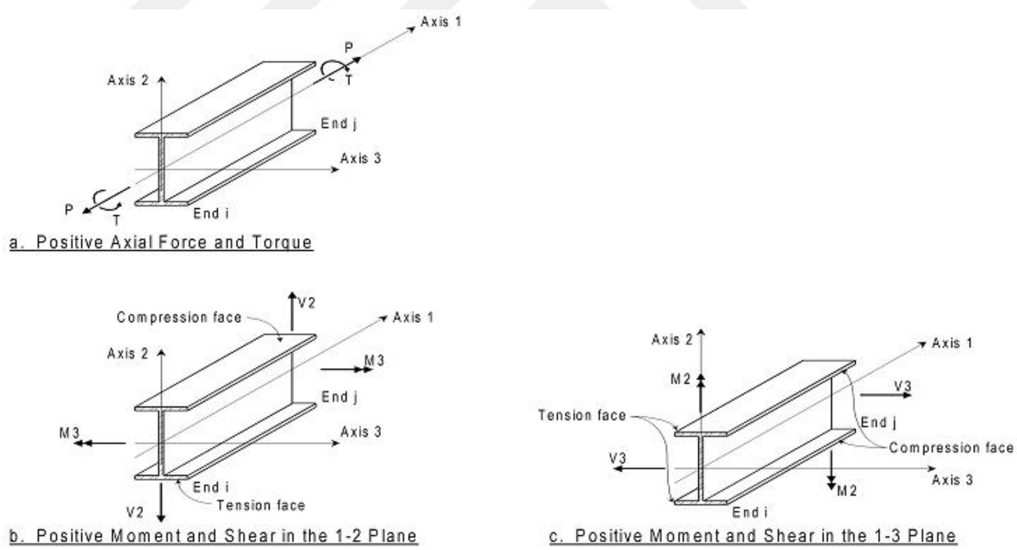

Figure 4.54 The internal frame internal forces (CSI America)

Figure 4.55 show that in the Case 1 analysis, the frames does not take M2, the bending moment in the 1-3 plane (about the 2-axis).

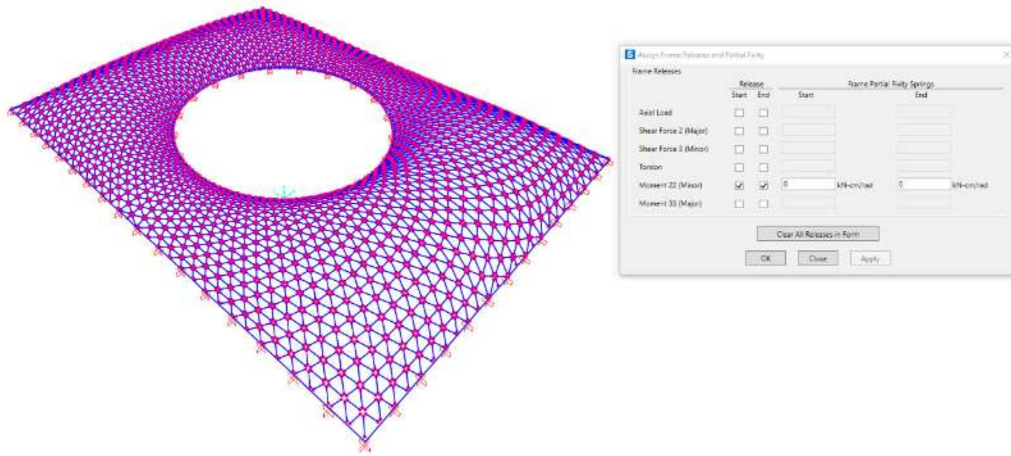

Figure 4.55 Frame releases for Case 1

Figure 4.56 show that in the Case 2 analysis, the frames take internal forces and moments

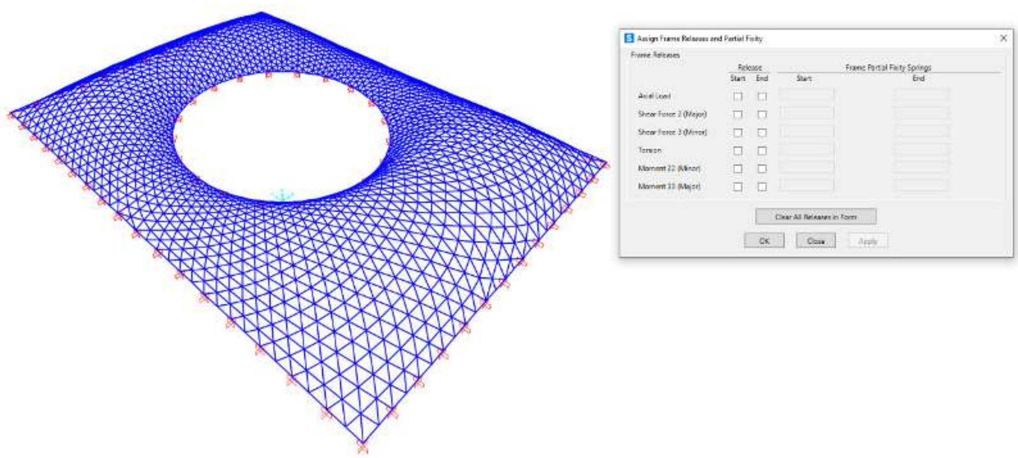

Figure 4.56 Frame releases for Case 2

4.5.5 von Mises criterion

von Mises stress theory is a criterion often used in the field of material strength to predict the point at which a material will fail due to plastic deformation. The theory is named after the Austrian engineer Richard von Mises, but is also known as the Maximum Shear Stress Theory or the Distortion Energy Theory.

von Mises stress theory plays a significant role in various engineering disciplines, including structural civil engineering. von Mises stress summarizes the stress state of a material in three dimensions as a single scalar value. This value is used to determine the stress condition at which a material reaches its yield strength. The yield strength is the stress level at which the material starts to exhibit plastic deformation. If a material reaches or exceeds this yield strength in terms of von Mises stress, it can exhibit permanent shape change or failure.

von Mises stress is typically used in Computer Aided Engineering (CAE) analyses to support material selection and design optimization. This theory can more accurately predict the behavior of materials under various loads in the real world, hence its widespread use in engineering applications.

When defining the stress state on a material, there are various stress components, including normal and shear stresses. von Mises stress theory is used to provide a single scalar value that summarizes these stress components and shows how they combine on a material.

Von Misses Stress is a distinct state of material measure at a certain location of an element. It is not a measure of stress variations between two points. The equations below demonstrate how to calculate the Von Misses Stress for an element under various states/types of stresses.

Table 4.13 von Mises stress formula

State of stress	Boundary conditions	von Mises equations
General	No restrictions	$\sigma_v = \sqrt{\frac{1}{2}\left[(\sigma_{11}-\sigma_{22})^2+(\sigma_{22}-\sigma_{33})^2+(\sigma_{33}-\sigma_{11})^2\right]+3\left(\sigma_{12}^2+\sigma_{23}^2+\sigma_{31}^2\right)}$
Principal stresses	$\sigma_{12}=\sigma_{31}=\sigma_{23}=0$	$\sigma_v = \sqrt{\frac{1}{2}\left[(\sigma_1-\sigma_2)^2+(\sigma_2-\sigma_3)^2+(\sigma_3-\sigma_1)^2\right]}$
General plane stress	$\sigma_3=0$ $\sigma_{31}=\sigma_{23}=0$	$\sigma_v = \sqrt{\sigma_{11}^2-\sigma_{11}\sigma_{22}+\sigma_{22}^2+3\sigma_{12}^2}$
Principal plane stress	$\sigma_3=0$ $\sigma_{12}=\sigma_{31}=\sigma_{23}=0$	$\sigma_v = \sqrt{\sigma_1^2-\sigma_1\sigma_2+\sigma_2^2}$
Pure shear	$\sigma_1=\sigma_2=\sigma_3=0$ $\sigma_{31}=\sigma_{23}=0$	$\sigma_v = \sqrt{3}\lvert\sigma_{12}\rvert$
Uniaxial	$\sigma_2=\sigma_3=0$ $\sigma_{12}=\sigma_{31}=\sigma_{23}=0$	$\sigma_v = \sigma_1$

Where: σ_1 is the normal stress x component, σ_2 is the normal Stress y component, σ_3 is the normal Stress y component, τ_{12} is the Shear Stress 12 plane, τ_{23} is the Shear Stress 23 plane, τ_{31} is the Shear Stress 31 plane

These equations provide a single value that represents the stress state. If this von Mises stress value exceeds the material's yield strength, the material may undergo plastic deformation and thus fail. Therefore, in structural design, the von Mises stress theory is used to predict how materials will behave under loads and determine whether a material is safe under a certain load. This aids in material selection and design optimization, leading to the design of safer and more cost-effective structures.

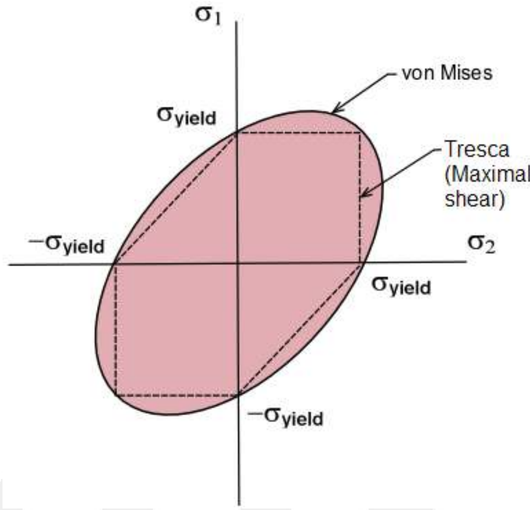

Figure 4.57 von Mises yield criterion in planar (Melchoir, 2006)

von Mises yield criterion in 2D (planar) loading conditions: if stress in the third dimension is zero (σ_3=0) (no yielding is predicted to occur for stress coordinates σ_1, σ_2 within the red area. Because Tresca's criterion for yielding is within the red area, von Mises' criterion is more lax.

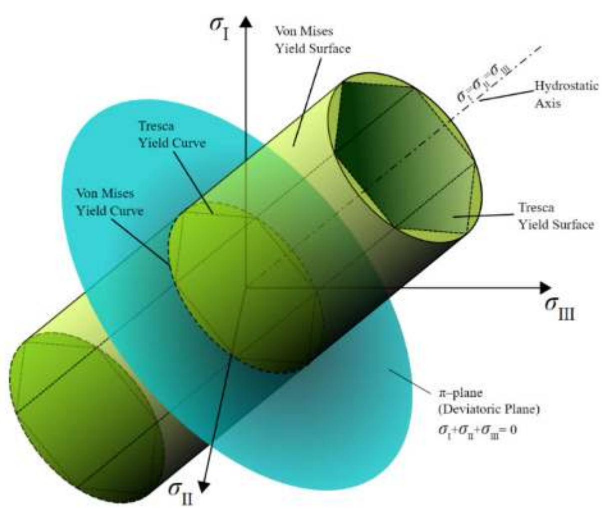

Figure 4.58 The von Mises yield surfaces (Rswarbrick, 2009)

Equivalent stress is widely used to represent a material’s status for ductile material. Engineers use this simple scalar value to determine if the material has yield or failed.

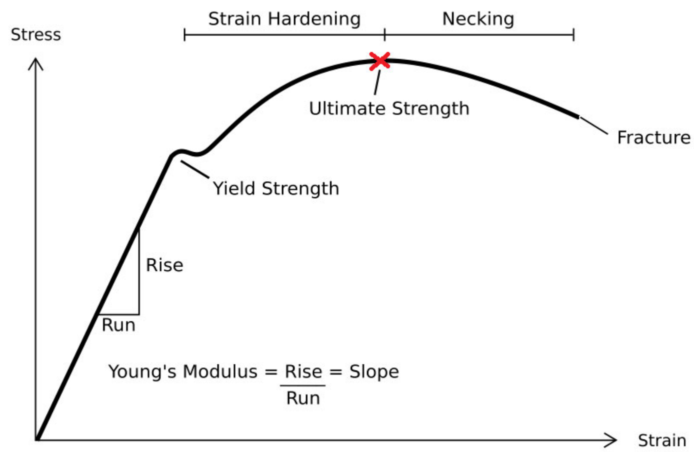

Figure 4.59 Material failure diagram (Breakdown, 2008)

4.5.6 Load assignments and model generation

The model transferred to the SAP2000 software, which is a CSI software, has been prepared by assigning supports and applying loads.

Figure 4.60 Geometry of Free-From, Side View

The 3D visuals of the free-form system created in the model are given in Figure 4.61.

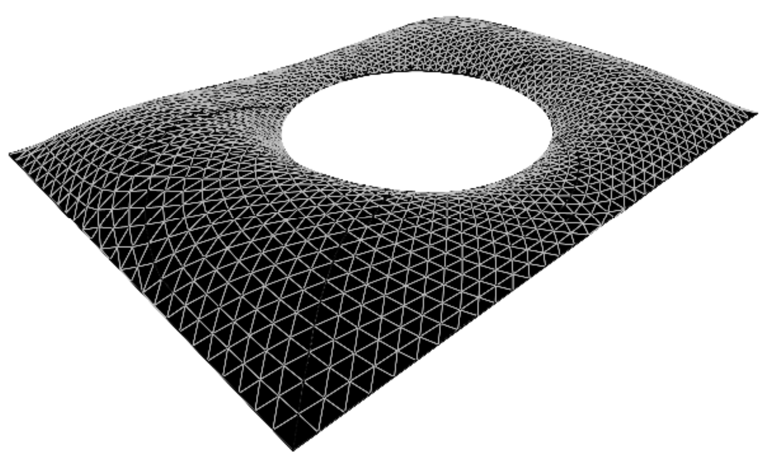

Figure 4.61 Geometry of Free-From, Isometric View

Regarding the loads:

• The system is designed so that it is not affected by temperature loads.

• The self-weight of the profiles is automatically considered in the calculations.

• Wind and snow loads, as well as the self-weight of the glass surface, are distributed over the surface elements covering the space between the steel profiles. Interpolation transfers snow and wind loads to the areas, and the loads affecting each segment are determined through iteration and entered into the program.

Load assignments have been made for the free-form system, and the generated visualizations from the program are shown in figures 4.62-67.

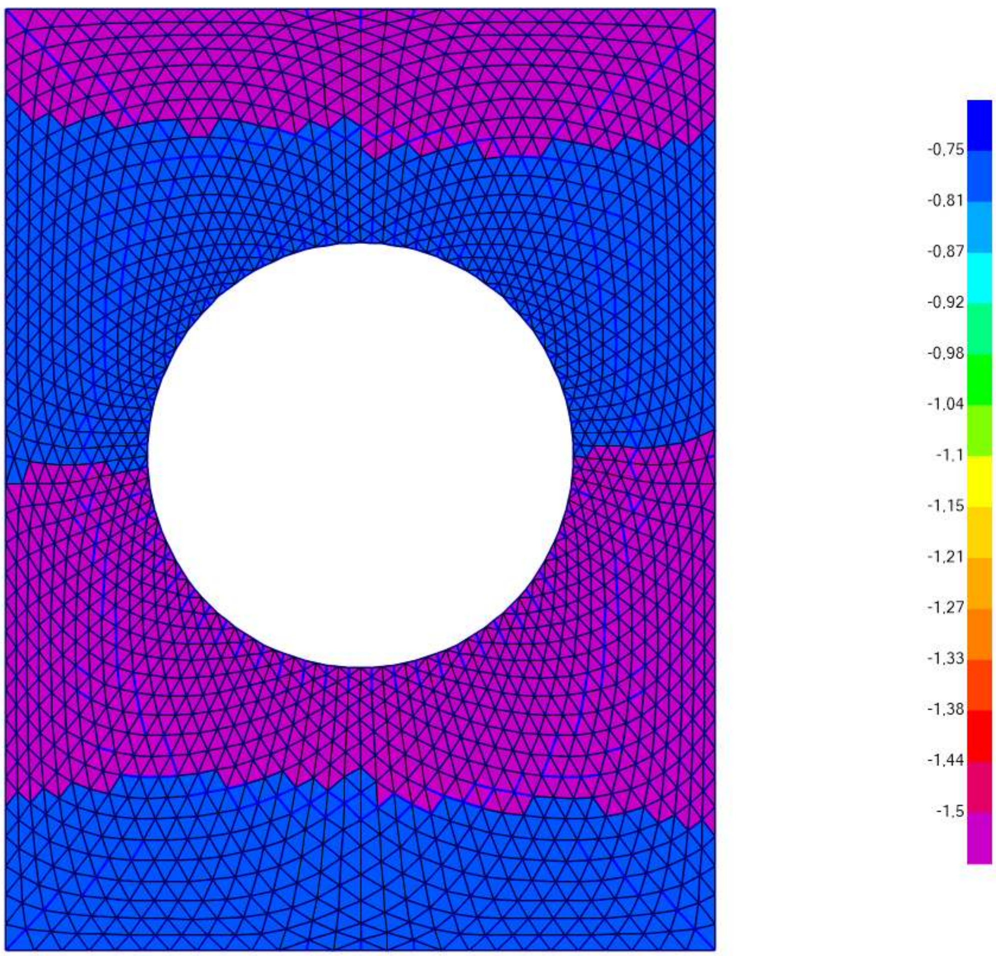

Figure 4.62 Snow load accumulation

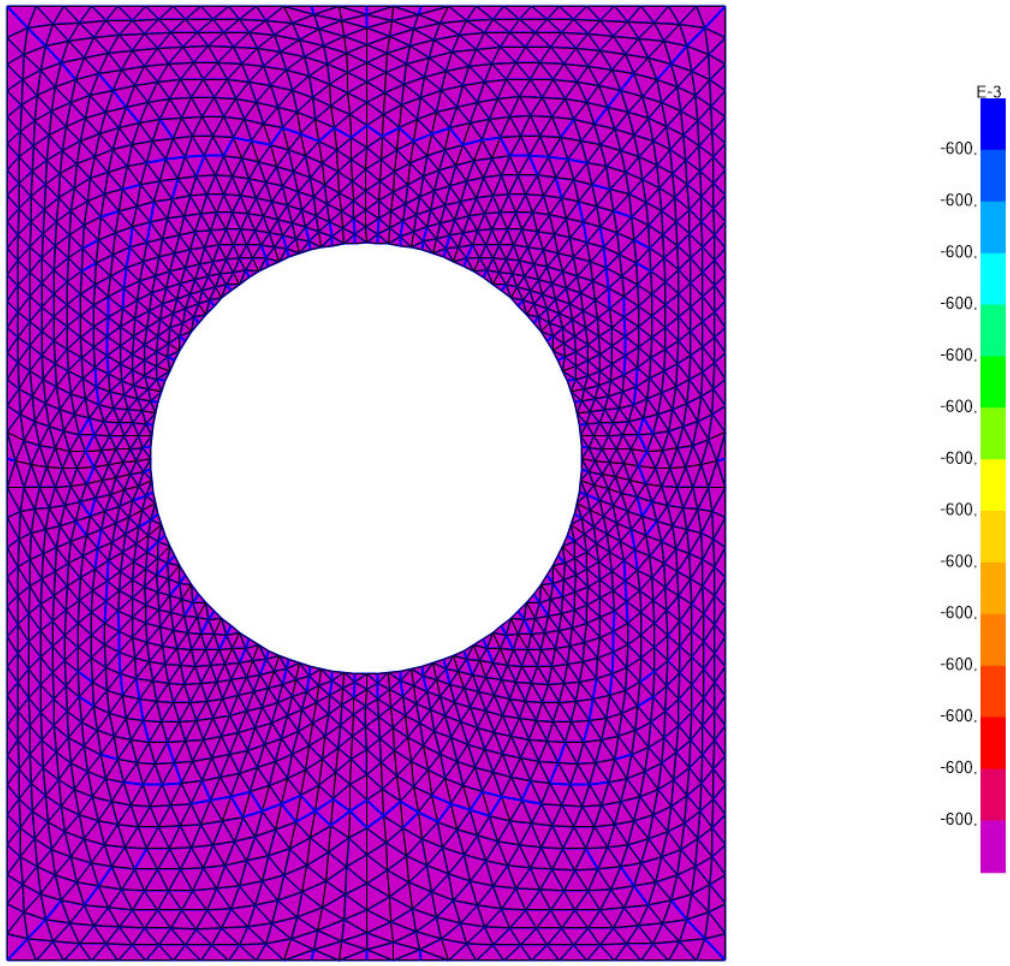

Figure 4.63 Balanced snow load assignments

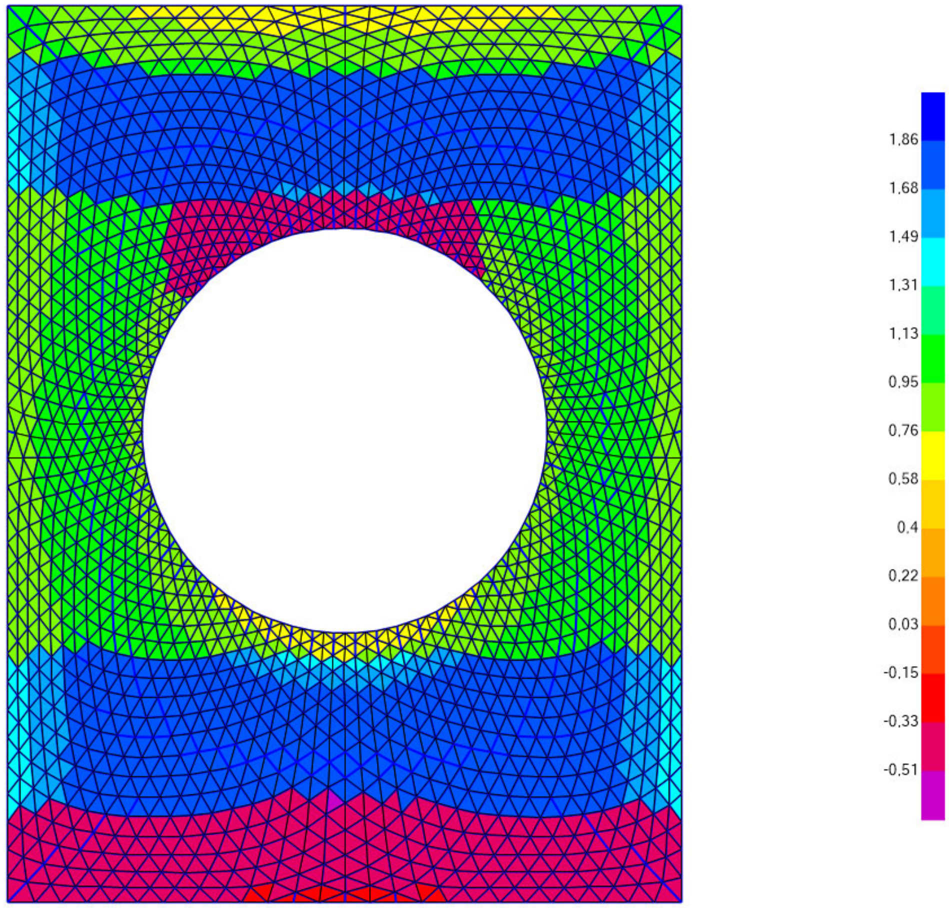

Figure 4.64 Representation of wind load assignments in the Y direction

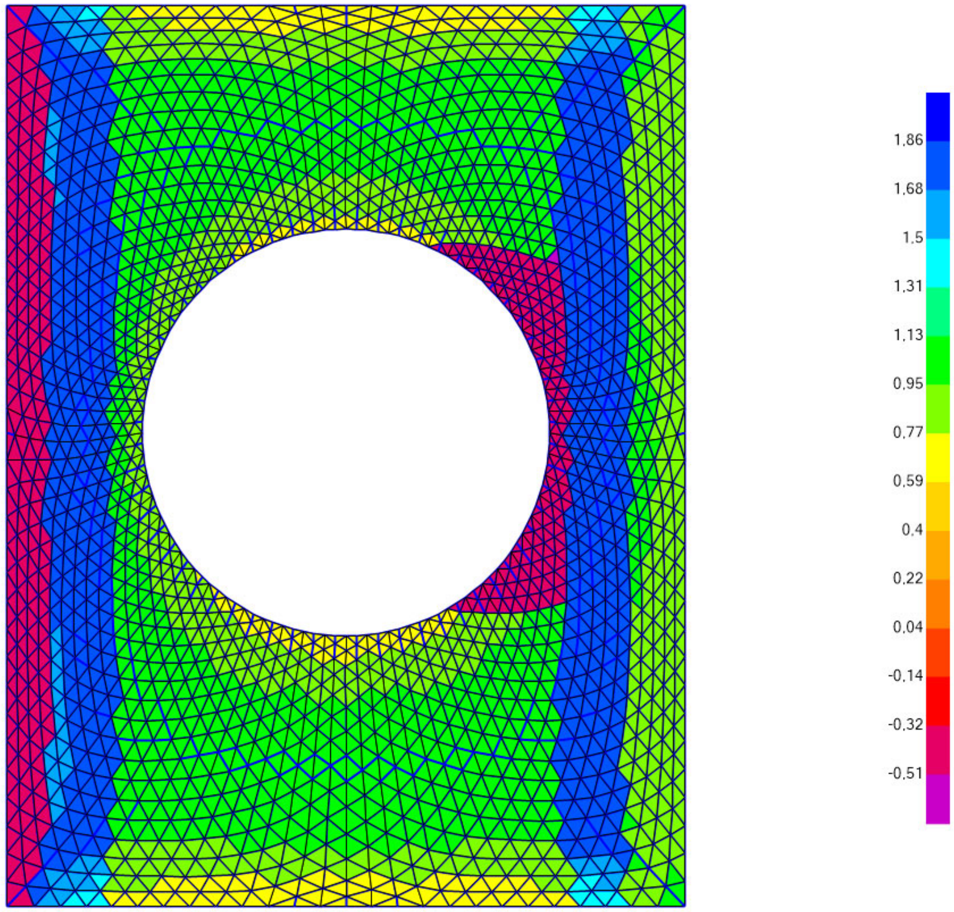

Figure 4.65 Representation of wind load assignments in the X direction

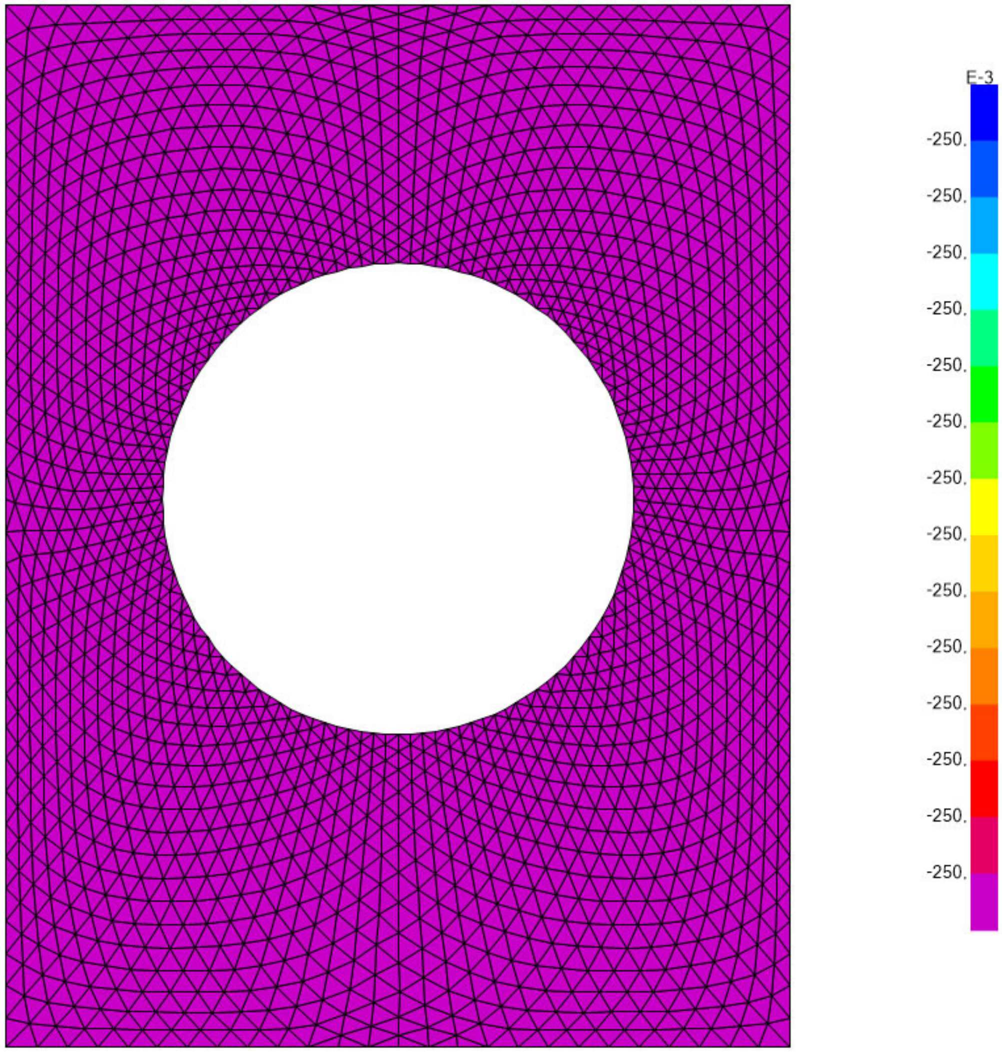

Figure 4.66 Live load assignments (kN/m^2)

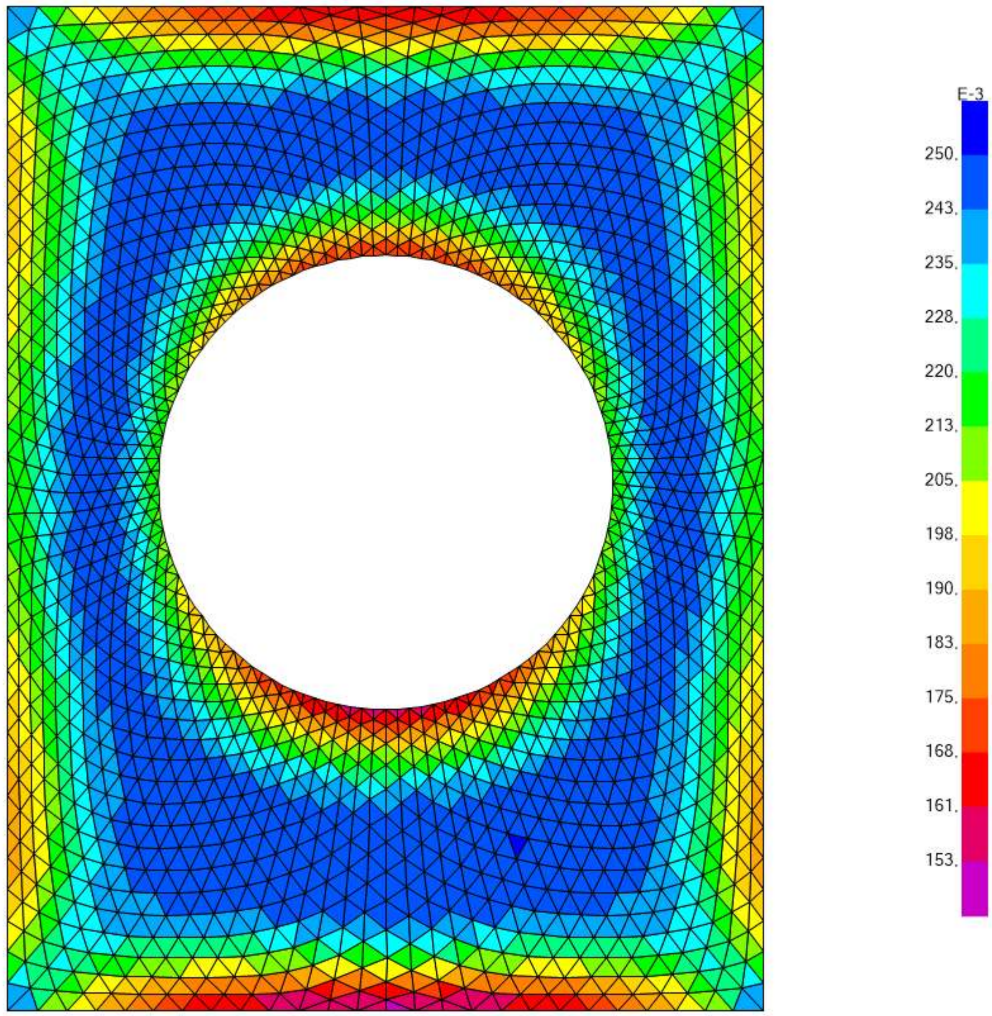

Figure 4.67 Live Load assignments (kN/m^2)

4.6 Analysis and evaluation

4.6.1 Frame P-M ratios

The P-M ratios of the 20 most critical profiles for Case 1 and Case 2 are provided in Figures 4.68-4.70.

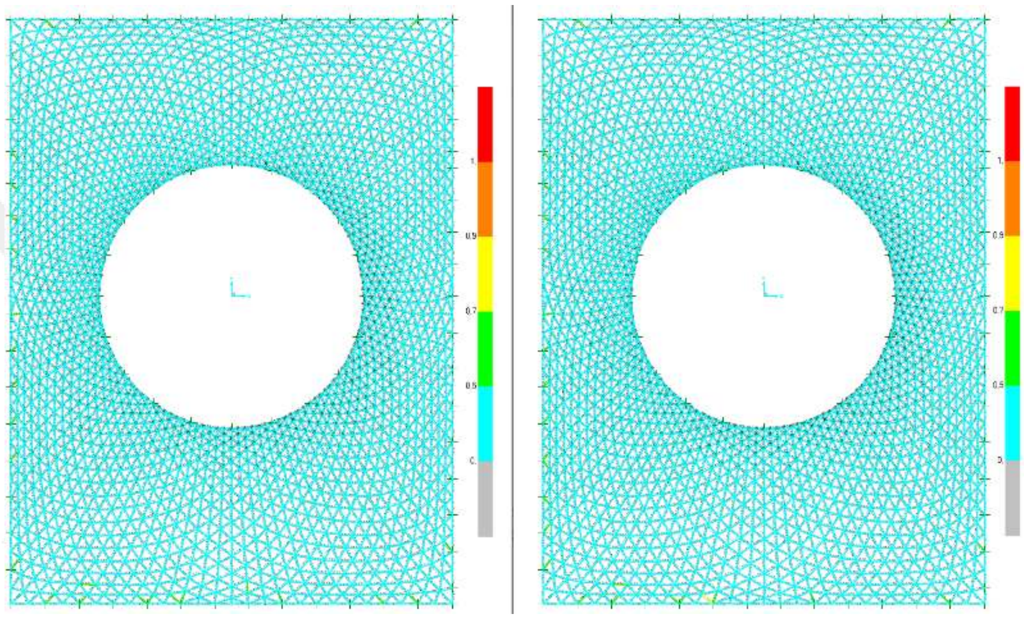

Figure 4.68 Stress-diagram for P-M ratios (Left Case 1 / Right Case 2)

TABLE: Steel Design 2 - PMM Details - AISC 360-16						
Frame	**DesignSect**	**Status**	**Combo**	**TotalRatio**	**ErrMsg**	**WarnMsg**
Text	Text	Text	Text	Unitless	Text	Text
502	RHS120x80x15x8	No Messages	1,2G + 1,0Q + 0,5S2 + 1,6Wp	0,683	No Messages	No Messages
451	RHS120x80x15x8	No Messages	1,2G + 1,6S2 + Q	0,655	No Messages	No Messages
424	RHS120x80x15x8	No Messages	1,2G + 1,0Q + 0,5S2 + 1,6Wp	0,642	No Messages	No Messages
149	RHS120x80x15x8	No Messages	1,2G + 1,0Q + 0,5S1 + 1,6Ws	0,597	No Messages	No Messages
161	RHS120x80x15x8	No Messages	1,2G + 1,0Q + 0,5S1 + 1,6Ws	0,589	No Messages	No Messages
195	RHS120x80x15x8	No Messages	1,2G + 1,0Q + 0,5S1 + 1,6Ws	0,576	No Messages	No Messages
339	RHS120x80x15x8	No Messages	1,2G + 1,6S1 + Q	0,558	No Messages	No Messages
219	RHS120x80x15x8	No Messages	1,2G + 1,0Q + 0,5S2 + 1,6Ws	0,558	No Messages	No Messages
2049	RHS120x80x15x8	No Messages	0,9G + 1,6Wp	0,552	No Messages	No Messages
175	RHS120x80x15x8	No Messages	1,2G + 1,0Q + 0,5S1 + 1,6Ws	0,542	No Messages	No Messages
342	RHS120x80x15x8	No Messages	1,2G + 1,6S1 + Q	0,537	No Messages	No Messages
250	RHS120x80x15x8	No Messages	1,2G + 1,0Q + 0,5S1 + 1,6Ws	0,535	No Messages	No Messages
155	RHS120x80x15x8	No Messages	1,2G + 1,0Q + 0,5S1 + 1,6Ws	0,530	No Messages	No Messages
381	RHS120x80x15x8	No Messages	1,2G + 1,6S1 + Q	0,524	No Messages	No Messages
679	RHS120x80x15x8	No Messages	1,2G + 1,6S2 + Q	0,523	No Messages	No Messages
689	RHS120x80x15x8	No Messages	1,2G + 1,6S2 + Q	0,518	No Messages	No Messages
384	RHS120x80x15x8	No Messages	1,2G + 1,6S1 + Q	0,513	No Messages	No Messages
303	RHS120x80x15x8	No Messages	1,2G + 1,6S1 + Q	0,509	No Messages	No Messages
306	RHS120x80x15x8	No Messages	1,2G + 1,6S1 + Q	0,509	No Messages	No Messages
298	RHS120x80x15x8	No Messages	1,2G + 1,6S1 + Q	0,508	No Messages	No Messages

Figure 4.69 Most critical frames for case 1

TABLE: Steel Design 2 - PMM Details - AISC 360-16					
Frame	**DesignSect**	**Combo**	**TotalRatio**	**ErrMsg**	**WarnMsg**
Text	Text	Text	Unitless	Text	Text
502	RHS120x80x15x8	1,2G + 1,0Q + 0,5S2 + 1,6Wp	0,708	No Messages	No Messages
451	RHS120x80x15x8	1,2G + 1,6S2 + Q	0,661	No Messages	No Messages
424	RHS120x80x15x8	1,2G + 1,0Q + 0,5S2 + 1,6Wp	0,659	No Messages	No Messages
149	RHS120x80x15x8	1,2G + 1,0Q + 0,5S1 + 1,6Ws	0,582	No Messages	No Messages
161	RHS120x80x15x8	1,2G + 1,0Q + 0,5S1 + 1,6Ws	0,578	No Messages	No Messages
195	RHS120x80x15x8	1,2G + 1,0Q + 0,5S1 + 1,6Ws	0,571	No Messages	No Messages
219	RHS120x80x15x8	1,2G + 1,0Q + 0,5S2 + 1,6Ws	0,562	No Messages	No Messages
2049	RHS120x80x15x8	0,9G + 1,6Wp	0,559	No Messages	No Messages
298	RHS120x80x15x8	1,2G + 1,6S2 + Q	0,546	No Messages	No Messages
236	RHS120x80x15x8	1,2G + 1,0Q + 0,5S1 + 1,6Ws	0,545	No Messages	No Messages
175	RHS120x80x15x8	1,2G + 1,0Q + 0,5S1 + 1,6Ws	0,537	No Messages	No Messages
339	RHS120x80x15x8	1,2G + 1,6S1 + Q	0,534	No Messages	No Messages
679	RHS120x80x15x8	1,2G + 1,6S2 + Q	0,531	No Messages	No Messages
303	RHS120x80x15x8	1,2G + 1,6S1 + Q	0,529	No Messages	No Messages
689	RHS120x80x15x8	1,2G + 1,6S2 + Q	0,528	No Messages	No Messages
250	RHS120x80x15x8	1,2G + 1,0Q + 0,5S1 + 1,6Ws	0,527	No Messages	No Messages
201	RHS120x80x15x8	1,2G + 1,0Q + 0,5S1 + 1,6Ws	0,521	No Messages	No Messages
155	RHS120x80x15x8	1,2G + 1,0Q + 0,5S1 + 1,6Ws	0,521	No Messages	No Messages
342	RHS120x80x15x8	1,2G + 1,6S1 + Q	0,516	No Messages	No Messages
306	RHS120x80x15x8	1,2G + 1,6S1 + Q	0,512	No Messages	No Messages

Figure 4.70 Most critical frames for case 2

4.6.2 Deflection

The displacement representation of each free-form system model under the most unfavorable conditions is given in table 4.71-72. The maximum deflection value under the most critical load combination is approximately 63mm in both cases. Also, as stated in Sischka (2000), “The maximum theoretical deflection is 142 mm.”

Deflectionf Check

f=63mm < L/300=29125/300=97,08mm,

The deflection value is appropriate.

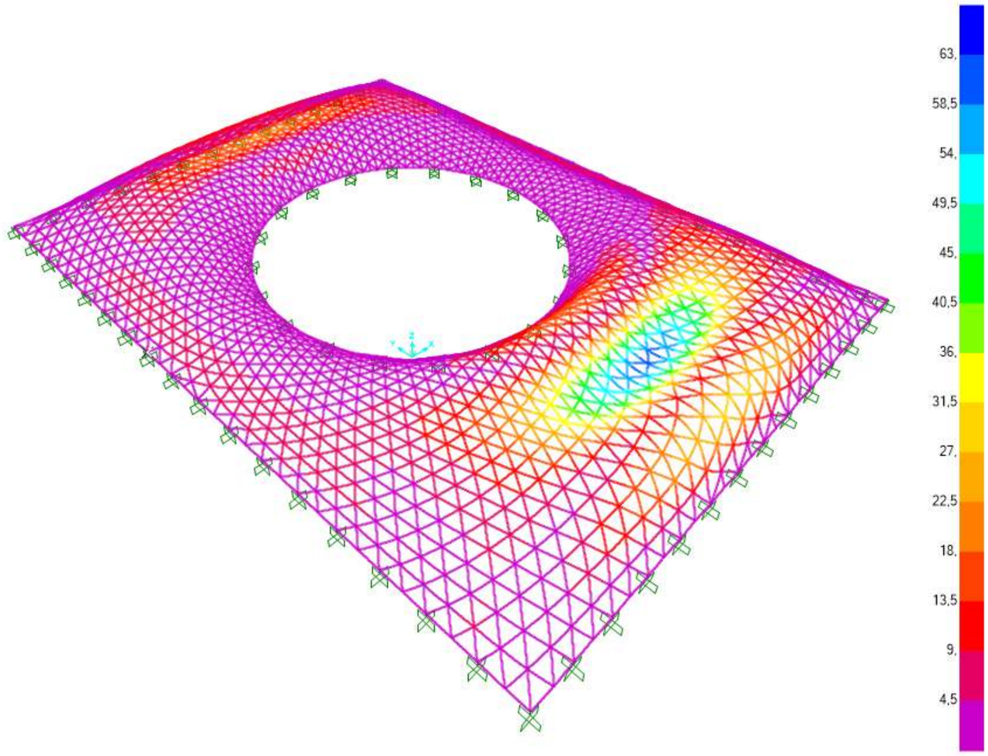

Figure 4.71 Deformed shape (G+0,5S1 unit: mm) Case 1

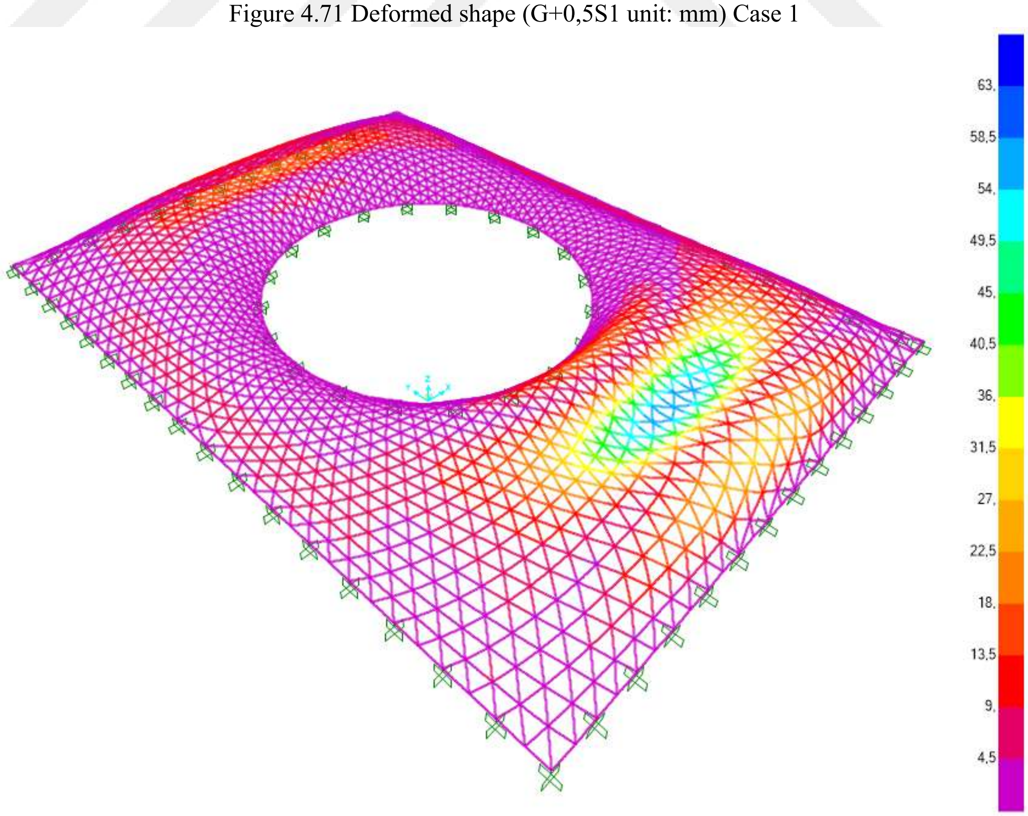

Figure 4.72 Deformed shape (G+0,5S1 unit: mm) Case 2

The free-form system model has been subjected to the load resistance factor design (LRFD) method according to the AISC specifications. The section carrying capacities related to bending, axial force, and shear strength have been checked.

The dominant effect on the elements is axial load, while the values of moments and shear forces remain relatively low. The most unfavorable results, including unbalanced (asymmetric) load combinations with snow loading, have been obtained for all models. A diagram of the axial load and moment variations for the most unfavorable combination and the sectional effects obtained from envelope combinations are provided in Table 4.27-4.30.

Table 4.14 Internal Force Diagrams (1,2G + 1,0Q + 0,5S2 + 1,6Wp)

Case 1	Case 2
Axial Force Diagram	Axial Force Diagram
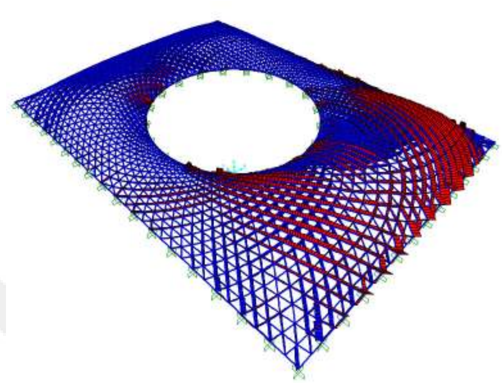	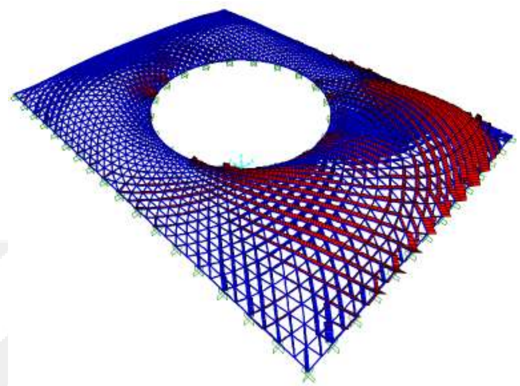
Shear Force 2-2 Diagram	Shear Force 2-2 Diagram
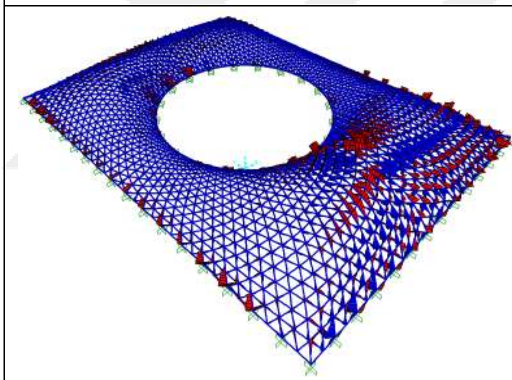	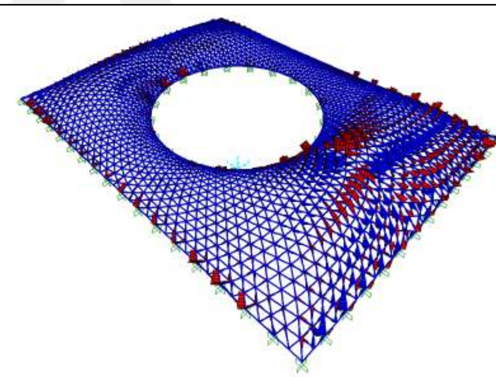
Shear Force 3-3 Diagram	Shear Force 3-3 Diagram
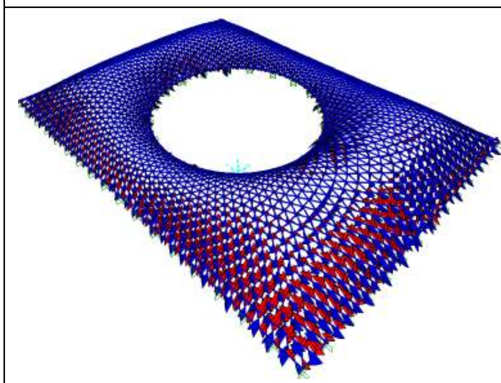	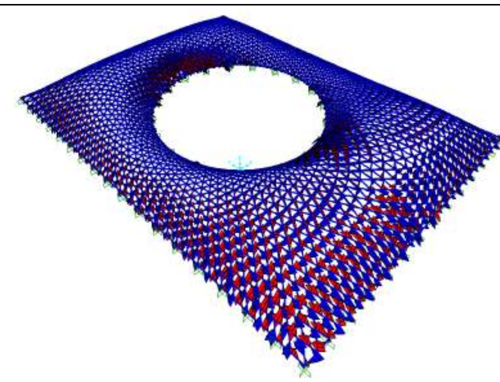

Table 4.15 Internal Force Diagrams (1,2G + 1,0Q + 0,5S2 + 1,6Wp)

Case 1	Case 2
Torsion Diagram	Torsion Diagram
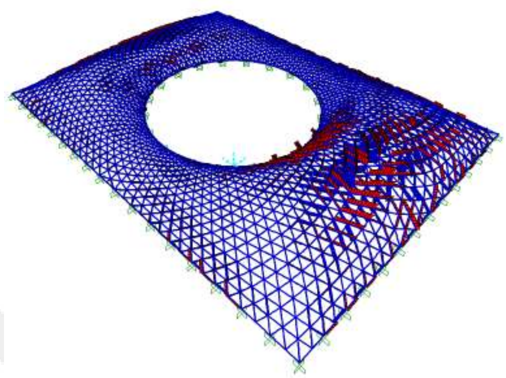	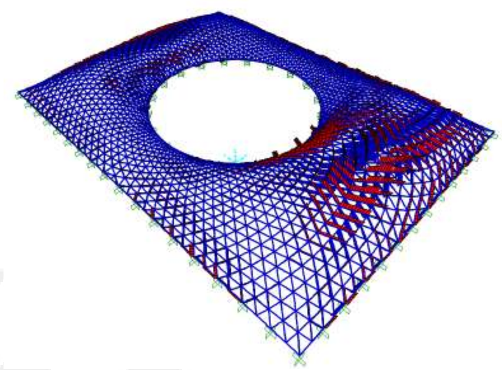
Moment 2-2 Diagram	Moment 2-2 Diagram
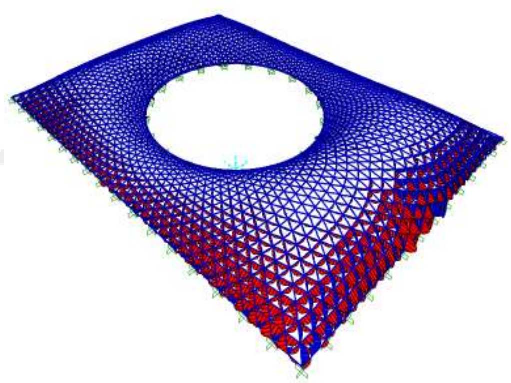	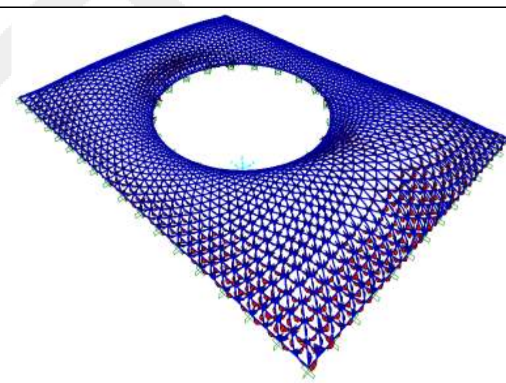
Moment 3-3 Diagram	Moment 3-3 Diagram
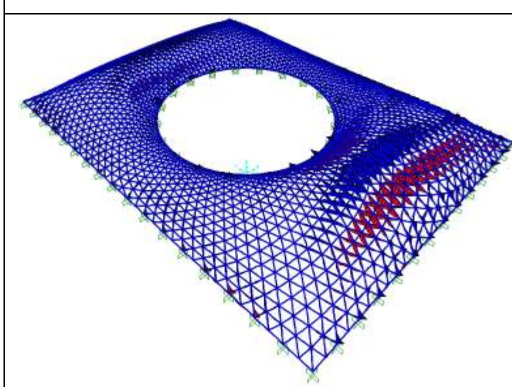	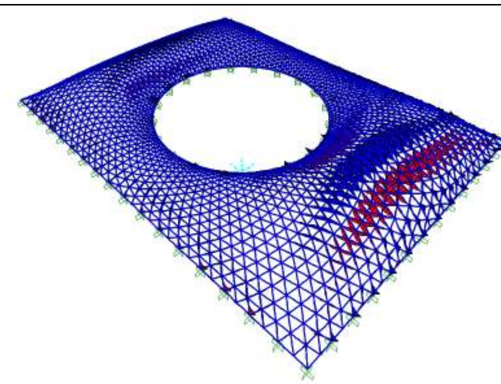

$N_{compressure}$ = -218,90 kN $N_{tension}$ = 253,51 kN $M_{Max, 2-2}$ = 1,57 kNm $M_{Max, 3-3}$ = 12,07 kNm $V_{Max, 2-2}$ = 9,51 kN $V_{Max, 3-3}$ = 1,56 kN	$N_{compressure}$ = -218,48 kN $N_{tension}$ = 251,27 kN $M_{Max, 2-2}$ = 1,11 kNm $M_{Max, 3-3}$ = 11,95 kNm $V_{Max, 2-2}$ = 9,54 kN $V_{Max, 3-3}$ = 1,84 kN

4.6.3 Buckling stability evaluation

The buckling factor determines the buckling load carrying capacity of a structural system and is typically a critical criterion in structural design. Particularly for free-form structures, which have more complex and geometric designs, these values are of particular importance.

Determining the buckling factor is usually part of the structural analysis process, and a specific value is typically dictated by design codes or industry standards. However, as a general rule, it is accepted that the buckling factor should be greater than 1. A buckling factor below 1 indicates that the structural system is insufficient and cannot withstand the buckling load.

However, when determining a target buckling factor, the type of structural system, materials used, expected loads, and other environmental conditions should be considered. Particularly for structures with complex geometry like free-form structures, a higher buckling factor may be targeted to provide a safer design and extra buckling capacity.

Lastly, when determining a specific structural design and buckling factor target, it's important to consult with a structural engineer or structural design professional.

In the analysis models, the most unfavorable load combinations are identified in table 4.16. The buckling load factors were determined by incorporating second-order effects into the buckling analysis, which was carried out separately for these combinations. The results of the buckling analysis, including the buckling load factors obtained for both case scenarios, can be found in table 4.17-18. As stated in Sischka (2000), “The first eigen frequency is at approximately 1 Hz, the overall buckling factor approximately 2.9 for factored loads.” The minimum buckling factor for Case 1 is

1.22, while for Case 2, it is 3.22. In conclusion, the buckling factor derived from the Case 2 analysis closely aligns with the actual value in the real model.

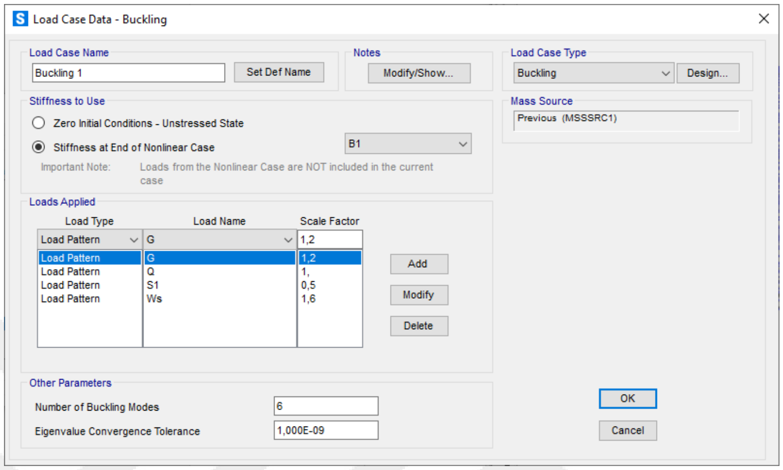

Figure 4.73 Definition made in the program for buckling

Table 4.16 Most critical load combination for buckling

No	Combination
Bucking 1	1,2G + 1,0Q + 0,5S1 + 1,6Ws
Bucking 2	1,2G + 1,0Q + 0,5S2 + 1,6Wp
Bucking 3	1,2G + 1,0Q + 0,5S2 + 1,6Wp
Bucking 4	1,2G + 1,0Q + 0,5S2 + 1,6Ws
Bucking 5	1,2G + 1,6S1 + Q
Bucking 6	1,2G + 1,6S2 + Q
Bucking 7	0,9G + 1,6Wp
Bucking 8	0,9G + 1,6Ws

Table 4.17 Buckling Factors for Case 1

OutputCase	**StepType**	**StepNum**	**ScaleFactor**
Text	Text	Unitless	Unitless
Buckling 1	Mode	1	4,08
Buckling 2	Mode	1	1,54
Buckling 3	Mode	1	1,38
Buckling 4	Mode	1	4,33
Buckling 5	Mode	1	1,22
Buckling 6	Mode	1	1,73
Buckling 7	Mode	1	1,73
Buckling 8	Mode	1	-6,09

Table 4.18 Buckling Factors for Case2

OutputCase	StepType	StepNum	ScaleFactor
Text	Text	Unitless	Unitless
Buckling 1	Mode	1	14,27
Buckling 2	Mode	1	7,47
Buckling 3	Mode	1	7,04
Buckling 4	Mode	1	14,91
Buckling 5	Mode	1	3,22
Buckling 6	Mode	1	3,65
Buckling 7	Mode	1	-7,07
Buckling 8	Mode	1	-12,66

4.6.4 Natural frequencies

As stated in Sischka (2000), "The first eigen frequency is at approximately 1 Hz, the overall buckling factor approximately 2.9 for factored loads."

Figures 4.74-75 display the lowest eigenfrequencies computed for the described finite element (FE) model. Presented frequencies are higher than the design criteria lower limit of 1.0Hz.

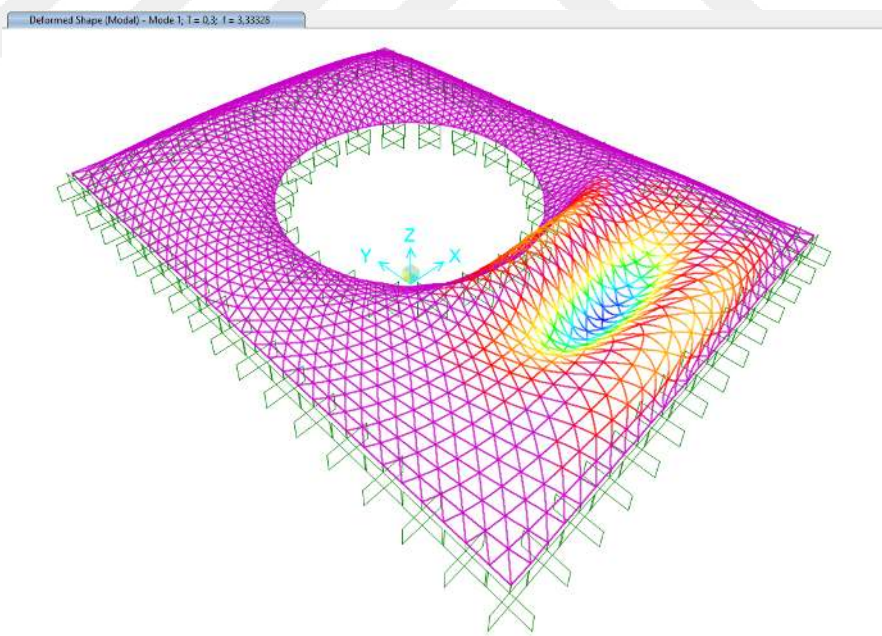

Figure 4.74 1st natural frequency at 3.33 Hz for case 1

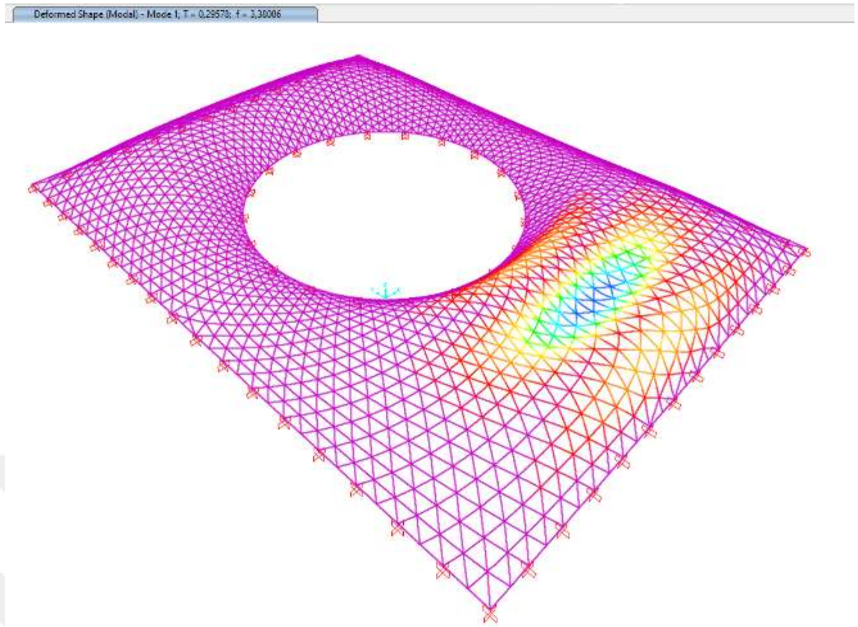

Figure 4.75 1st natural frequency at 3.38 Hz for case 2

4.6.5 Frames' forces

Frame forces for the free-form system are provided in Annex 2

4.6.6 Support reactions

The most critical support reaction responses are provided in figure 4.76-4.77. These figures contain data relevant to the various support reactions occurring within the structure, providing a deeper understanding of the system's stability under different load conditions.

Tables for the support reactions in the free-form system are provided in Annex 1.

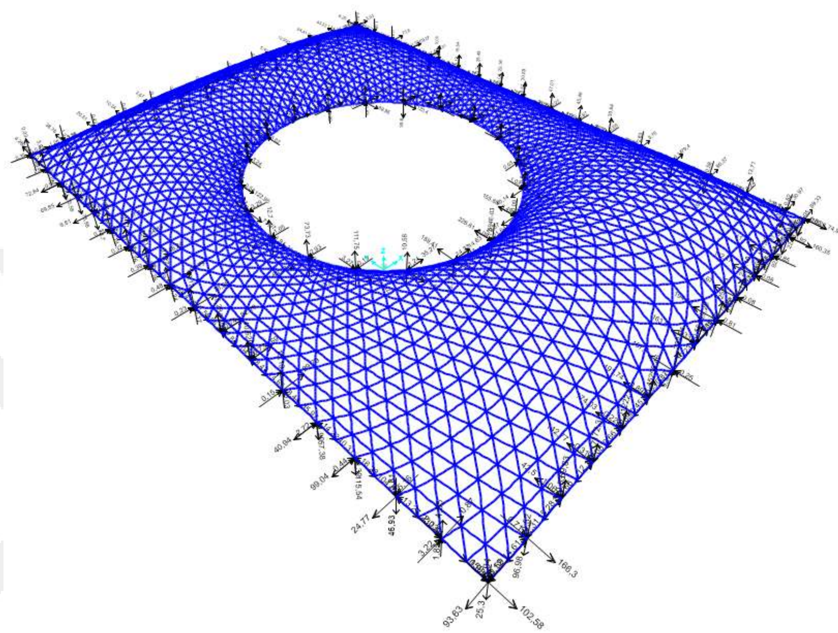

Figure 4.76 Maximum Reaction Forces for case 1
Load combination: 1,2G + 1,0Q + 0,5S2 + 1,6Wp

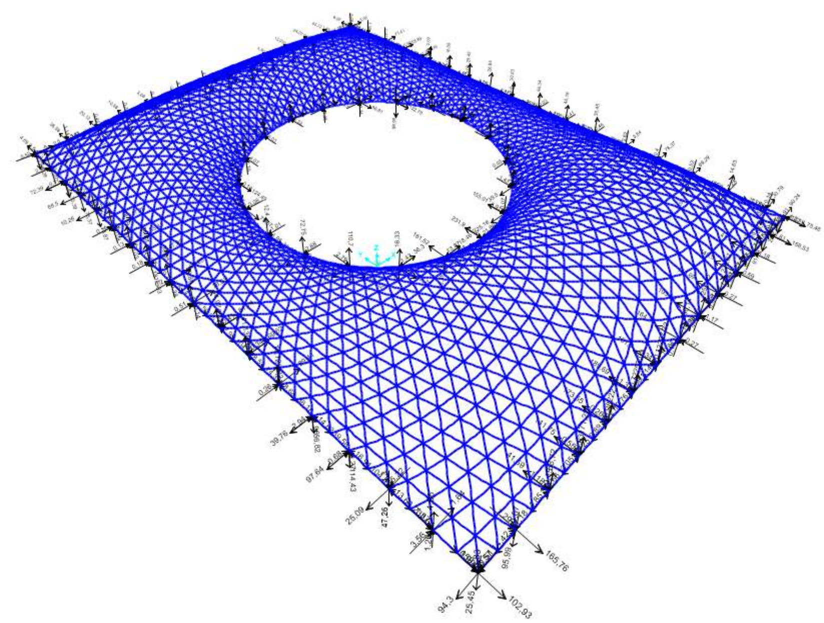

Figure 4.77 Maximum Reaction Forces for case 2
Load combination: 1,2G + 1,0Q + 0,5S2 + 1,6Wp

4.6.7 Weight of the structure

The table of steel tonnages for the structure is shown in table 4.15. This table presents comprehensive data on the amount of steel used in various parts of the structure.

Table 4.19 Material List - By Section Property

Section	Object Type	Num Pieces	Total Length	Total Weight
Text	Text	Unitless	m	KN
RHS120x80x15x8	Frame	5178,00	10772,80	3184,18

4.7 Node Analysis

Prior to proceeding with the computations, it is pertinent to deliberate upon the merits and demerits associated with both welded and bolted node points:

	Welded Node Points	Bolted Node Points
Structural Integrity	Provides high structural integrity and load capacity by transforming parts into a single continuous element.	Are robust, but may not provide the same structural continuity as welded connections. There is a risk of bolts loosening over time.
Aesthetic Considerations	Offers a continuous, seamless look, contributing to the aesthetics of free-form structures.	The mechanical aesthetic can sometimes contribute to the desired design intent but generally doesn't offer as seamless a look as welded connections.
Fabrication & Assembly	Represents a more complex process that requires skill. Mistakes often involve serious rework or component replacement.	Represents a simpler and faster process, requiring less expertise. Mistakes or adjustments can be easily remedied by replacing or adjusting bolts.
Cost and Time	May lead to higher costs and time, especially when complex geometries are involved.	Provides advantages of lower costs and time, especially in large-scale projects.
Maintenance	Maintenance of welded connections is generally more difficult and often involves more time and costs.	Maintenance and alterations are generally easier and less costly.

The most critical node point in the structure system can be observed in Figure 4.78.

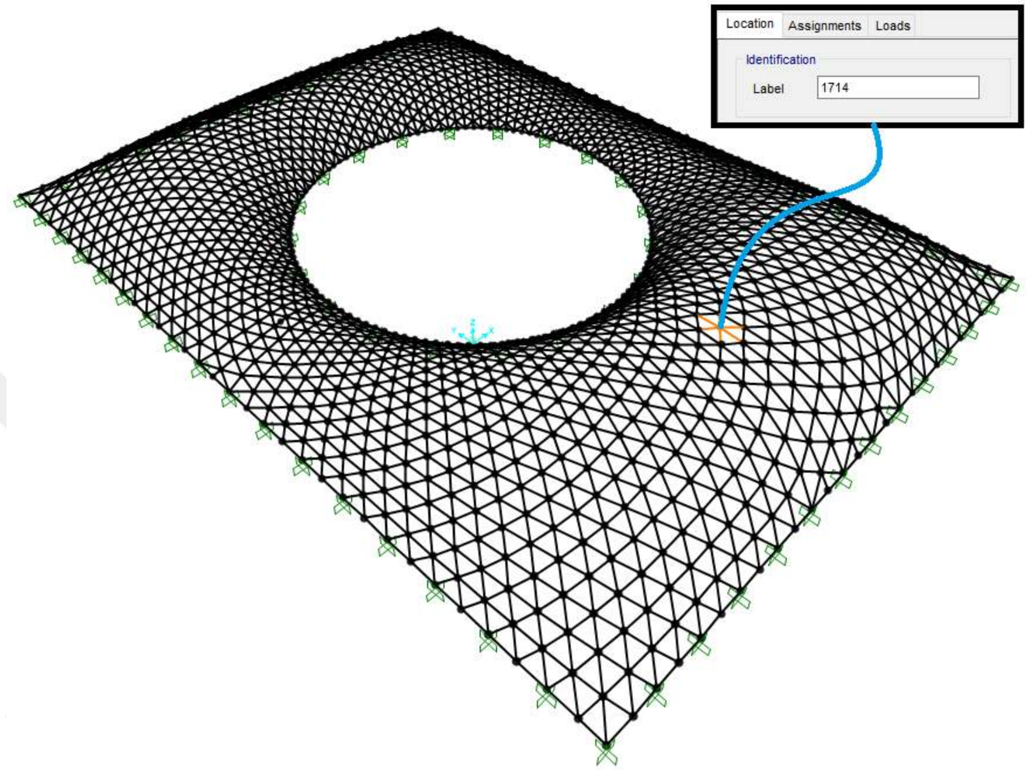

Figure 4.78 Most critical node for both cases

Table 4.20 Internal Force Diagrams (1,2G + 1,0Q + 0,5S2 + 1,6Wp)

Case 1	Case 2
Axial Force Diagram	Axial Force Diagram
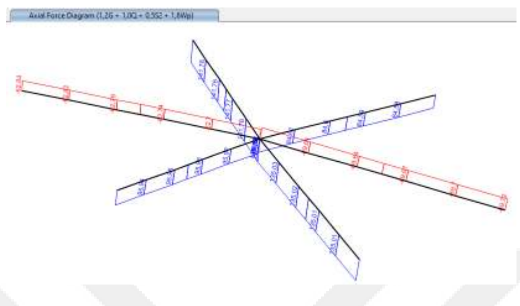	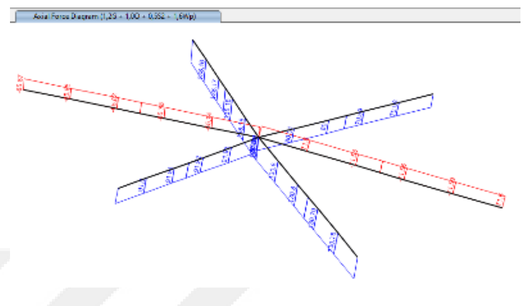
Shear Force 2-2 Diagram	Shear Force 2-2 Diagram
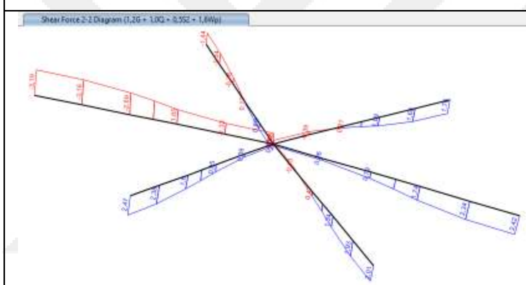	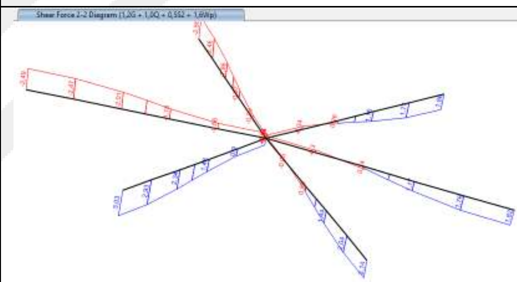
Shear Force 3-3 Diagram	Shear Force 3-3 Diagram
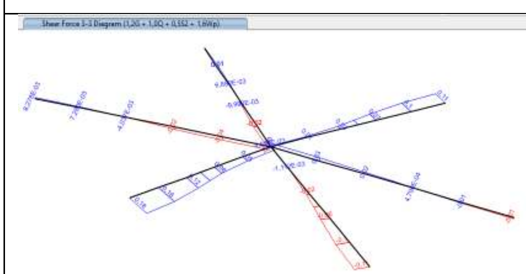	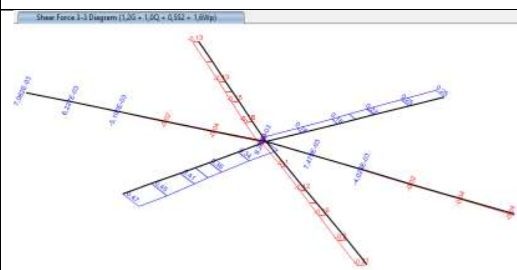

Table 4.21 Internal Force Diagrams (1,2G + 1,0Q + 0,5S2 + 1,6Wp)

Case 1	Case 2
Torsion Diagram	Torsion Diagram
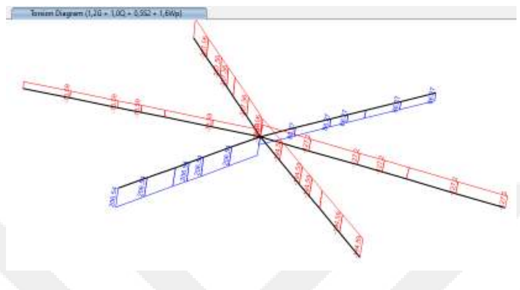	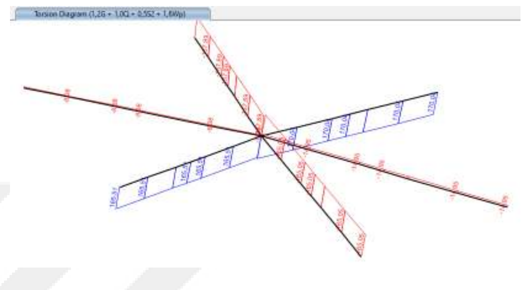
Moment 2-2 Diagram	Moment 2-2 Diagram
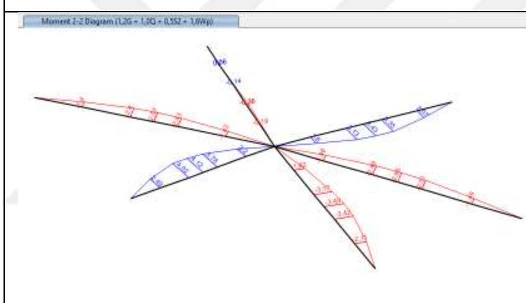	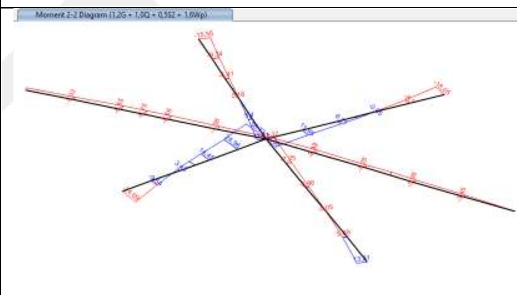
Moment 3-3 Diagram	Moment 3-3 Diagram
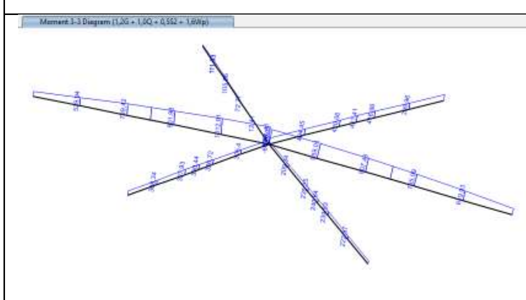	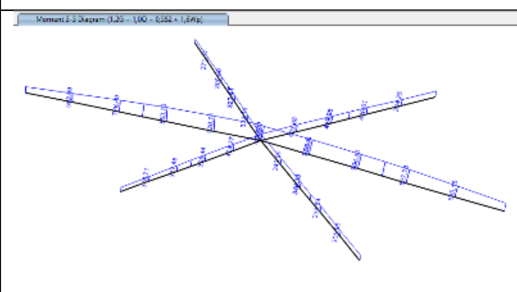

Table 4.22 Element Joint Forces - Frames for Case 1

Frame	OutputCase	P	V2	V3	T	M2	M3
Text	Text	KN	KN	KN	KN-cm	KN-cm	KN-cm
5077	1,2G + 1,0Q + 0,5S2 + 1,6Wp	-62,69	-1,27	-0,04	-73,59	0,00	1091,41
5102	1,2G + 1,0Q + 0,5S2 + 1,6Wp	-69,60	0,21	0,03	-127,20	0,00	976,02
5131	1,2G + 1,0Q + 0,5S2 + 1,6Wp	84,62	-0,48	0,01	86,27	0,00	389,44
5140	1,2G + 1,0Q + 0,5S2 + 1,6Wp	141,79	0,78	-0,02	-207,56	0,00	-60,45
5141	1,2G + 1,0Q + 0,5S2 + 1,6Wp	95,98	0,30	0,04	206,54	0,00	280,52
5142	1,2G + 1,0Q + 0,5S2 + 1,6Wp	135,03	-0,22	0,00	-194,59	0,00	180,33

Table 4.23 Element Joint Forces - Frames for Case 2

Frame	OutputCase	P	V2	V3	T	M2	M3
Text	Text	KN	KN	KN	KN-cm	KN-cm	KN-cm
5077	1,2G + 1,0Q + 0,5S2 + 1,6Wp	-65,72	-0,61	-0,04	-8,38	-5,51	973,89
5102	1,2G + 1,0Q + 0,5S2 + 1,6Wp	-71,49	-0,34	0,01	-14,95	-6,67	905,99
5131	1,2G + 1,0Q + 0,5S2 + 1,6Wp	80,01	-0,44	0,15	170,04	18,66	427,56
5140	1,2G + 1,0Q + 0,5S2 + 1,6Wp	138,19	-0,30	-0,16	-157,89	11,61	320,25
5141	1,2G + 1,0Q + 0,5S2 + 1,6Wp	91,93	0,82	0,33	165,51	36,73	411,60
5142	1,2G + 1,0Q + 0,5S2 + 1,6Wp	130,81	-0,15	-0,09	-165,05	-11,37	337,55

The CAD model of the structure was made with the Ansys SpaceClaim program.

4.7.1 Bolted node analysis

S355 steel grade is defined for each part of the model.

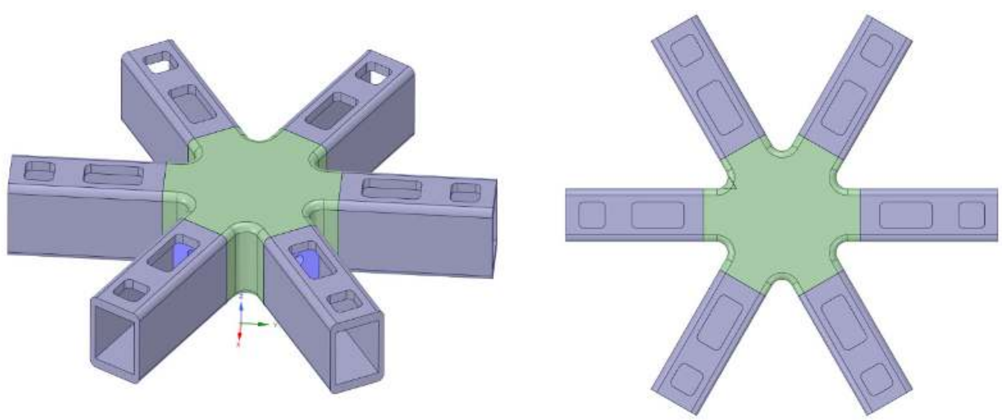

Figure 4.79 Designed structural node connecting to six members

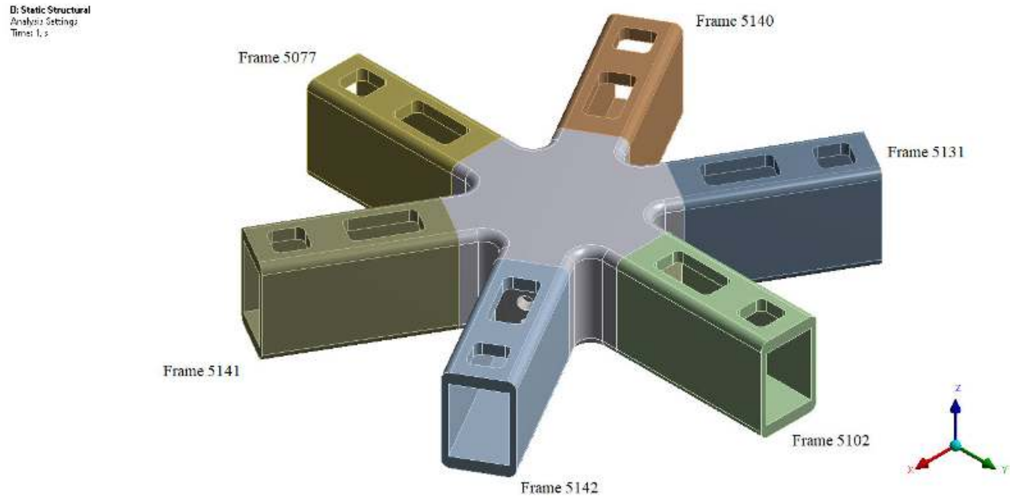

Figure 4.80 Frame Labels

The accuracy of results will depend on the mesh quality, so choosing a mesh size that balances accuracy with computational effort is essential.

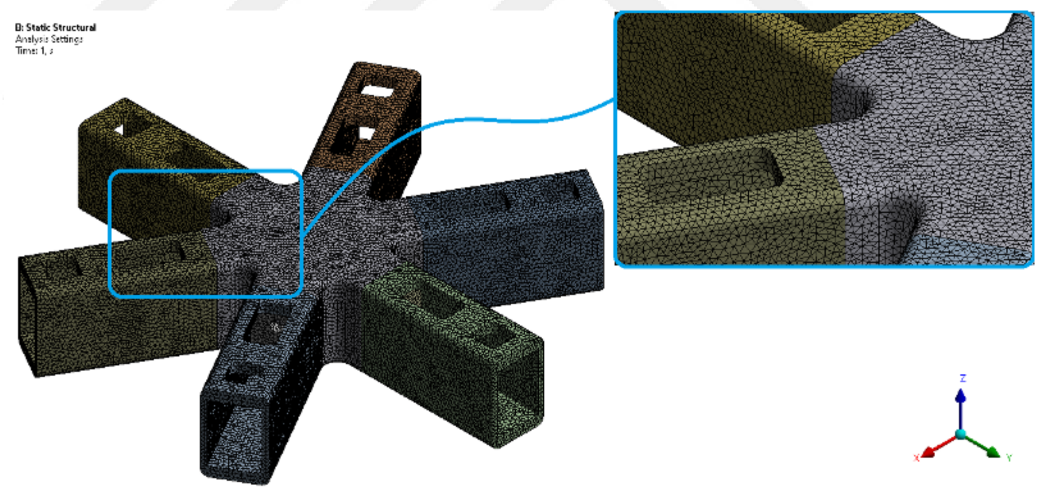

Figure 4.81 Mesh

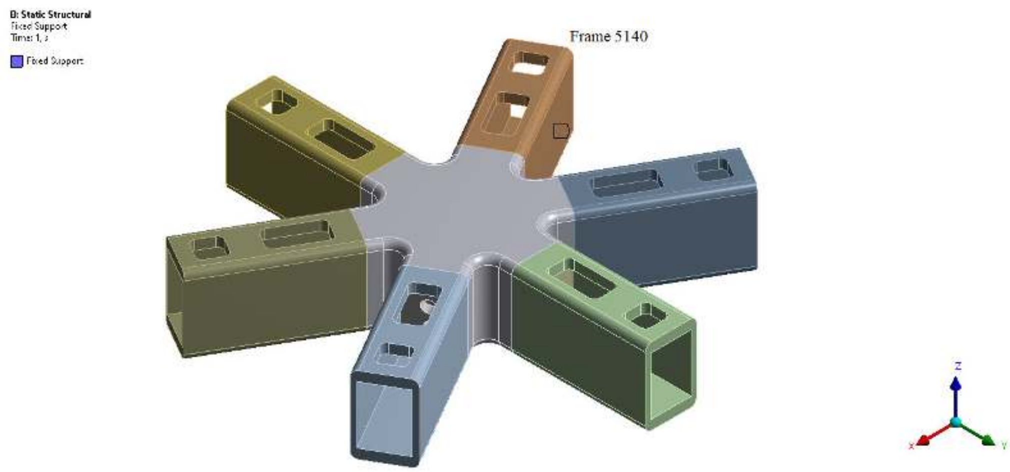

Figure 4.82 Boundary condition

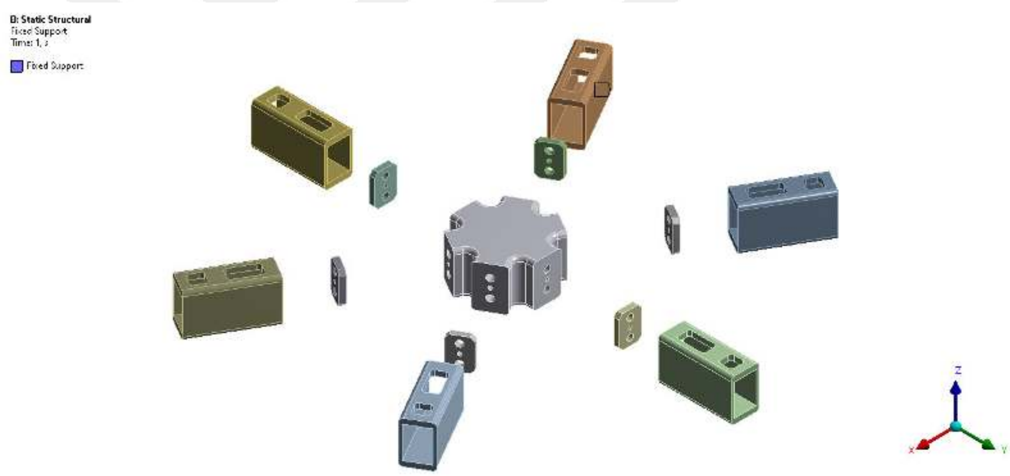

Figure 4.83 Assembling of structural node showing their internal structure

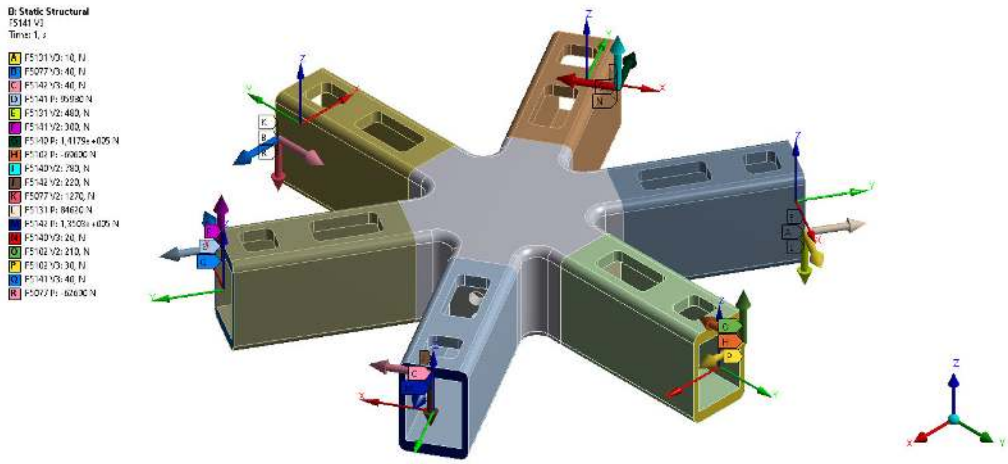

Figure 4.84 Applied forces (axial and shear forces)

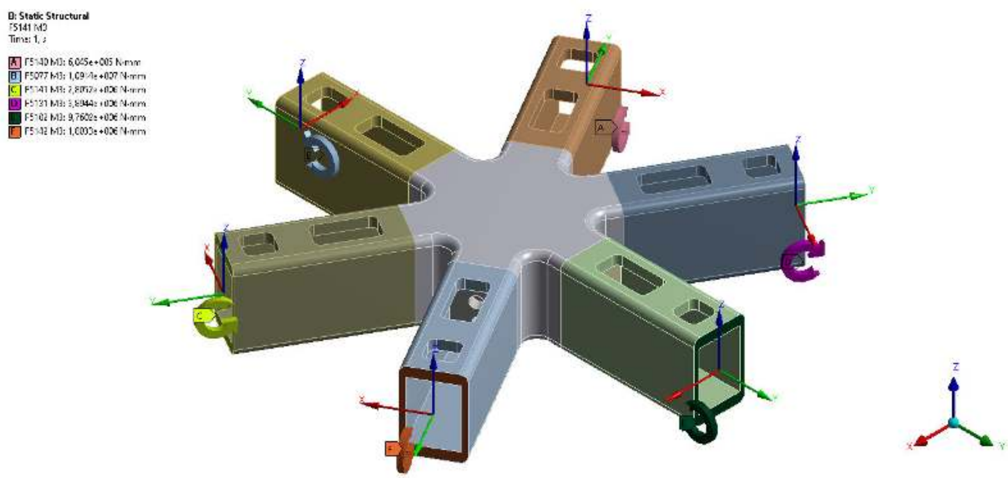

Figure 4.85 Applied moments (M2-2, M3-3 and torsion moment)

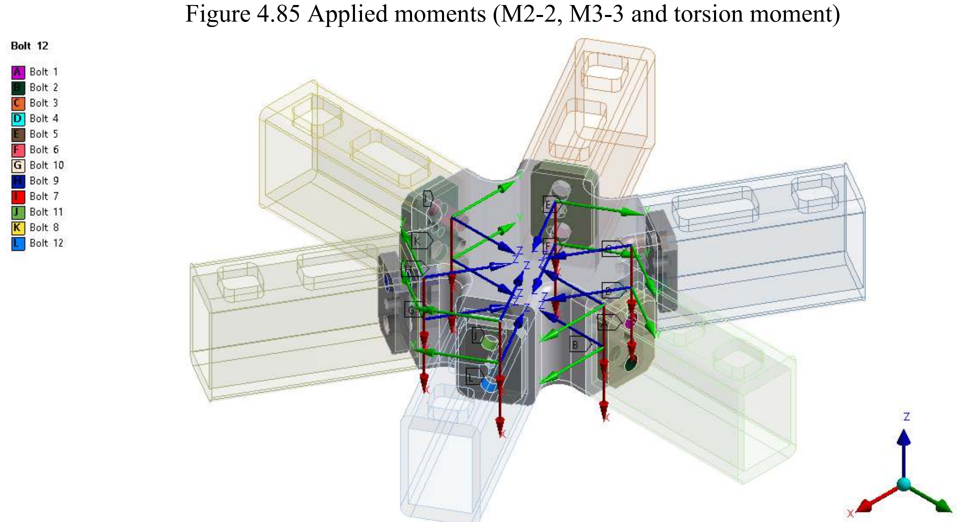

Figure 4.86 Connection between node and profile

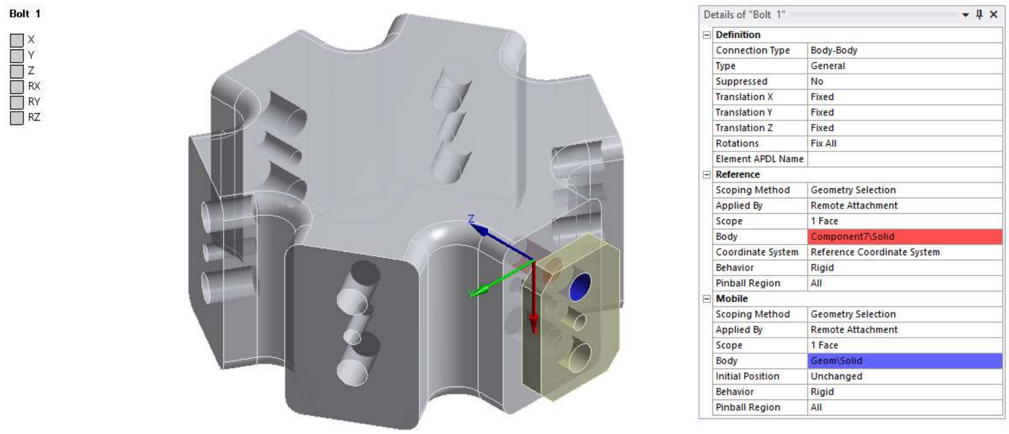

Figure 4.87 Bolt connection definition

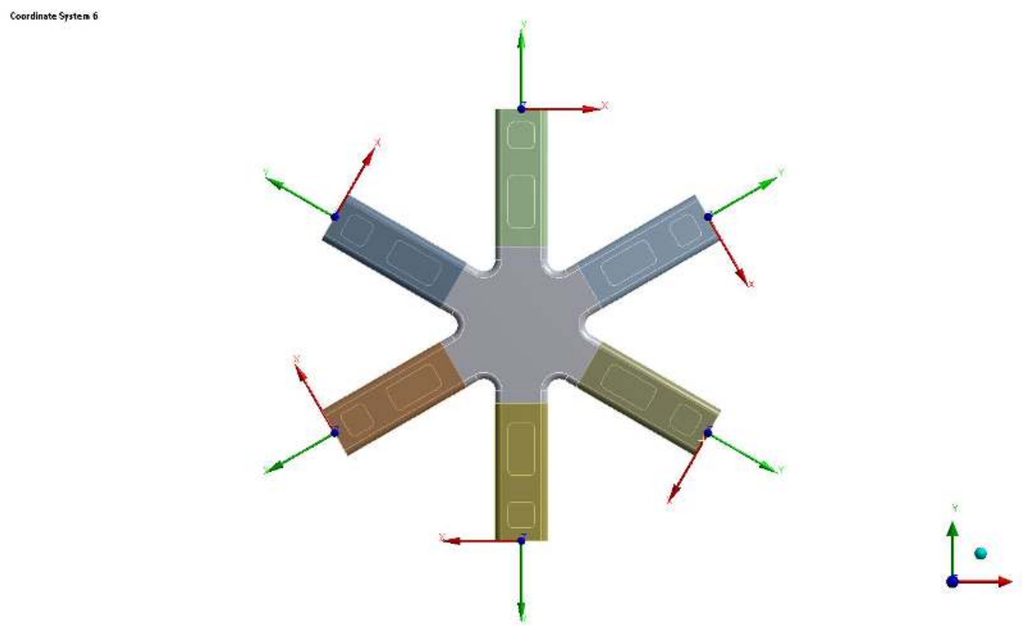

Figure 4.88 Frame local axes

The displacements and stresses in the node will be checked for node calculations.

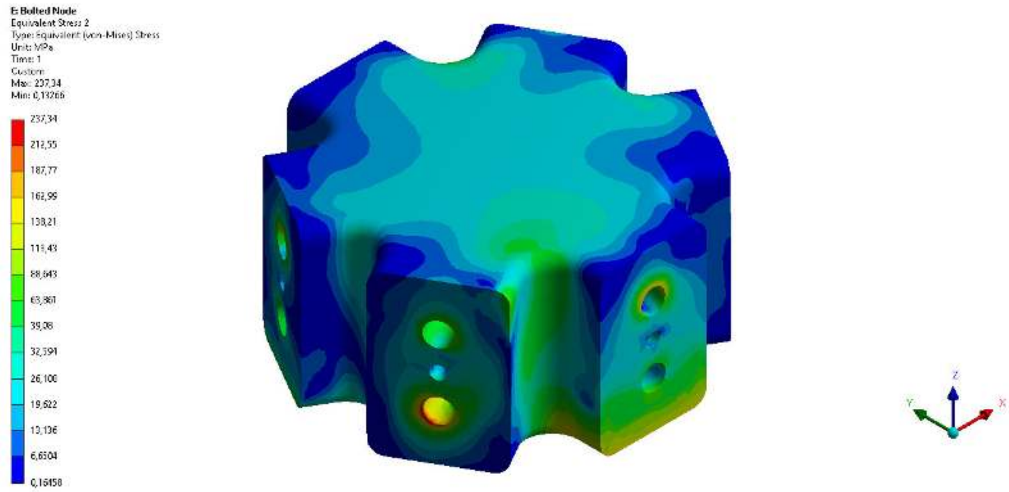

Figure 4.89 von Mises stress contours of structural nodes
under loading condition σ_{max} = 237,34 MPa

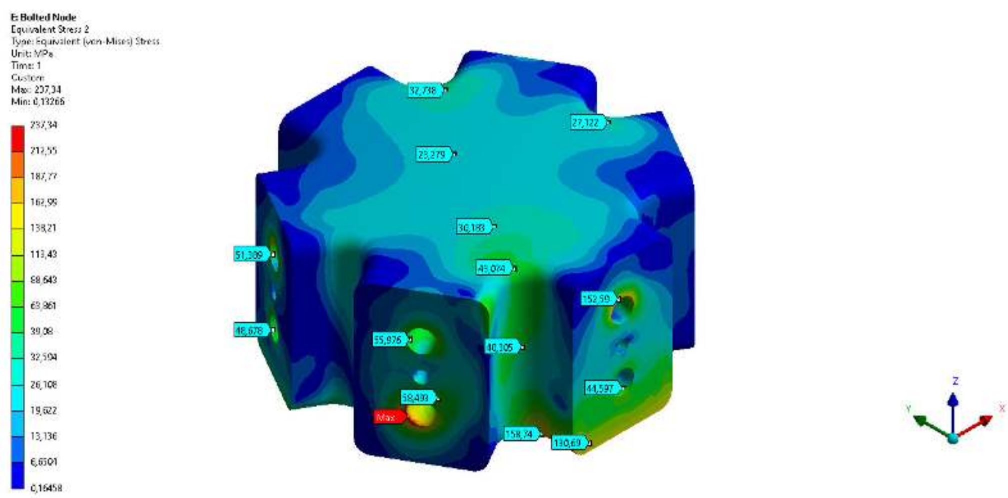

Figure 4.90 von Mises stress contours of structural nodes
under loading condition σ_{max} = 237,34 MPa

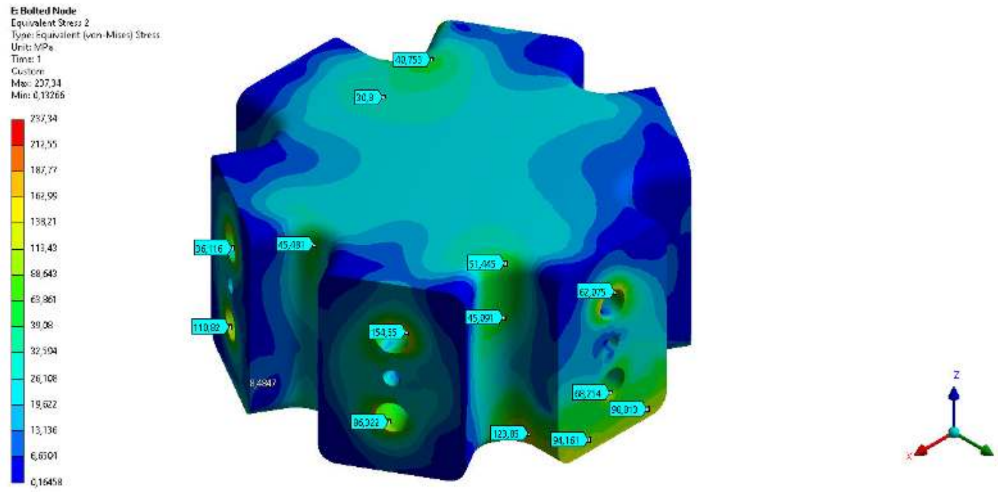

Figure 4.91 von Mises stress contours of structural nodes
under loading condition σ_{max} = 237,34 MPa

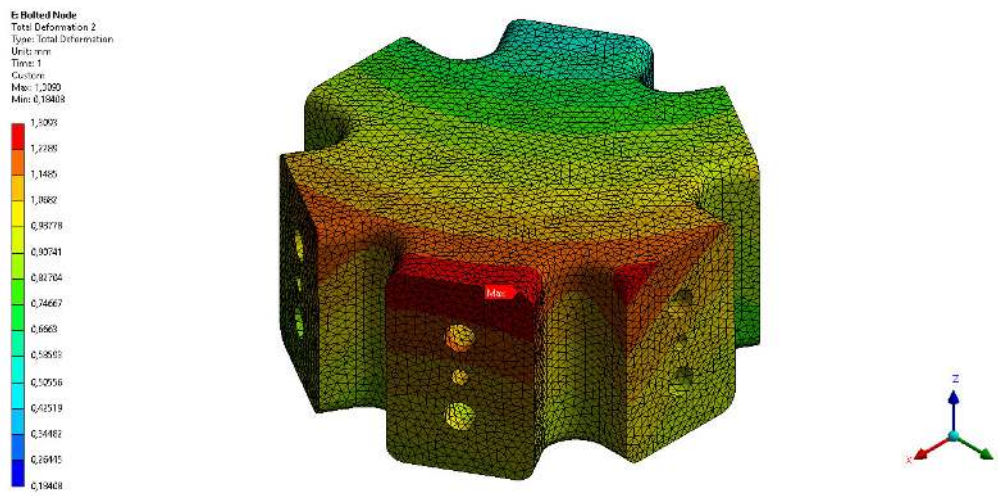

Figure 4.92 Deformed shape of node
under loading condition f_{max} = 1,31mm

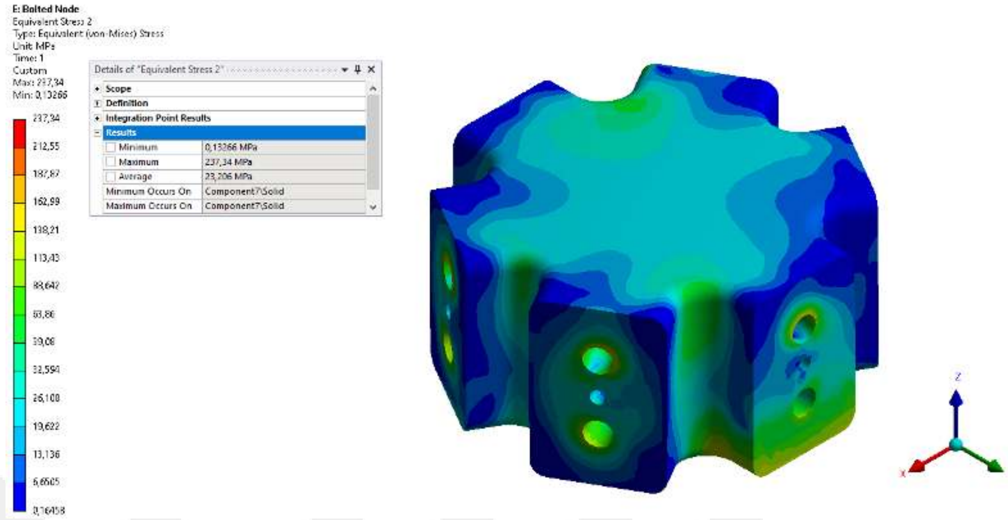

Figure 4.93 von Mises stress contours maximum, minimum and average results

Details of "Component7\Solid"

Material	
Assignment	Structural Steel
Nonlinear Effects	Yes
Thermal Strain Effects	Yes
Bounding Box	
Length X	246,6 mm
Length Y	238,56 mm
Length Z	120, mm
Properties	
Volume	4,8977e+006 mm³
Mass	38,447 kg
Centroid X	-194,12 mm
Centroid Y	-9,6453e-003 mm
Centroid Z	30,889 mm
Moment of Inertia Ip1	1,7565e+005 kg·mm²
Moment of Inertia Ip2	1,7569e+005 kg·mm²
Moment of Inertia Ip3	2,5872e+005 kg·mm²

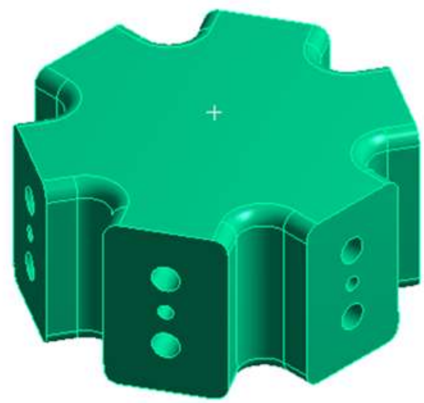

Figure 4.94 Mass of node

4.7.2 Welded node analysis

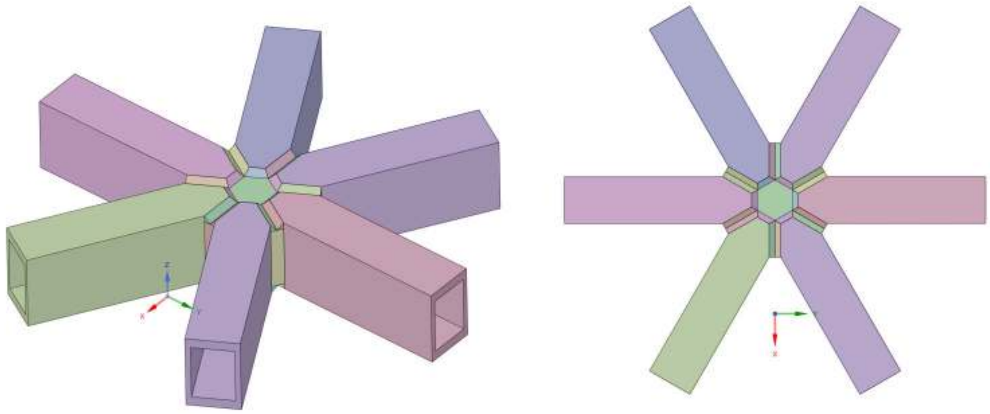

Figure 4.95 Designed structural node connecting to six members

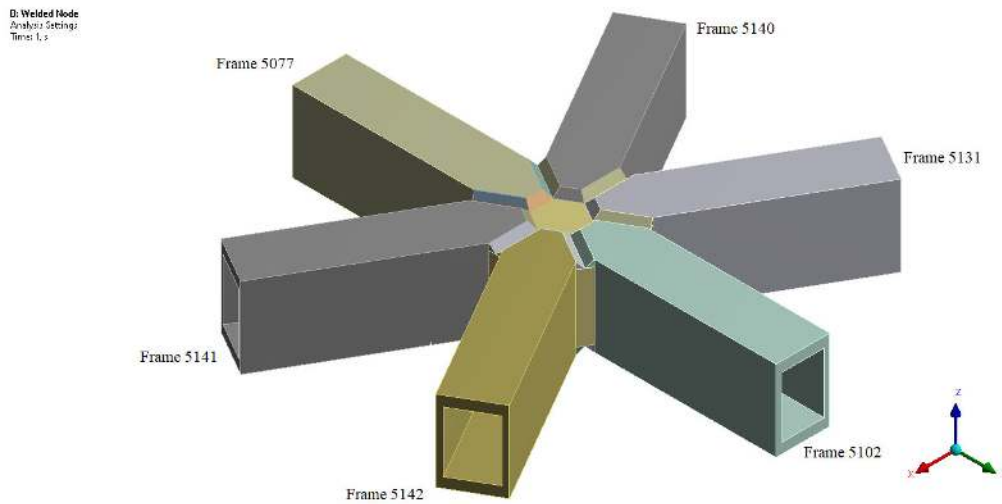

Figure 4.96 Frame Labels

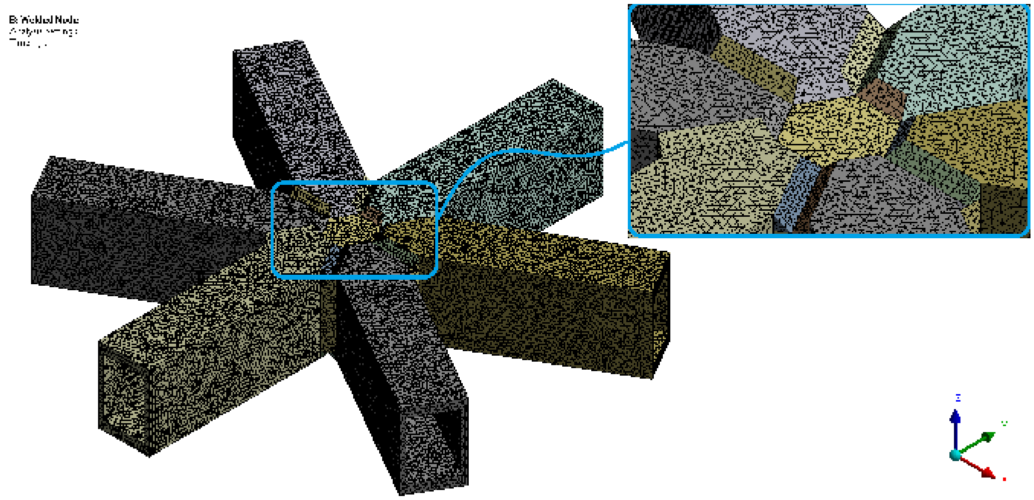

Figure 4.97 Mesh

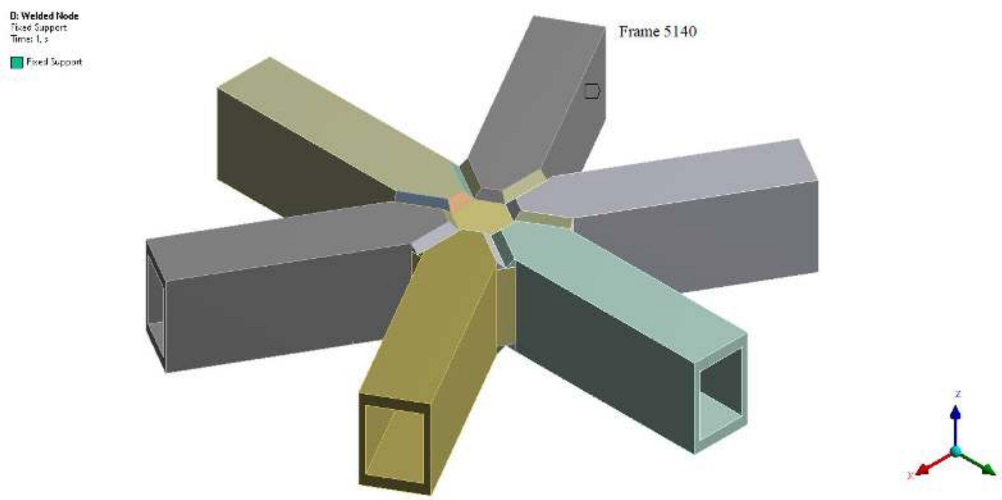

Figure 4.98 Boundary condition

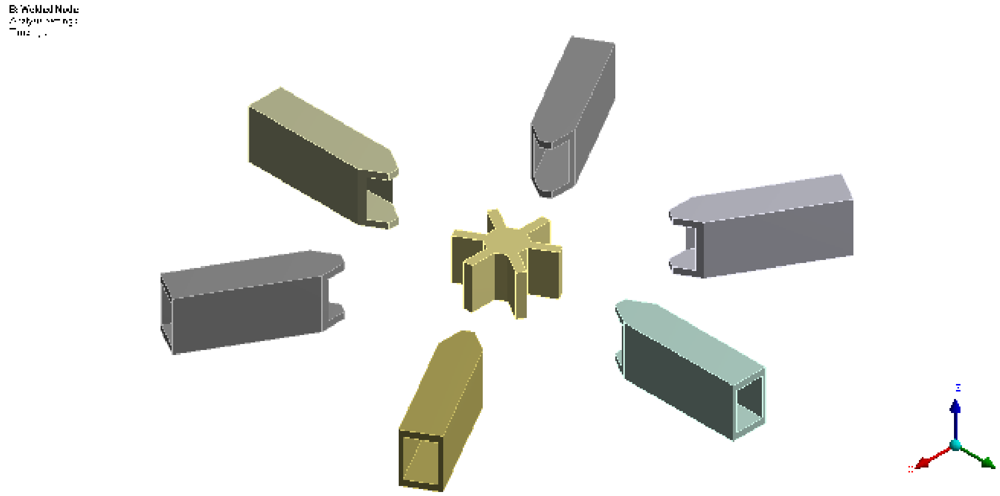

Figure 4.99 Assembling of structural nodes showing their internal structure

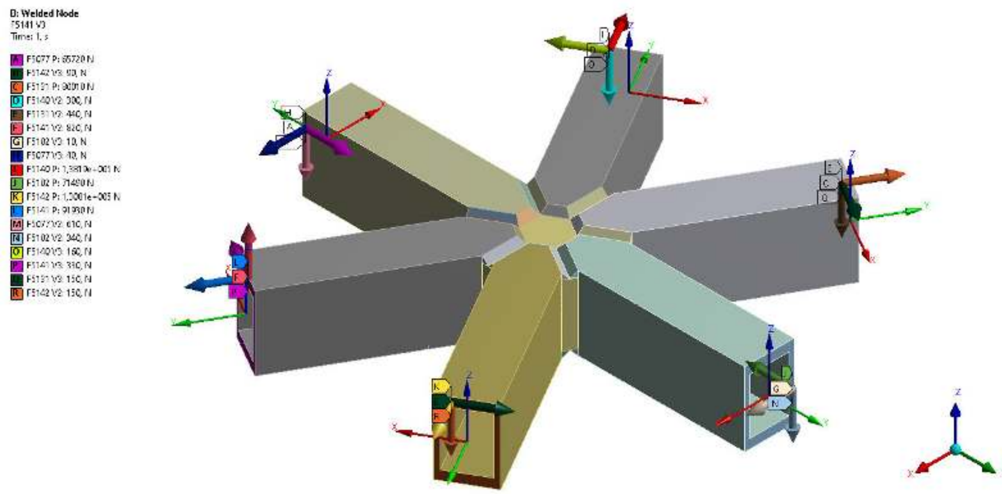

Figure 4.100 Applied forces (axial and shear forces)

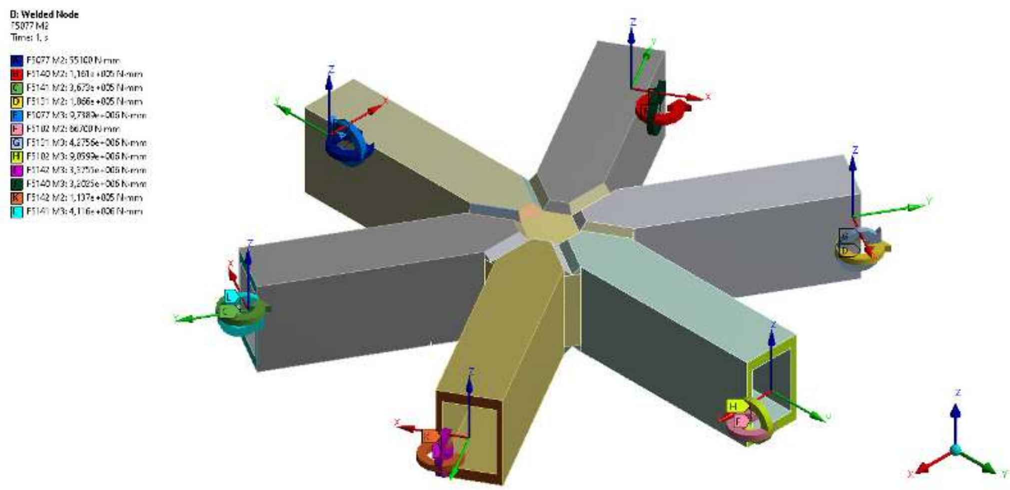

Figure 4.101 Applied moments (M2-2, M3-3 and torsion moment)

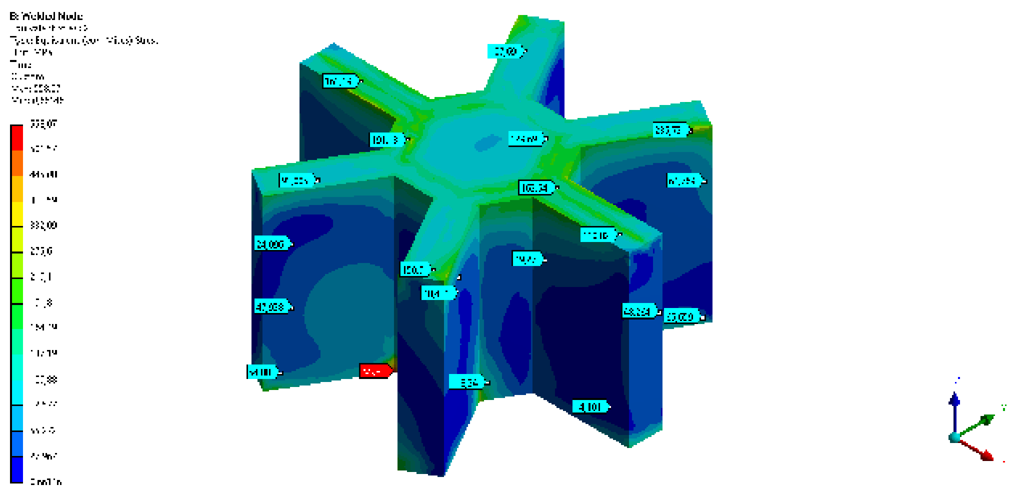

Figure 4.102 von Mises stress contours of structural nodes under loading condition σ_{max} = 558,07 MPa

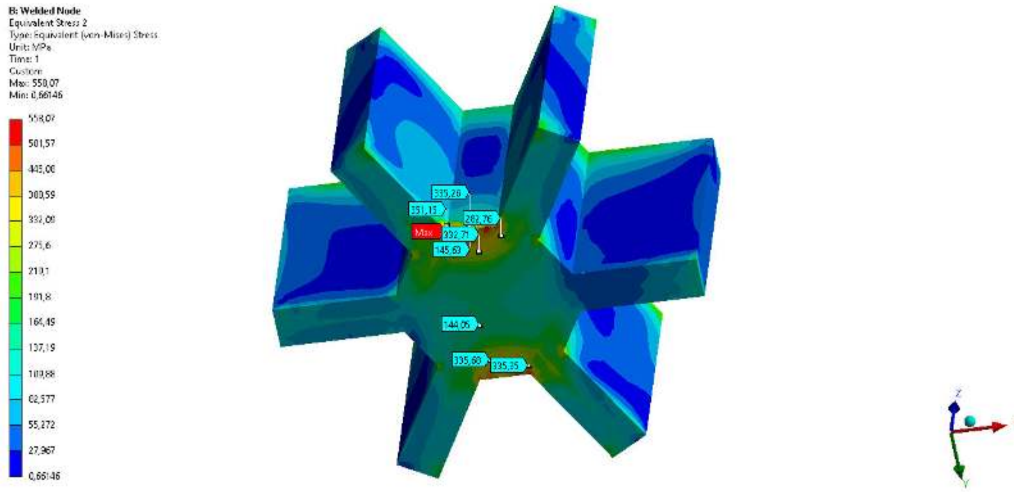

Figure 4.103 von Mises stress contours of structural nodes
under loading condition σ_{max} = 558,07 MPa

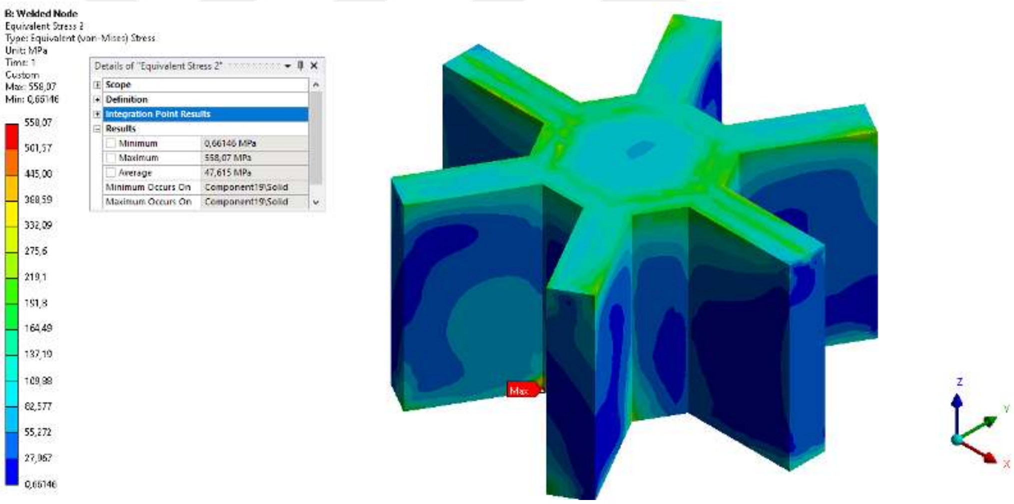

Figure 4.104 von Mises stress contours max., min. and average results

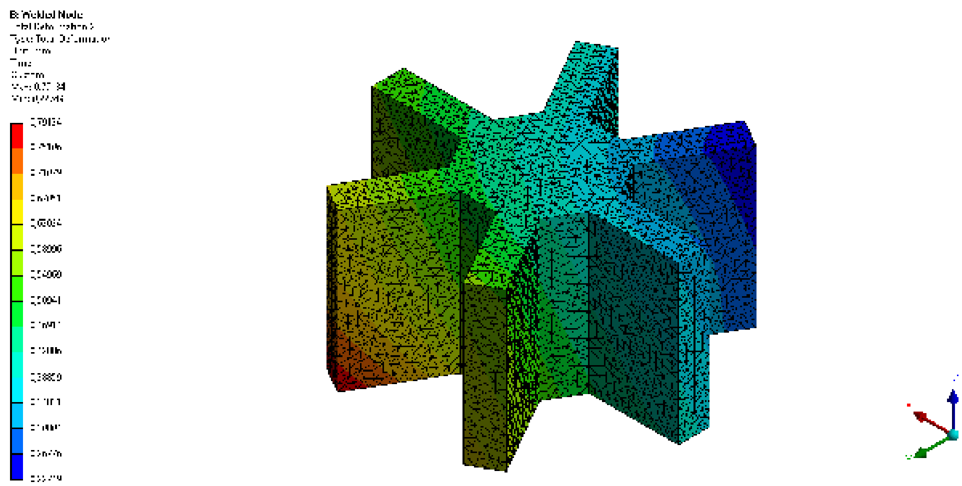

Figure 4.105 Deformed shape of node
under loading condition f_{max} = 0,79mm

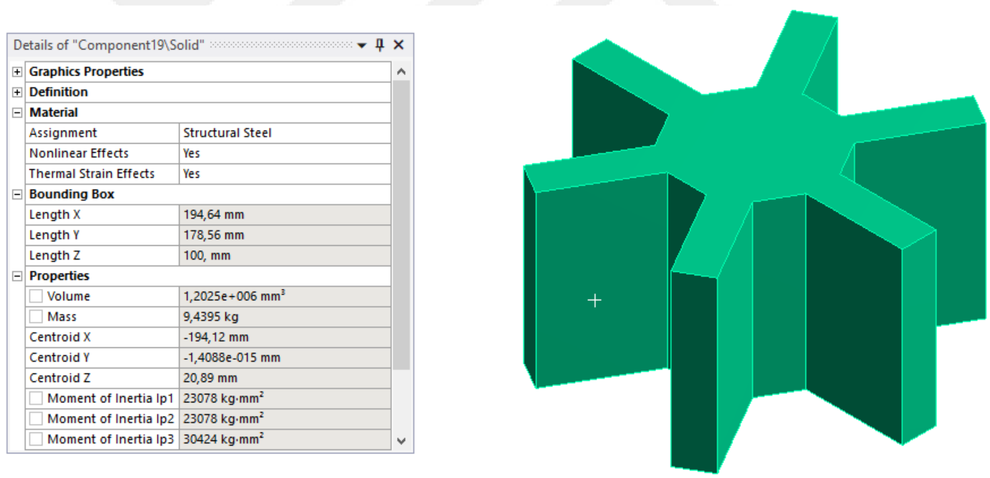

Figure 4.106 Mass of node

5. RESULTS, CONCLUSIONS, AND FUTURE WORK

5.1 Result and Conclusions

In recent years, single-layer free-form systems have gained popularity in architectural design projects for constructing unique and original structures. These designs have attracted significant local and international attention due to their impressive appearance. The use of single-layer free-form systems allows for the realization of creative and boundary-pushing designs while adding a different dimension to the external appearance and functionality of the structures. Compared to traditional methods, these systems can be constructed using less material, making them more environmentally friendly and cost-effective.

This MSc thesis thoroughly examines the technical details of single-layer free-form systems from architectural and engineering perspectives. The different connection types, welded and bolted connections at the system's joints, are investigated. The advantages and disadvantages of these connection types are discussed in detail. The architecture of the Queen Elizabeth II Great Court British Museum serves as an example in this thesis, and the single-layer free-form structure assumed to be constructed in the Yeşilköy neighborhood, Bakırköy district, Istanbul, is analyzed using SAP2000. The critical joint obtained from this analysis is also analyzed as the welded and bolted connection using ANSYS. The applied loads, including static, snow, earthquake, and wind, are evaluated based on relevant codes.

Two different case analyses are carried out for the single-layer free-form system. In the first case, the moment in the weak direction (2-2 direction) is released, assuming the structure does not resist moments in the weak direction. This case is analyzed with bolted connections at the joints. In the second case, the structure is assumed to transfer all forces, and the analysis is conducted with welded connections at the joints.

Based on the analysis results, the following findings are obtained:

- The joint reactions yield approximately the same results for both cases.
- The critical buckling value for the first case is 1.22, while 3.65 for the second case. It indicates that the welded connection provides more stability in terms of torsion compared to the bolted connection.
- The modal analysis results for the first and the second cases are 3.32 Hz and 3.38 Hz. Similar results are obtained in terms of mode shapes for both cases.

- In terms of deflection, the same deflection value is obtained for both cases under the G+0.5S1 load combination. This result implies that the release of moments in the weak direction does not affect the moment of inertia in the strong direction.
- The joint analysis reveals that the maximum stress value in the welded connection is approximately 60% higher than that in the bolted connection, while the maximum deflection value in the bolted connection is approximately 65% higher than that in the welded connection.
- The stress ratio of the profiles is in the range of 0.70, and while this stress ratio could potentially be increased, it would risk reducing the buckling factor to inadequate levels.
- In a welded system, transporting the elements that have been welded in the factory to the construction site poses a significant logistical challenge due to the irregular and often large-scale nature of these elements. Conversely, bolted systems, which tend to have a more regular shape, offer greater ease of transport due to their modularity, making them more advantageous from a logistical perspective.

In conclusion, it is observed that the load combinations causing the most critical torsion factors in the model involve asymmetric loads, which highlights their importance in the design stage. When considering the differences between the bolted and welded connections, the most significant variation is observed in the torsion factor. The welded connection shows more stable behavior in terms of torsion. However, there are advantages and disadvantages associated with each connection type.

Welded connections offer a strong and secure connection but may require high temperatures and specialized equipment, and their recyclability and reassembly can be challenging. On the other hand, bolted connections allow easy and quick assembly, disassembly, maintenance, and repair and provide an aesthetically pleasing appearance.

Different profile types can be explored for future studies to obtain different results. The impact of different profile types on joint connection design can be investigated. Additionally, the effect of different joint connection designs on the overall structure can be studied. Lastly, further research can focus on optimizing joint connection designs and their impact on the structure.

REFERENCES

Ahmed, M., & Stutzki, C. (2015). Steel/Aluminum Grid Shells for Skylights. Structures Congress 2015,

AISC 360-16. (2016). AISC 360-16, Specification for Structural Steel Buildings. Chicago.

Ali, H. (2013). Rtionalisation of Freeform Glass Facades from Concept to Construction.

Andreu, P. (2013). The Osaka Maritime Museum Retrieved from https://www.japan-experience.com/all-about-japan/osaka/museums-galleries/osaka-maritime-museum

Andrieu, P. (2000). The Osaka Maritime museum Retrieved from https://www.hda-paris.com/project/maritime-museum-osaka-japon/

ANSI/AISC 360-10. 2010. Specification for Structural Steel Buildings. American Institute of Steel Construction, pp. 1–612.

ANSYS INC. (2015). ANSYS User Manual Version 16.0. Canonsburg, Pennsylvania.

Arup. Watercube Beijing Retrieved from https://archello.com/fr/story/422/attachments/photos-videos/5

Bobbarton, (2012). Mainheim Multihalle. Arup and Frie Otto. The first and still the biggest gridshell in timber.

Breakdown, (2008). Stress Strain Ductile Material Retrieved from https://commons.wikimedia.org/wiki/File:Stress_Strain_Ductile_Material.png

Brown, S. (2000). Engineering the British Museum Great Court Roof. In Widespan Roof Structures (pp. 283-286). Thomas Telford Publishing.

Chow, S. (2021). The Astrodome Retrieved from https://www.khou.com/article/sports/astrodome-future-houston/285-1d29cb48-eb8b-47ae-b0eb-635aa7f28c15

Clerk, G. (2018). Sage Gateshead Retrieved from https://www.accountingweb.co.uk/tech/accounting-software/sage-business-cloud-accounting-debuts-at-gateshead

Cowing, K. (2013). The South Pole Dome Retrieved from https://spaceref.com/science-and-exploration/deconstruction-of-the-south-pole-dome/

Crystal, E. (2009). The Roman Pantheon Retrieved from https://www.teggelaar.com/en/rome-day-5- continuation-2

CSI Analysis Reference Manual. (2017). Analysis Reference Manual. The USA.

Didier, Boy De La Tour (2010). Centre Pompidou-Metz Retrieved from https://www.archdaily.com/490141/centre-pompidou-metz-shigeru-ban architects

Diliff, (2013). Panorama of the Great Court of the British Museum Retrieved from https://commons.wikimedia.org/wiki/File:British_Museum_Great_Court,_London,_UK_-_Diliff.jpg

Ding, Y., Chen, Z.-T., Zong, L., & Yan, J.-B. (2017). A theoretical strut model for severe seismic analysis of single-layer reticulated domes. Journal of Constructional Steel Research, 128, 661-671.

DiStefano, G. (2017). Palazzetto dello sport a Roma Retrieved from https://www.radiocolonna.it/gioie-e-dolori/roma-ecco-lufficio-gare-per-lo-sport-diario-stop-a-tempi-biblici-per-i-bandi/

Dragone, G. (1979). Wind Effect on Hemispherical Domes MSc Thesis, University of Surrey.

Eckersley O'Callaghan. (2018). Iona Skydome Retrieved from https://www.eocengineers.com/projects/iona-skydome-370/

Economic, U. N. D. o., & Division, S. A. P. (2006). World urbanization prospects: the 2009 revision. UN.

Evanson, T. (2013) Kogod Courtyard - northeast corner and floor - Smithsonian American Art Museum Retrieved from https://www.flickr.com/photos/timevanson/8349341128

GDR, (2023). Graves Development Resources Retrieved from https://gonebraska.com/what-to-know-before-moving-to-omaha/

Graitec, Comparison figure, Retrieved from https://advantage.graitec.com/en-ca/knowledgebase/article/KA-02006

Halbe, R. (2017). Abu Dhabi, United Arab Emirates Retrieved from https://parametric-architecture.com/louvre-abu-dhabi-by-ateliers-jean-nouvel/

Harris, R., Haskins, S., & Roynon, J. (2008). The Savill Garden gridshell: Design and construction. The Structural Engineer, 86(17), 27-34.

Heki, K. (1984). Analysis, Design and Realization of Space Frames. Bulletin of LASS, 84, 96-406.

Helbig, T., Giampellegrini, L., & Oppe, M. (2014). "Carioca Wave"–A free-form steel-and-glass canopy in Rio de Janeiro, Brazil. Steel Construction, 7(4), 252-257.

Helbig, T., Riederer, J., Kamp, F., & Oppe, M. (2016). Free-form on every scale: " Tornado "roof structure for Bory Mall, Bratislava, Slovakia. Steel Construction, 9(3), 249-254.

Hurstley, T. (2019). Jewel Changi Airport, Singapore Retrieved from https://worldlandscapearchitect.com/jewel-changi-airport-singapore-pwp-landscape-architecture/?v=ebe021079e5a

Huth, D. (2006). Beehive Hut. Retrieved from https://commons.wikimedia.org/wiki/File:Dingle_beehive_hut.JPG

Hwang, K., Knippers, J., & PARK, S.-W. (2009). Influence of various types of node conectors on the buckling loads of grid shells. Symposium of the International Association for Shell and Spatial Structures (50th. 2009. Valencia). Evolution and Trends in Design, Analysis and Construction of Shell and Spatial Structures: Proceedings,

Janberg, N. (1897). Vyksa Steel Production Hall.

Janberg, N. (2003). Palazzetto dello Sport, Rome Retrieved from https://structurae.net/en/media/11325-palazzetto-dello-sport-rome

Janberg, N. (2007). Ctesiphon Palace. Retrieved from https://www.britannica.com/place/Taq-Kisra

Janberg, N. (2009). Bourse de Commerce Retrieved from https://structurae.net/en/media/146082-bourse-de-commerce

Janberg, N. (2020). Great Zeiss Planetarium Berlin Retrieved from https://structurae.net/en/media/340710-great-zeiss-planetarium-berlin

Kara, T. (2019). Tek tabakali kubbelerin taşiyici sistemlerinin yönetmelikler açisindan değerlendirilmesi.

Knippers Helbig. (2016). “Tornado” roof structure for Bory Mall, Bratislava, Slovakia Retrieved from https://www.knippershelbig.com/en/projects

Lam, M. Watercube Beijing Retrieved from https://archello.com/fr/story/422/attachments/photos-videos/1

Li, H., Wang, J., Ren, X., & Lu, W. (2015). Dynamic Collapse Analysis of Reticulated Shell Structures with Substructures. 2015 International Conference on Structural, Mechanical and Material Engineering,

Liddell, I. (2015). Frei Otto and the development of gridshells. Case Studies in Structural Engineering.4: 39-49.

lunamtra (2008). Steel-cupola built by F.W. Schwedler in Berlin in 1874.

Maten, R.N. 2011. Ultra High Performance Concrete in Large Span Shell Structures. Master Thesis, Delft University of Technology, Delft, the Netherlands, pp. 266.

Melchoir, (2006). Von Mises stress 2D Retrieved from https://commons.wikimedia.org/wiki/File:Tresca_stress_2D.png

Melissa. (2009). Beehive Tomb. Retrieved from http://art103fall2009.pbworks.com/w/page/10992785/Mycenaean%20Art.

Metal Yapı. (2014) Bory Mall Retrieved from https://www.metalyapi-eng.com/projects-bory-mall.html

Mirtschin, J. (2012). British Museum Great Court Roof Cad Model Retrieved from http://geometrygym.blogspot.com/2009/11/british-museum-great-court-roof-using.html

Mittendorf, J., & Dodson, D. (2015). The Art of Reading Buildings. Fire Engineering Books.

Murphy, J. (2008). The Spruce Goose Retrieved from https://commons.wikimedia.org/wiki/File:Queen_Mary_Dome_(3298007004).jpg

NGI, (2022). Sage Gateshead Retrieved from https://www.ngi.org.uk/resources/news/sage-gateshead-is-changing-its-name-and-inviting-people-to-get-involved/

Özcan, M. (2019). Tek katmanlı uzay kafes kubbelerde çapraz eleman kullanımının tasarıma etkisinin belirlenmesi.

Özuygün, Ş. (2004). Statik itme yöntemiyle bina tahkiki ve güçlendirme hesabı. (Master’s thesis). İstanbul Teknik Üniversitesi, Fen Bilimleri Enstitüsü, İstanbul. (örnek tez yazımı)

Paco, (2007). Sketch of the missing "Recoletos Fronton" of Madrid, Retrieved from https://commons.wikimedia.org/wiki/File:Fronton_Recoletos.png

Prat, R. (2005). The New Milan Trade Fair Retrieved from https://www.architonic.com/es/project/studio-fuksas-the-new-milan-trade-fair/5103915

Quan, G., Qi, J., Wu, H., Ye, J., Gao, B., Xu, N., & Hu, B. (2022). Experimental and numerical study on the performance of new prefabricated connections for free-form grid structures. In Structures (Vol. 36, pp. 1050-1067). Elsevier.

Rotunda, Bourse de Commerce – Pinault Collection, Paris Retrieved from https://www.museos.com/en/paris/bourse-de-commerce/

RSP, (2020). Architects Planners & Engineers Retrieved from https://rsp.sg/rsp_work/jewel-changi-airport/

Rswarbrick, (2009). Von mises and Tresca yield surfaces in the principle stresses Retrieved from coordinate https://commons.wikimedia.org/wiki/File:Yield_surfaces.svg

SAP2000 Integrated Structural Analysis and Design Software, Computer and Structure Inc., Berkeley, California, 2000.

Saraç, Y. (2005). Optimum design of pın-jointed 3-D dome structures using global optimization techniques Middle east technical university].

Savaşır, K., & Tuğrul, F. (2014). Uzay Kafes Sistemlerle Yaratılabilecek Üst Örtülerin Yüzey Geometrilerinin İncelenmesi: Heydar Aliyev Merkezi Örneği, 7. Ulusal Çatı & Cephe Sempozyumu, 3-4.

Schlaich, J., Schober, H., & Kürschner, K. (2005). New trade fair in Milan—grid topology and structural behaviour of a free-formed glass-covered surface. International Journal of Space Structures, 20(1), 1-14.

Schlegelmilch, C. (2009). "Circlehouse/Fichtebunker" Retrieved from http://www.cordiaschlegelmilch.de/fotografie/architektur/?DOC_INST=5,%2026.02.2019

Seele Austria. Carioca Wave Retrieved from https://seele.com/locations/se-austria-gmbh-co-kg-at

Seele Pilsen. Carioca Wave Retrieved from https://seele.com/references/carioca-wave

Seifi, H. (2019). Topology optimisation and additive manufacturing of structural nodes of gridshell structures (Doctoral dissertation, RMIT University).

Sischka, J. (2000). Engineering the construction of the great court roof for the British Museum. Widespan roof structures, 199.

Sta, C. (2015). Fukuoka Seaside Momochi Aerial Shoot Retrieved from https://commons.wikimedia.org/wiki/File:Fukuoka_Seaside_Momochi_Aerial_Shoot.jpg

Stephan, S., Sánchez-Alvarez, J., & Knebel, K. (2004). Reticulated structures on free-form surfaces. Stahlbau, 73(8), 562-572.

Stephan, S., Sánchez-Alvarez, J., & Knebel, K. (2004). Reticulated structures on free-form surfaces. Stahlbau, 73(8), 562-572.

Strelau, D. (2011). Hagia Sophia I Retrieved from https://commons.wikimedia.org/wiki/File:Interior_of_Hagia_Sophia.jpg

Tonelli, D., Pietroni, N., Puppo, E., Froli, M., Cignoni, P., Amendola, G., & Scopigno, R. (2016). Stability of statics aware voronoi grid-shells. Engineering Structures, 116, 70-82.

TS EN 1991-1-3. 2007. Eurocode 1: Actions on structures - Part 1-3: General actions - Snow loads (Eurocode TS-EN 1991-1-3). TSE, Ankara, 52 s.

TS EN 1991-1-4. 2007. Eurocode 1: Actions on structures - Part 1-4: General actions - Wind actions (Eurocode TS-EN 1991-1-4). TSE, Ankara, 126 s.

VCG, (2018). The Harbin Opera House in Northeast China's Harbin Retrieved from http://europe.chinadaily.com.cn/a/201801/05/WS5a4eea9ba31008cf16da5469_4.html

Wade Fund, J. H. (1974). Interior of the Pantheon, Rome Retrieved from https://www.clevelandart.org/art/1974.39

Wagner Biro, (2015). Louvre Abu Dhabi Retrieved from https://www.wb-sg.com/projects/louvreabudhabi/

Wagner Biro,(2000). The British Museum Retrieved from https://www.wb-sg.com/projects/britishmuseum/

Wheelahan, D. (2020). Shine Dome Retrieved from https://www.science.org.au/news-and-events/news-and-media-releases/towards-net-zero-emissions-australias-home-science

Williams, C. J. (2000). The definition of curved geometry for widespan structures. In Widespan roof structures (pp. 41-49). Thomas Telford Publishing.

Williams, C. J. (2001). The analytic and numerical definition of the geometry of the British Museum Great Court Roof. *Mathematics & design*, *200*, 434-440.

Xiong, Z., Guo, X., Luo, Y., & Zhu, S. (2017). Elasto-plastic stability of single-layer reticulated shells with aluminium alloy gusset joints. Thin-Walled Structures, 115, 163-175.

Yilmaz, G. (2021) Tek katmanli uzay kafes kubbelerde berkitme elemani kullaniminin tasarima etkisinin belirlenmesi.

Young, N. (2000). Great Court at the British Museum, London Retrieved from https://arquitecturaviva.com/works/renovacion-del-british-museum-2

Zhi, X., Nie, G., Fan, F., & Shen, S. (2012). Vulnerability and risk assessment of single-layer reticulated domes subjected to earthquakes. Journal of Structural Engineering, 138(12), 1505-1514.

ANNEX

Annex 1: Joint Reactions

Joint	OutputCase	F1	F2	F3	M1	M2	M3
Text	Text	KN	KN	KN	KN-cm	KN-cm	KN-cm
R20	1,2G + 1,6S2 + 0,8Wp	***293,66***	160,61	259,43	467,86	64,26	112,14
R5	1,2G + 1,6S1 + Q	96,90	-466,91	447,61	-114,86	632,39	***-580,91***
R18	1,2G + 1,0Q + 0,5S2 + 1,6Wp	41,64	7,96	53,61	***3358,82***	-15,65	-111,97
R18	1,2G + 1,6S2 + Q	1,58	***422,74***	***462,53***	-854,58	-0,56	27,43
R1	1,2G + 1,0Q + 0,5Qr + 1,6Wp	-0,81	224,76	-258,67	***-2266,96***	-11,46	2,97
R1	1,2G + 1,0Q + 0,5S2 + 1,6Wp	-1,73	228,81	***-265,37***	-2163,87	-8,41	-0,16
R37	1,2G + 1,0Q + 0,5Qr + 1,6Wp	-7,73	-206,97	-4,02	-822,16	-486,93	***617,83***
R50	1,2G + 1,0Q + 0,5S1 + 1,6Ws	-24,22	55,75	38,03	-66,49	***-4290,16***	-26,24
R4	1,2G + 1,6S1 + Q	-92,17	***-475,33***	452,58	-97,09	-627,35	592,30
R49	1,2G + 1,6S1 + Q	-181,49	-2,43	140,10	-146,71	***1974,31***	101,74
R16	1,2G + 1,0Q + 0,5S2 + 1,6Wp	***-283,80***	52,15	195,38	642,85	323,53	-29,10

Annex 1 : Joint reactions for Case 1

Joint	OutputCase	F1	F2	F3	M1	M2	M3
Text	Text	KN	KN	KN	KN-cm	KN-cm	KN-cm
R4	1,2G + 1,6S1 + Q	-94,30	***-467,26***	447,48	-78,96	-598,60	***625,43***
R16	1,2G + 1,0Q + 0,5S2 + 1,6Wp	***-281,98***	55,51	197,72	738,64	406,83	75,77
R49	1,2G + 1,6S1 + Q	-181,01	-2,13	140,12	-174,68	***1973,92***	72,46
R20	1,2G + 1,6S2 + 0,8Wp	***286,67***	162,66	260,16	515,53	118,60	44,78
R1	1,2G + 1,0Q + 0,5Qr + 1,6Wp	-0,13	228,61	-262,31	***-2296,58***	-8,12	12,66
R1	1,2G + 1,0Q + 0,5S2 + 1,6Wp	-1,28	231,90	***-267,99***	-2188,75	-8,82	11,64
R18	1,2G + 1,6S2 + Q	0,62	***420,18***	***458,53***	-871,85	-6,69	9,07
R18	1,2G + 1,0Q + 0,5S2 + 1,6Wp	44,31	4,46	51,51	***3393,53***	31,60	-54,11
R50	1,2G + 1,0Q + 0,5S1 + 1,6Ws	-25,87	55,55	37,76	-219,88	***-4272,78***	-125,57
R5	1,2G + 1,6S1 + Q	95,28	-466,57	446,91	-77,04	602,31	***-609,16***

Annex 2 : Joint reactions for Case 2

Annex 2: Frame Forces

Frame	Station	OutputCase	P	V2	V3	T	M2	M3
Text	cm	Text	KN	KN	KN	KN-cm	KN-cm	KN-cm
149	0,00	1,2G + 1,0Q + 0,5S1 + 1,6Ws	-1,65	***26,59***	0,27	103,80	0,00	***3016,54***
124	105,57	1,2G + 1,6S1 + Q	-203,76	***-17,97***	0,19	36,66	0,00	1668,00
332	0,00	1,2G + 1,6S1 + Q	-9,54	6,42	***2,86***	-5,01	202,03	723,87
333	115,22	1,2G + 1,6S1 + Q	-8,72	-6,24	***-2,90***	5,00	204,52	721,45
339	0,00	1,2G + 1,6S1 + Q	***-323,82***	3,03	-0,90	43,13	0,00	130,00
339	271,40	1,2G + 1,0Q + 0,5Qr + 1,6Wp	***181,12***	1,91	0,60	-20,90	0,00	-112,08
349	172,43	1,2G + 1,6S1 + Q	-99,12	0,02	0,10	-117,96	***231,88***	-249,18
352	174,68	1,2G + 1,6S1 + Q	-99,00	0,02	-0,10	116,84	***-237,70***	-253,03
1323	215,04	1,2G + 1,0Q + 0,5S2 + 1,6Ws	38,72	-0,77	-0,43	***264,78***	0,00	"
1264	185,32	1,2G + 1,0Q + 0,5S2 + 1,6Ws	-29,15	-0,19	-0,40	***-277,99***	0,00	-836,94
570	161,02	1,2G + 1,0Q + 0,5S1 + 1,6Ws	-2,19	2,87	-0,22	-74,94	0,00	***-1205,65***

Annex 3: Frame forces for Case 1

Frame	Station	OutputCase	P	V2	V3	T	M2	M3
Text	cm	Text	KN	KN	KN	KN-cm	KN-cm	KN-cm
149	0,00	1,2G + 1,0Q + 0,5S1 + 1,6Ws	-4,89	***25,40***	-0,02	155,40	-14,86	***2907,54***
124	105,57	1,2G + 1,6S1 + Q	-203,54	***-18,13***	1,25	71,52	-66,71	1661,61
333	115,22	1,2G + 1,6S1 + Q	-9,43	-6,50	***-3,43***	6,63	***221,50***	723,80
332	0,00	1,2G + 1,6S1 + Q	-10,86	6,47	***3,43***	-7,10	221,46	718,96
339	0,00	1,2G + 1,6S1 + Q	***-322,32***	2,48	-1,07	37,52	-73,24	77,65
349	344,87	1,2G + 1,6S1 + Q	-97,05	-1,49	2,00	-120,63	***-148,99***	-104,31
339	271,40	1,2G + 1,0Q + 0,5Qr + 1,6Wp	***179,12***	2,31	0,52	-13,84	-25,23	-217,19
1323	215,04	1,2G + 1,0Q + 0,5S2 + 1,6Ws	37,49	-1,59	-0,41	***257,52***	15,11	-525,52
1264	185,32	1,2G + 1,0Q + 0,5S2 + 1,6Ws	-29,83	-0,71	-0,57	***-263,24***	32,11	-804,56
570	161,02	1,2G + 1,0Q + 0,5S1 + 1,6Ws	-6,31	3,76	-0,32	-72,48	15,57	***-1238,36***

Annex 4 : Frame forces for Case 2

CURRICULUM VITAE

Personal Information

Surname, Name	Serhat, Faruk
Web Page (Research Gate, Academia, etc.)	

Education

Degree	Institution	Year of Graduation
MS	Dicle University	2023
BS	Dicle University	2014
High School	Gazi Anatolian	2010

Work Experience

Period (Year)	Company, Institution	Enrollment
06.2022-Present	Minister of Environment, Urbanisation and Climate Change	Civil Engineer
02.2020-06.2022	Mimsa Alüminyum	Civil Engineer
11.2016-02.2020	Aygün Alüminyum	Civil Engineer
12.2014-11.2015	Uzay Sistem	Civil Engineer

Foreign Languages

English

Hobbies

Book, Technological Developments, Travel

DİCLE ÜNİVERSİTESİ
FEN BİLİMLERİ ENSTİTÜSÜ
TEZ BENZERLİK BİLDİRİMİ FORMU

Öğrencinin Adı, Soyadı	Faruk, Serhat		
Öğrenci No	20806051		
Ana Bilim Dalı	İnşaat Mühendisliği		
Program Türü	Proje ☐	Yüksek Lisans ☒	Doktora ☐
Tez Danışmanı (Ünvanı, Adı, Soyadı)	Doç. Dr. Mehmet Emin ÖNCÜ		
(Varsa) II. Tez Danışmanı (Ünvanı, Adı, Soyadı)			
Tez Başlığı	**Design of Single-Layer Free-Form Steel Structures: A Case Study on The British Museum Great Court Roof**		
RAPOR BİLGİLERİ			
Raporlama Aşaması	Tez Savunma Sınavı Sonrası		
Sayfa Sayısı	186		
Raporlama Tarihi	12.07.2022		
Benzerlik Oranı (%)	19%		

Yukarıda bilgileri verilen tez çalışmamın toplam 186 sayfalık kısmına ilişkin, 12/07/2023 tarihinde şahsım/tez danışmanım tarafından Turnitin isimli intihal tespit programından aşağıda belirtilen filtrelemeler uygulanarak alınmış olan intihal raporuna göre, tezimin benzerlik oranı % 19 olarak tespit edilmiştir.

Uygulanan filtrelemeler:

☐Başlangıç Bölümleri (Kabul ve Onay sayfası, Teşekkür sayfası, Özet/Abstract) hariç

☐Kaynaklar hariç

☐Alıntılar hariç/dâhil

☒Diğer (Her şey dahil)

Tezimin benzerlik oranı, Dicle Üniversitesi Fen Bilimleri Enstitüsü İntihal Raporu Uygulama Esaslarında belirtilen üst sınır benzerlik oranını aşmamaktadır. Benzerlik oranım üst sınır benzerlik oranının altında olsa dahi aksinin tespit edilmesi durumunda her türlü yasal sorumluluğu kabul ettiğimi ve hukuki sonuçlarına razı olduğumu bildirir,
gereğini arz ederim.

Öğrencinin Adı, Soyadı: Faruk Serhat
Tarih: 12.07.2023
İmza:

Danışman Adı, Soyadı: Doç. Dr. Mehmet Emin ÖNCÜ Tarih:12.07.2023	İmza:
Ana Bilim Dalı Başkanı Adı, Soyadı: Prof. Dr. Z. Fuat TOPRAK Tarih:12.07.2023	İmza: